TRANSVERSE CRACK INITIATION AND PROPAGATION IN UNIDRECTIONAL COMPOSITES WITH MANUFACTURING DEFECTS

A Dissertation

by

ASWATHI SUDHIR

Submitted to the Office of Graduate and Professional Studies of
Texas A&M University
in partial fulfillment of the requirements for the degree of

DOCTOR OF PHILOSOPHY

Chair of Committee,	Ramesh Talreja
Committee Members,	J N Reddy
	Vikram Kinra
	Mohammed Naraghi
Head of Department,	Rodney Bowersox

August 2019

Major Subject: Aerospace Engineering

ABSTRACT

The objective of the current work is to study damage initiation and propagation in unidirectional fiber-reinforced polymeric composites under transverse loading. In the study conducted, a systematic analysis is carried out to analyze the effects of manufacturing induced defects such as random distribution of fibers and presence of voids in matrix on the damage initiation in unidirectional composites under transverse tension. As illustration, this study focuses on the resin infusion manufacturing process and the defects hence formed. Upon infusing resin, the initial fiber configuration undergoes perturbation and results in a random distribution with regions of resin rich areas and fiber clusters. In addition, micro voids (between the fibers in a bundle) and macro voids (between fiber bundles) are usually formed from the manufacturing process. Effort is laid on quantifying the effect of manufacturing defects to the failure events.

Representative Volume Elements (RVEs) are constructed to capture essential features of the composite microstructure that determine the local stress fields and hence damage initiation followed by further events of damage. Stress analysis of the RVEs is conducted using Abaqus FEA software. A novel methodology is put forward to generate random distributions of fibers that would simulate different levels of perturbations of the fibers from initial (dry bundle) positions during the manufacturing process resulting in different configurations of fiber clusters. An embedded RVE approach has been adopted in a finite element model to calculate the stress fields to avoid artificial effects of the RVE boundary. Damage initiation is then monitored using a previously proposed energy based criterion for cavitation induced fiber/matrix debonding in polymers. The first event of failure is determined by the energy based criterion. This work also throws light on the significance of energy based failure initiation in polymeric composites. The local stress field determines the first failure

event out of the two competing mechanisms- dilatation driven and distortional driven.

Subsequent events of damage in the form of crack formation by coalescence of the debond cracks is also analyzed by the energy based approach. The cavitation based damage initiates in the matrix region close to the fiber matrix interface and results in debond formation. These debonds coalesce to form cracks of different length based on the number of fibers debonding. The energy released during the crack growth is monitored for increasing crack length and the criticality is compared to homogeneous case at different crack lengths. The strains at cracking are monitored for varying radial mobility. The effect of non-uniformity in fiber distribution is gauged by comparing the total J Integral of the RVEs with homogeneous and matrix medium.

Ongoing and future work is aimed at studying ply cracking process to its full extent and its consequence on crack deflection into inter-ply regions leading to delamination.

DEDICATION

To my parents and my brother

ACKNOWLEDGMENTS

First and foremost, I am very much pleased to express my gratefulness and indebtedness to **Dr. Ramesh Talreja**, for his outstanding support and patience through out my research. It is needless to say that he has been extremely helpful in providing quality guidance, precious time and of course, support on various facets of the research work and other situations in life. No words can explain how amazing advisor he is! I am always grateful to him for his extreme patience and kindness.

I would also like to thank my committee members, Dr. Vikram Kinra, Dr. Mohammed Naraghi and Dr. J. N. Reddy for their guidance and sharing their knowledge. I am grateful to all my Teachers without whom I would not have reached here. I cannot proceed without thanking Dr. Suhasini Gururaja for inspiring me and for her guidance during my masters study. I am also thankful to my family, who always encouraged me to pursue my dreams. Nothing can substitute their unconditional love and support. Special thanks to my brother who was always my support system.

I am also grateful to my fellow researchers Sarah and Linqi for their extensive support, fruitful discussions and timely help. I am also thankful to my friends, co-research students, who helped me with materials, moral and intellectual support at the time of need. Special thanks to my friends: Atanu, Hari, Sruthi, Nithin and my roommates- Christy, Seles, Arundhathi, Panchami, Donna.

I am deeply indebted to Binu aunty and Paul uncle for taking care of me like their daughter. Also, Dr. Moble Benedict for all his motivation at the right time. I am also thankful to Gail and Karen for their support and advice from the beginning of this degree.

I would like to take this opportunity to thank all those who helped me in whatever capacity to see that the dissertation attains completion.

Last but not least I thank God Almighty for his blessings for whatever I have and giving me inner solace and strength to overcome the ups and downs of life.

CONTRIBUTORS AND FUNDING SOURCES

Contributors

This work was supported by a dissertation committee consisting of Dr, Ramesh Talreja, Dr. Vikram Kinra and Dr. Mohammed Naraghi of the Department of Aerospace Engineering and Dr. Junnuthala N Reddy of the Department of Mechanical Engineering.

All the work conducted for the dissertation was completed by the student independently.

Funding Sources

Graduate study was supported by an assistantship from Texas A&M University. The research is supported by the Office of Naval Research (ONR) under Grant Award No. N00014-16-1-2173

NOMENCLATURE

v_m	Volume Fraction of Matrix
v_f	Volume Fraction of Fiber
PMC	Polymer Matrix Composite
MMC	Metal Matrix Composite
CMC	Ceramic Matrix Composite
FRC	Fiber Reinforced Composite
PRC	Particle Reinforced Composite
RVE	Representative Volume Element
RUC	Repeating Unit Cell
FEA	Finite Element Analysi
UD	Uni Directional
CTE	Coefficient of Thermal Expansion
K(r)	Second Order Intensity Function
g(r)	Radial Distribution Function
σ	Far Field Stress
σ_1	Maximum Principal Stress
σ_2	Maximum Principal Stress
σ_3	Maximum Principal Stress
E	Young's Modulus
ν	Poison's Ratio

U_v	Dilatational Strain Energy Density
U_d	Distortional Strain Energy Density
U_v^{crit}	Critical Dilatational Strain Energy Density
ΔR	Radial Mobility
$\Delta\theta$	Angular Mobility
A	Area of Realization
N	Number of Points within the Realization
w_k	Ratio of Circumferences within Area to total Circumference
r	radius
$I_k(r)$	Number of Points in circle
NOR	Number of Rings around Central Fiber
L	Size of the Model Assembly
R	Radius of the RVE Perimeter
Φ	Diameter of the Fiber
r_v	Radius of Voids
E_0	Young's Modulus of 0° plies
E_{90}	Young's Modulus of 90° plies
$WWFE$	Worldwide Failure Exercise
σ_L	Longitudinal Stress
σ_T	Transverse Stress
σ_{LU}	Longitudinal Strength
σ_{TU}	Transverse Strength
ϵ_L	Longitudinal Strain

ϵ_T	Transverse Strain
ϵ_{LU}	Maximum Longitudinal Strain
ϵ_{TU}	Maximum Transverse Strain
θ_{fp}	Failure Plane Inclination Anlge

TABLE OF CONTENTS

Page

LIST OF FIGURES

FIGURE Page

LIST OF TABLES

TABLE Page

1. INTRODUCTION AND LITERATURE REVIEW

1.1 Introduction

Ever since, mankind started building structures, finding the best suitable material has been of concern. Often, it was a choice based on the mechanical properties of the material, that matched the specific task. However, with the advancement of technology, the material selection has become a complicated task that involves meeting a number of simultaneous requirements. This is much evident and demanding in aerospace industry. The aerospace industry has always been one of the driving forces that lead tor the development of advanced materials like composite materials.

A composite material is defined as a material having two or more chemically and/or physically distinct constituents/phases combined in a certain configuration to form a new material on a macroscopic scale. The constituents present in the composite material retain their individual identities and properties, yet act together to produce an entirely different material with superior properties. These materials have been used in civil structures-like reinforced concrete, for a long time. But in the past few decades, the advancement in research has facilitated the use of these materials into other industries like aerospace, automotive and wind turbine industries as well.

Usually, for composite materials, one of the constituent material generally consists of a bulk material - referred to as matrix and holds the other constituents together- referred to as inhomogeneity/reinforcement (which may be fillers of some type- fibers, whiskers, or particulates). The effective behavior of the composite is strongly influenced by the volume fraction and properties of the phases present. For a typical two-phase reinforced composite material, v_f represents the volume fraction of the fibers and $v_m = 1 - v_f$ denotes the volume fraction of the matrix.

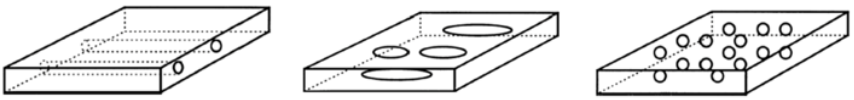

(a) (b) (c)

Figure 1.1: Classification of Composites: a) Fiber Reinforced Composite b) Flake Reinforced Composite c) Particle Reinforced Composite Adapted from [1]

Composites are typically classified on the basis of (a) type of matrix material and (b) type of reinforcement. Depending on the nature of the matrix material used, the composites are classified as i) Polymer Matrix Composites (PMCs), ii) Metal Matrix Composites (MMCs) and iii) Ceramic Matrix Composites (CMCs). Based on the size and shape of reinforcement, composites can be further subdivided as i) Fiber-Reinforced Composites (FRCs), ii) Particle-Reinforced Composites (PRCs), and iii) Flake Reinforced Composites (see Figure 1.1). In FRCs, one of the dimensions of the reinforcement is much larger than the two other dimensions while in Flake-Reinforcement one dimension (thickness) is much smaller than the other two. In PRCs, all three dimensions are of the same order. Amongst FRCs, further distinction is possible as follows: i) long or continuous FRCs, ii) woven/textile composites and iii) short fiber reinforced composites. The properties of a composite material is dependent on fiber architecture, fiber volume fraction, fiber orientation angle and the constitutive properties of the constituents[1, 12].

PMCs are an important of class of composites in which the fibers are reinforced in thermoset or thermoplastic polymer. Over the past few decades, there is a rising need for PMCs as a choice of structural material. They are by far the most commonly used reinforced composite material with applications ranging from tennis rackets to bicycles, aircraft and wind turbine blades. Boeing 787 and A350 uses atleast 50$\%$ by weight composites, as shown in figure1.2. Figure shows the use of composite materials in A350 (52$\%$)[3]. Some of the

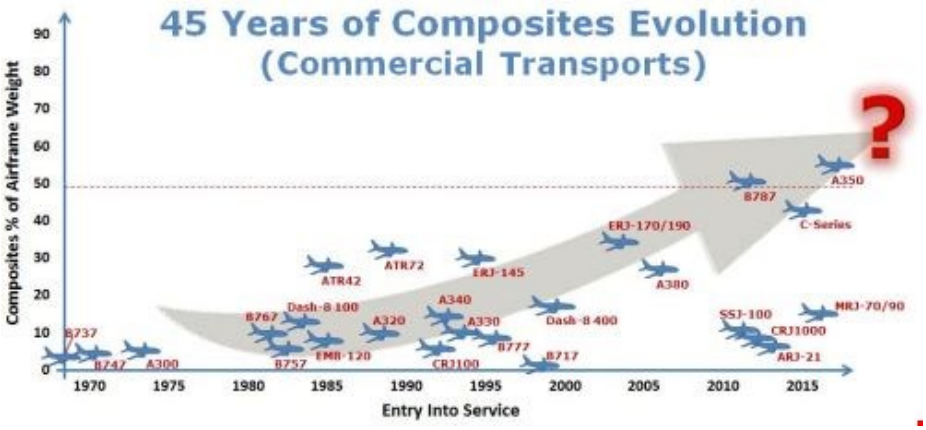

Figure 1.2: Composite Materials in Aerospace Industry Reprinted from [2]

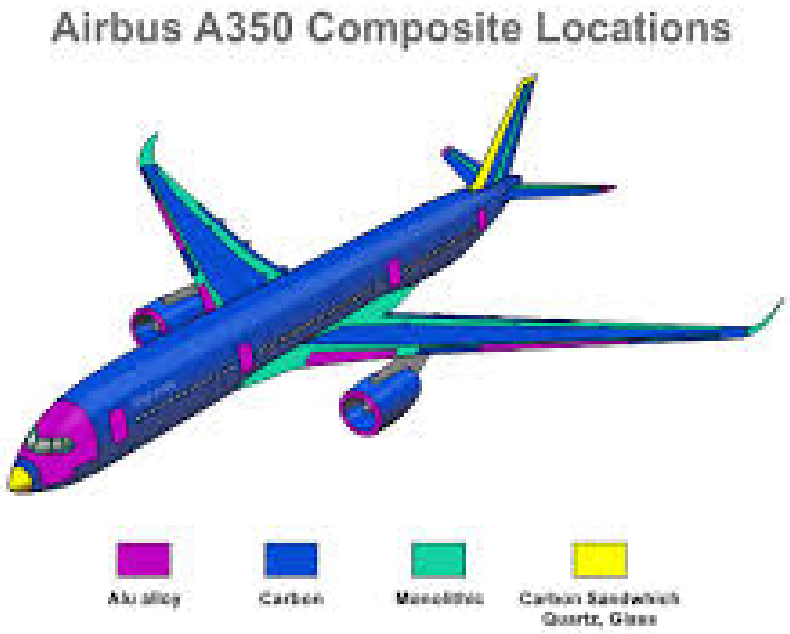

Figure 1.3: Composite Materials in A350 (52% by weight) Reprinted from [3]

key advantages of PMCs are:

- **High Specific Strength**: They are high strength material made from lightweight constituent materials. The specific gravities of the constituents of PMCs are low when compared to metals. Thus PMCs have high strength to weight ratio compared to conventional metals.

- **Design Flexibility**: Fibers in PMCs can be selectively placed or oriented in the matrix to carry load in particular direction. Hence, directionality can be introduced in the material rather than using isotropic materials.

- **Ease of Manufacturing**: PMCs have relatively simple processing techniques which do not require very high temperature and pressure like other composites.

The other reasons that make them desirable are they are resistant to corrosion, high thermal stability, better fatigue performance etc[13].

On the other hand, PMCs do not show yielding/ plastic deformation like metals. Also, they have lower ductility and fracture toughness compared to metals. The stress-strain diagram of PMCs can still be nonlinear. This non-linearity in the behavior is due the damage mechanisms such as fiber-matrix debonds, matrix cracking, delamination, fiber breakage, etc. Failure process in composites consists of multiple crack formation, coalescence of cracks, fiber failure etc. There may not be an immediate failure, but a progressive degradation of the material property is observed. The location of damage initiation is highly dependent on the local stress fields and perturbation in the stresses affect the damage initiation. Hence, the effect of defects especially from manufacturing plays an important role in the damage initiation and propagation in PMCs.

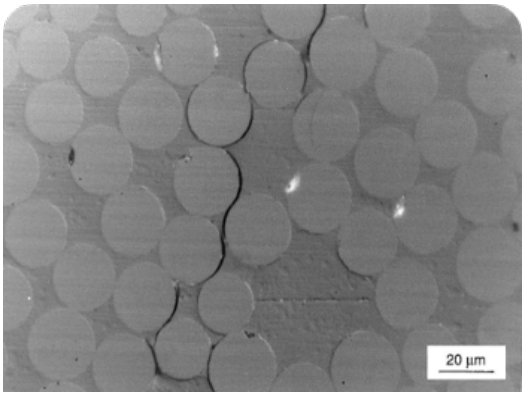

(a) Matrix Crack leading to Debonds

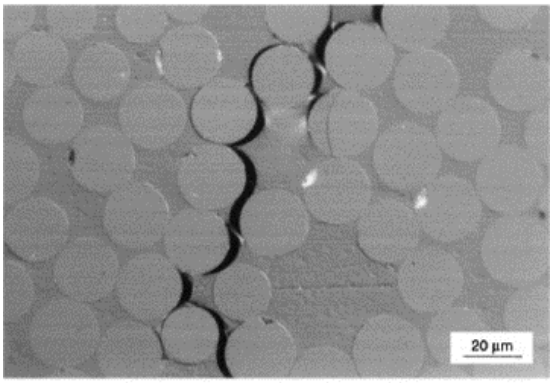

(b) Transverse Crack formation in Matrix

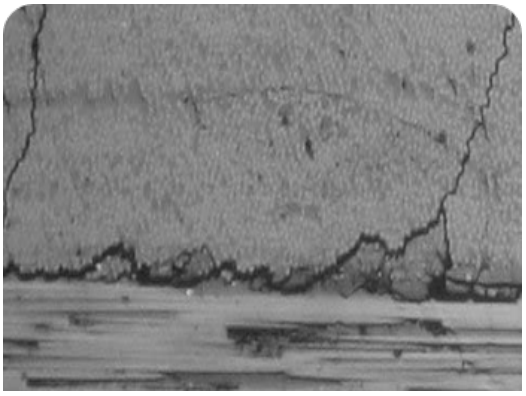

(c) Delamination

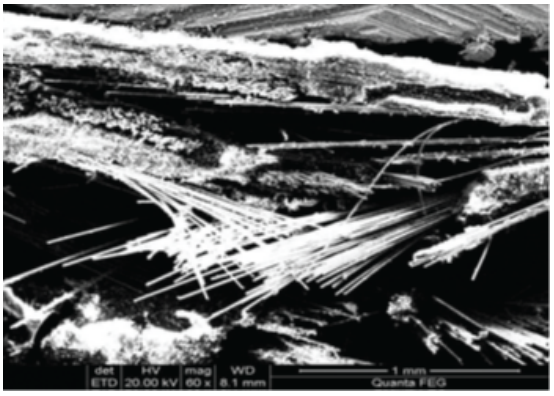

(d) Fiber Breakage

Figure 1.4: Damage Modes in PMCs: Figure 1.4a shows the formation of debonds along the fiber matrix interface. These debonds coalesce to form a transverse crack in the matrix in Figure 1.4b. These cracks propagate into the interface between the plies causing delamination (Figure 1.4c) and then lead to fiber breakage (Figure 1.4d) Reprinted from [4] Based on [5]

1.1.1 PMCs: Constituents and Manufacturing Methods

Polymer matrix composites (PMCs) comprise more than 90% of the composite materials available. They are used extensively within industry due to their high stiffness and strength, low density, long fatigue life, corrosion resistance, crash worthiness and other improved performance. These materials can also be tailored to exhibit stealth characteristics, sensor capabilities, and high thermal or electrical conductivity]cite[14, 9, 15, 16].

1.1.1.1 Constituents

Polymer matrix composites consist of matrices made of polymeric materials, such as plastics or resins that are either thermosetting or thermoplastic, and fibrous reinforcements. The reinforcements can be short or continuous fibers bound together by an organic polymer matrix. PMC is designed so that the mechanical loads to which the structure is subjected in service are supported by the reinforcement. The function of the matrix is to bond the fibers together and to transfer loads between them. As such, they are divided into two categories: reinforced plastics, and advanced composites [17]. The distinction is based on the level of mechanical properties (usually strength and stiffness). Reinforced plastics, which are relatively inexpensive, typically consist of polyester resins reinforced with low-stiffness glass fibers.

The matrix properties determine the resistance of the PMC to most of the degradative processes that eventually cause failure of the structure. These processes include impact damage, delamination, water absorption, chemical attack, and high-temperature creep. Thus, the matrix is typically the weak link in the PMC structure.The matrix phase of commercial PMCs can be classified as either thermoset or thermoplastic.

The common properties of thermoset polymers are:

- Do not melt once hardened

- Develop well-bonded 3-D structures
- Require a curing process: Uncured resins are susceptible to moisture and temperature effects, and contamination Under-cured resins are too soft to transmit loads efficiently between the matrix and the fibers Over-cured resins become embrittled and crack prematurely.
- Can be left in a partially cured state
- Most often used in chopped fiber composites
- Examples: Epoxies, unsaturated polyesters, phenolics, vinylesters, bismaleimides
- Commonly used for aircraft, space, military, and automotive parts
- Produced by condensation polymerization or by addition polymerization, followed by a condensation rearrangement reaction to form heterocyclic entities Both produce water, making it difficult to produce void-free parts or structures

Ther properties of Thermoplastic polymers are:

- 1-D or 2-D in molecular structure
- Soften at high temperatures, showing a discrete melting point
- Become rigid with cooling
- Examples: polyethylenes, polyesters, polyketones, polysufones, polypropylenes, polyamides
- Can be crystalline or amorphous
- Creep is a concern, but can be minimized with the proper reinforcement selection
- No chemical reactions are needed, thus no excess heat or product gas are released

- The limiting factors in production are time to heat, shape, and cool
- Materials can be salvaged and re-worked
- Lose strength at high temperature

A brief overview of several manufacturing process for PMCs is required to understand the corresponding process induced manufacturing process [18]. The following methods typically apply to both resin types.

Table 1.1: Manufacturing Process for PMCs

Hand Lay-up:	Reinforcing fibers are placed in the mold after a release film and gel coat in some instances); the resin material is then rolled into the reinforcing fibers. Hand lay-up is commonly used in the US aircraft industry to produce PMC parts.
Spray Lay-up:	The reinforcements are chopped and sprayed simultaneously with the resin into the mold. A roller is then used to ensure that the resin fully wets the fiber bundles. This technology produces low specific strength structures and is used to join back-up structures to composite face sheets on composite tools.
Manual Prepreg Lay-up:	The prepreg is cut into several layers, as needed for the mold. The shaped prepregs are then layered within the mold
Automatic Prepreg Lay-up:	A tape-laying machine lays the prepreg in the mold, cutting the prepreg when the mold edge is reached. This process is repeated until the part is complete

Table 1.1 Continued

Compression Molding:	A specific amount of uncured resin and reinforcement are placed into the cavity of a matched mold in the open position. As the mold is closed, the pressure increases, causing the mold to fill and the part to form. This method may be used with prepregs also.
Liquid Composite Molding:	LCM processes include Resin Transfer Molding (RTM), Structural Reaction Injection Molding (SRIM), and Injection Compression Molding. A fiber preform is placed in the mold cavity and a polymeric resin is injected into the sealed mold. A curing reaction is initiated; the part solidifies and is then removed from the mold. Since LCM has a very high, non-recurring tooling cost, it is best suited for high production volumes to lower the cost
Vacuum-Assisted RTM:	The resin is injected into a mold that contains the reinforcement using pressure that is applied by the atmosphere against an evacuated system.
Resin Film Infusion:	The resin film is placed in the bottom of the mold. Heat and pressure are then applied, causing the resin viscosity to decrease and spread through the preform
Expansion RTM:	A material that expands when heated is placed in the preform. The resin is infused and the mold is heated, causing the core material to expand and subsequently forcing the resin into the remaining parts of the preform
Transfer Molding:	Similar to compression molding, but the mold is closed when the resin material is injected.

Table 1.1 Continued

Filament Winding:	Fiber spools are mounted to a creel; the strands from each spool are combined and pulled through a resin bath. The strands are then fully activated with an initiator or hardener and the excess resin is removed. Lastly, they are sent through a drying device and wound onto a mandrel, forming the desired part. Filament winding is used more extensively to manufacture composites than all other lay-up methods combined
Fiber Placement:	Similar to filament winding, but enables all axes of motion.
Pultrusion:	Continuous fibers are drawn from reels, formed into a general shape, and drawn through a resin bath. The wetted fibers are then shaped as they converge toward a heated die, where curing occurs. Upon die exit, the formed part enters a pulling system, which provides the force that pulls the materials through the entire system. The pultruded part is then cut and trimmed to the desired size.
Thermoforming:	Utilizes matrices that can repeatedly be softened or melted on heating and hardened or solidified on cooling, and that can provide increased fracture toughness and higher hot-wet use temperatures (thermoplastics).

Now, with the basic understanding of the manufacturing process, we are able to look at the process induced defects. Some of the major defects arising from the resin infusion process are :

- **Non Uniform Distribution of Fibers:** In almost all the manufacturing process discussed above, it is impossible to generate a uniform distribution of fibers in the matrix. Nevertheless, depending on the process of manufacturing the degree of nonuni-

form fiber distribution in the matrix can be controlled.

- **Voids/Pores:** These are another important inevitable defect present in the PMCs. They are formed from the entrapment of volatile gases air or other materials. They can also be formed from the improper pressure during the cure cycle and inadequate wetting of the fiber by the resin. Voids are typically of two types- micro voids(those that are trapped within the fiber tow) and macro voids (those that are trapped within the fiber tows).

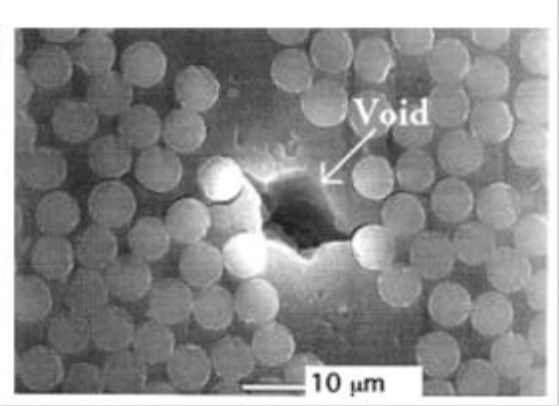

Figure 1.5: Microvoid in a PMC Reprinted from [6]

m The Figure 1.5 shows the image of a void trapped in a matrix. It can also be seen in the picture that a crack connecting the void and the debonds.

- **Inclusion:** Another important defect the inclusion of another foreign material which leads to physical and mechanical discontinuities within the material. These affect the local stress distribution and depending upon the entrapped material's physical and chemical properties, they react with the environment and the matrix. These can affect the strength and stiffness parameters of the matrix material.

- **Thermal Residual Stress:** Polymer materials are usually cured from a temperature of 100-150°. While curing it is possible to have uneven curing. This will lead to prestressing the composite which can be tensile or compressive in nature depending on the location . This residual stress from the thermal cool down affects the local stress state in the composite and affects the damage initiation.

Even though composites have many advanced properties than the conventional structural materials, they are still limited in usage. This is due to the complexity in the structural behavior of the material arising from the anisotropy and inhomogeneity in composite material. As a result, composites do not have a unique failure mechanism like metals. As shown in figure1.4, the damage mechanism in composites are typically series of events/ failure modes and requires multi scale analysis. For unidirectional composites, matrix cracking is mostly the first damage mode. Once the matrix cracking initiates, it leads to fiber matrix debonds followed by delamination and ultimately failure of the structure. Development of an accurate methodology to predict the failure initiation and propagation in composites has been a hot topic for the scientific society.

1.1.2 Failure theories

Over the years, a number of failure theories have been developed for composites. The Worldwide Failure Exercise (WWFE) is a platform which compares some of these analytical models to the experimental data. The comparison is analyzed[19] and turns out that none of the theories has the ability to correlate to the experimental data. Some of the failure theories and their limitations are examined in [5]. A brief description of the failure theories is provided here.

1. **Maximum Stress Theory:** The failure occurs if one of the stresses in the longitudinal or transverse direction exceeds the corresponding allowable stress. To avoid

failure, the material must satisfy the following inequalities in tension.

$$\sigma_L \leq \sigma_{LU} \tag{1.1}$$

$$\sigma_T \leq \sigma_{TU} \tag{1.2}$$

$$\tau_{LT} \leq \tau_{LTU} \tag{1.3}$$

and similarly in compression,

$$\sigma_L \leq \sigma^{'}_{LU} \tag{1.4}$$

$$\sigma_T \leq \sigma^{'}_{TU} \tag{1.5}$$

The major assumption is that the failure modes are independent.

2. **Maximum Strain Theory:** The failure occurs when one of the strains in the axis(longitudinal or transverse) exceeds the corresponding allowable strain. Again, the interaction between the failure modes is ignores in this criteria.

$$\epsilon_L \leq \epsilon_{LU} \tag{1.6}$$

$$\epsilon_T \leq \epsilon_{TU} \tag{1.7}$$

$$\gamma_{LT} \leq \gamma_{LTU} \tag{1.8}$$

and similarly in compression,

$$\epsilon_L \leq \epsilon^{'}_{LU} \tag{1.9}$$

$$\epsilon_T \leq \epsilon^{'}_{TU} \tag{1.10}$$

3. **Tsai Hill Theory:** It takes into account for the failure mode interactions in a multi

axial stress state. However, this theory is based on homogenized composite and a yield criteria is proposed for the materials taking orthotropy into account[20, 21].

$$(\frac{\sigma_L}{\sigma_{LU}})^2 + (\frac{\sigma_T}{\sigma_{TU}})^2 - \frac{\sigma_L}{\sigma_{LU}}\frac{\sigma_T}{\sigma_{LU}} + (\frac{\sigma_{LT}}{\tau_{LTU}})^2 \leq 1 \tag{1.11}$$

The above equation is conservative and one must transform the stress to the longitudinal and transverse direction.

4. **Tsai Wu:** Proposed a scalar function that accounted for ellipsoidal surface of failure in UD composites[22]. The quadratic expression under plane stress is

$$F_L\sigma_L + F_{LT}\sigma_L\sigma_T - 1 \tag{1.12}$$

5. **Hashin:** A more physically acceptable failure criterion. Proposed the failure mode to account for each failure mode individually[23]. He separated the matrix and fiber failure modes. For plane stress condition, tensile fiber failure mode is given by the following term

$$(\frac{\sigma_1}{\sigma_{LU}})^2 + (\frac{\sigma_6}{\tau_{LTU}})^2 - 1 \tag{1.13}$$

Similarly, for matrix tensile mode,

$$(\frac{\sigma_2}{\sigma_{TU}})^2 + (\frac{\sigma_6}{\tau_{LTU}})^2 - 1 \tag{1.14}$$

6. **Puck Theory :** Introduced three traction components σ_n,σ_{nl} and σ_{nt} , acting on the failure plane at an inclination angle θ_{fp}. As described in Puck et al[24], a function $f_E(h)$, called the stress exposure factor is defined based on suggestions in Hashin[23]

and fracture is assumed on the plane where this function takes its maximum with respect to the angle θ.

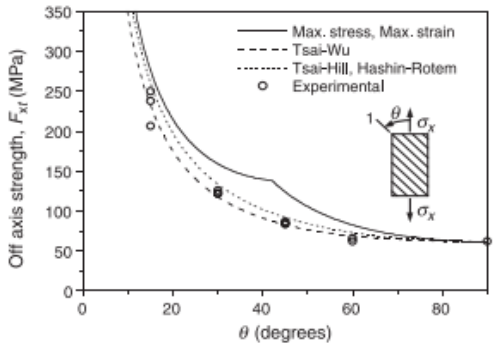

(a) Comparison of failure theories and off-axis strength data Reprinted from [25, 26]

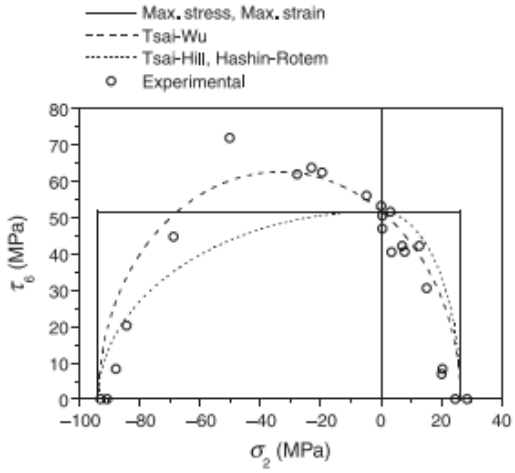

(b) Comparison of Failure envelope under transverse normal and shear loading Reprinted from [25, 27]

Figure 1.6: Comparison of Failure Theories and Failure Envelopes

After a rigorous review on the underlying assumptions, it is found that the early theories like Tsai-Hill and Tsai- Wu do not capture the physical failure mechanism. The later

theories like Hashin and Puck, which take the physics based mechanism into account, are based on homogenization theories. This makes these theories limited as they fail to capture the local stress fields.

Talreja et al[5] also provides remedies and strategies to improve the failure prediction in composites. Some of the main remedies suggested in the work are

- **Multiscale analysis of failure**: Composite materials are heterogeneous solids- matrix, fiber and interface. Under general imposed loading, damage initiates at a point/ weak zone and triggers subsequent events of the failure process. Failure initiation is local and depends on the local stress fields and the criticality condition for the local stress field.There may exist multiple modes which compete with each other and the one that reaches criticality first would be the damage initiation mode. The failure progression can take different paths depending on the fiber architecture and the nature of the imposed loading. The sequence of the events on those paths often involve coalescence of multiple debonds formed at interfaces and cracks in the matrix, and fiber failures in the later stages. Thus, the failure prediction requires multi-scale analysis. Bulsara et al[10] proposed that the sacle at which the analysis has to be carried out depends on the property to be evaluated. Hence, the scale for evaluating elastic properties are not same as the one for evaluating the damage properties.

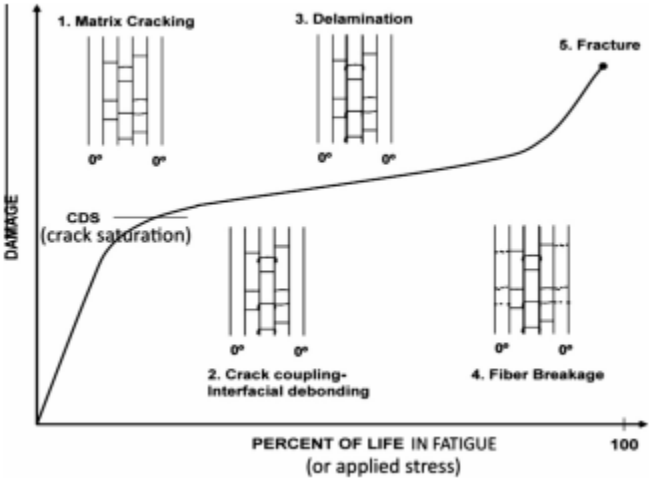

Figure 1.7: Progression of Failure Events in a Laminate Reprinted from [7]

- **Analysis of constrained failure**: Composite structures are made up of composite plies with straight fibers are stacked in different orientations to create laminates. In some cases, complex fiber architectures using woven fabrics are also generated. There exists interfaces between layers in the containing UD fibers or woven fabrics. The failure process within the layer is subjected to a constraint by the presence of other layers until delamination occurs. The classical failure theories, do not take into account this constrain effect by nearby layers. Jamison et al[28] studied the constraint failure process in laminates. The observation from a tension-tension fatigue of laminates is shown in figure1.7. The initial stage is multiple crack formation in the laminate which reaches a saturation in crack density on continued loading. Upon further increasing the loading, ply crack grows into the interface between the plies leading to delamination and the consequent fiber breakage and final failure. Hence, ignoring the failure progression from the ply constraints results in error in the failure prediction.

- **Analysis of manufacturing defects**: The current failure theories are formulated on homogenized solids with anisotropy induced from fiber orientations. Thus the stress fields in the composite thus created are averaged over the entire composite. In reality, composites cannot be manufactured without defects resulting from the corresponding manufacturing process.Some of the defects resulting from manufacturing processes are observed and quantified in [29, 30, 31]. These defects are either the failure initiation point or affect the failure initiation from weak sites such as interfaces. Traditional approach is to analyse the composite with embed defects into the homogenized solid for assessing their effects. This is inadequate as they fail to capture the interactions between the defects and the composite micro-structure. Hence, analysis of the real composite micro structure includes manufacturing defects in multi-scale analysis as performed in Huang et al and Chowdhury et al[32, 33].

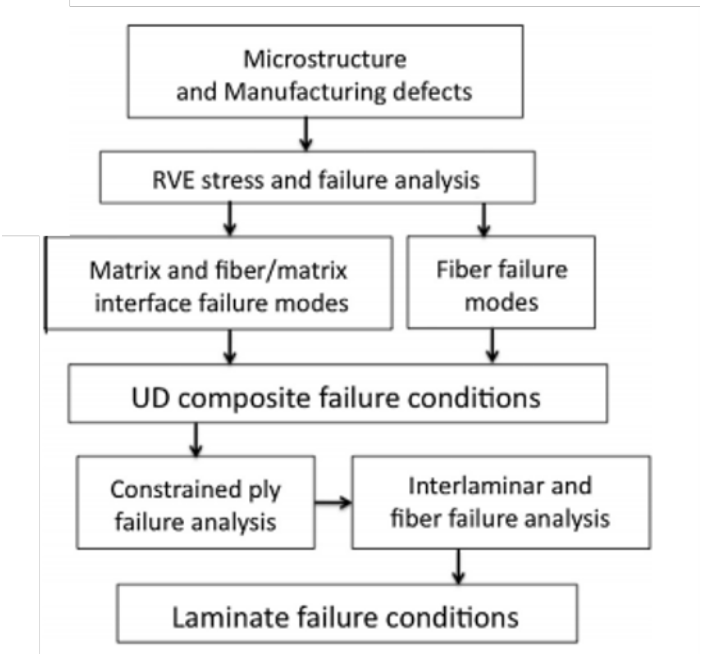

Figure 1.8: Analysis Scheme for Composites Reprinted from [5]

Incorporating these in the failure analysis would give us the following scheme as shown in figure1.8. To understand and predict the failure mechanisms in composites hence is a challenge and currently more emphasis is being given to this field. In the current research, particular focus is being given to UD composites under transverse loading.

1.2 Objective

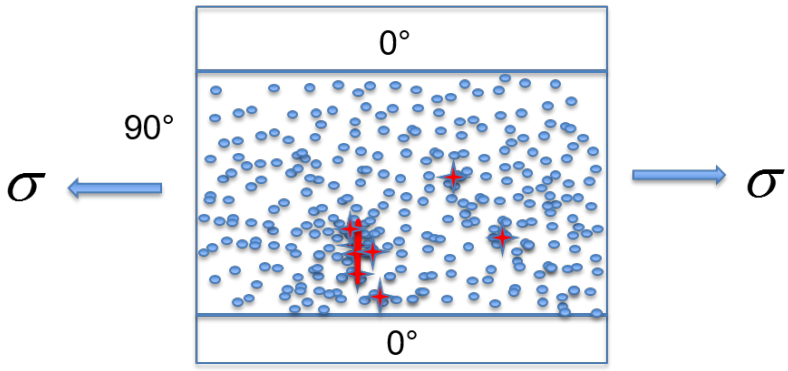

Figure 1.9: First Event of Failure

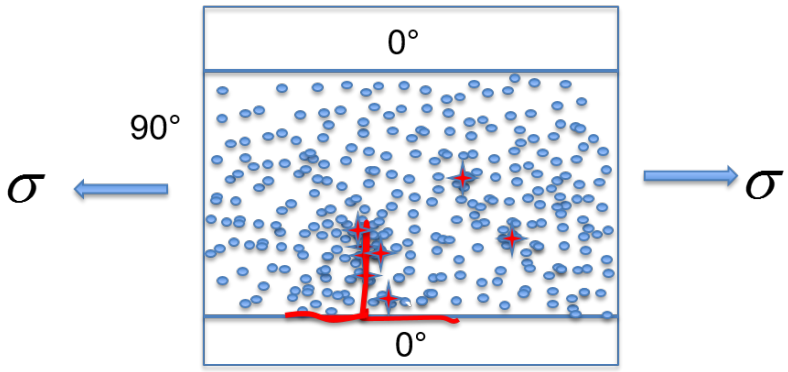

Figure 1.10: Further Failure Events

In this dissertation, the damage initiation and propagation in UD composites under transverse loading is investigated. As discussed above a multi scale analysis which incorporates the effect of manufacturing defects and constraints is adopted in the current study.

The main objectives of current work can be classified into two:

1. To identify the first failure event based on strain energy density criteria [34, 35] and to determine the effect of manufacturing defects on the same as shown in Figure 1.9.
    - Identify the location and mechanism of damage initiation: Quantify manufacturing process controls on the microstructure.
    - Monitor the points of failure initiation into formation of crack
    - Quantify the effect of manufacturing defects on the damage initiation
2. To monitor the crack formation and driving force for crack propagation. Comparison of the the evolution of transverse crack into delamination when it reaches interface as shown in Figure 1.10.

The following are the key concepts or methodology adopted in this research.

- **Generate a Representative Volume Element(RVE)**: A novel methodology for creating an RVE from resin infusion process has been adopted. The RVE incorporates manufacturing defects. The RVE generation is governed by two parameters, radial and angular mobility.
- and crack formation: At least 5 realizations each of the RVE is taken into account at each of the varying parameters, i.e, radial mobility and angular mobility.
- **Damage Initiation Criteria**: The location of damage initiation based on strain energy density criteria in the RVE is determined. The two strain energy based mecha-

nisms compete with each other and the local stress state determines the mechanism by which the first failure event occurs.

- **Finite Element Analysis- first failure event**: After the verification of the model generated, the RVE is analyzed for the local stress state and the failure initiation point is determined. The location and the mechanism is identified at the micro scale.

- **Further failure events : Crack Formation**: Coalescence of the debonds into the crack is carried out. Energy release rate for the advancing crack is monitored.

- **Effect of stiffener** : Presence of the 0° plies intensifies the crack propagation. This is studied by introducing the stiffener. The effect of the stiffener location and stiffness of the layer will be looked at.

1.2.1 Approach

A systematic approach has been adopted to carryout the damage initiation and propagation analysis in UD composites under transverse loading. The effect of process induced defects are also incorporated. In the current study, we focus on the resin infusion process for illustration and hence the defects of interest are nonuniform fiber distribution and presence of voids. The entire analysis is carried out in Abaqus FEA framework. Subroutines are written to monitor the damage initiation points. Modeling of crack and evaluation of J Integral was also carried out in Abaqus[36].

1.3 Outline of the Dissertation

As presented in the previous sections, this work can be grouped into 6 main chapters:

1. Chapter 1: The Introduction chapter throws light onto the current application of PMCs and the need for an accurate failure prediction methodology for PMCs. It also suggests the accurate method to model failure in PMCs. The objective of the current research is mentioned in this chapter.

2. Chapter 2: This chapter explains the methodology of generating an RVE for the current study. A brief explanation of the concept of RVE and RUC is also provided. In addition, the systematic procedure for determining the size of RVE is also explained in this chapter.

3. Chapter 3: This chapter deals with the failure initiation criteria. The conventional stress based failure criteria are discussed in detail. The current work focuses on the point failure initiation by strain energy density criteria. The corresponding failure mechanisms are explained in detail.

4. Chapter 4: This chapter is the beginning of the numerical simulations. To begin with the model verification simulations are provided and explained. Later the factors that affect the local stress state are identified and the effect of those on the first event of failure are also provided.

5. Chapter 5: This chapter essentially deals with the failure progression in the lamina. The J Integral is measured for the crack propagation. The effect of ply on crack propagation is also studied. The later part is the crack propagation into an interface where, the crack sees the 0° ply and how the local stress state affect the crack propagation.

6. Chapter 6: Summary, conclusion and recommendation for future work based on the current research is provided in detail in this chapter.

2. REPRESENTATIVE VOLUME ELEMENT

2.1 Introduction

The lightweight polymer matrix composites (PMCs) are gaining mainstay acceptance in aerospace, automobile and wind turbine industries. Although impressive applications of these materials have recently been achieved, much more are possible but depend on reducing the manufacturing cost. The less expensive manufacturing processes often leads to less control over the process and result in more manufacturing defects such as nonuniform distribution of fibers, matrix voids, misalignment of fibers etc. The current approach is to conduct tests and evaluate the effect of these defects on the composite performance. This is expensive and cumbersome process and requires the test to be conducted in case a manufacturing parameter is altered. A good design strategy is to conduct cost/performance trade-off, and this requires knowing how the manufacturing defects affect performance, in particular failure.

The PMCs can be manufactured in different ways, e.g. by autoclave curing of stacked prepregs or by resin infusion. Each process results in different types of defects with different severity. Rather than assuming arbitrary randomness in defect geometry and distribution, as is common in the literature, it would be useful to characterize the irregularities or non-uniformity of defects by parameters than can be related to the anomalies of a given manufacturing process. With this objective in mind, we develop here a systematic procedure for characterizing fiber distribution non-uniformity as it might result from resin infusion in spreading out the fibers from their initial positions in a fiber bundle. A brief introduction to the concept of RVE and RUC is provided.

2.2 Concept of RVE vs RUC

Continuum mechanics is based on the concept of a homogeneous medium at large length scale which can be subdivided into heterogeneous medium at smaller length scale. As a result the micromechanics deals with either a RVE of an RUC. An RVE is a represen-

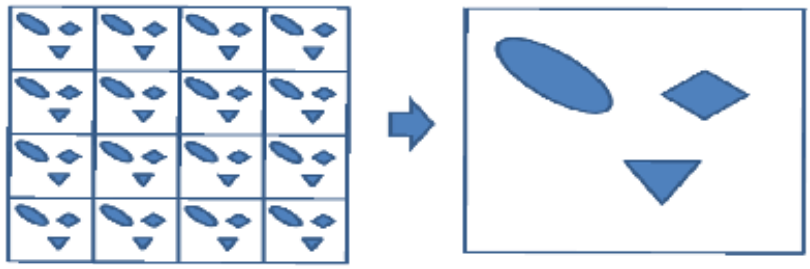

(a) RUC

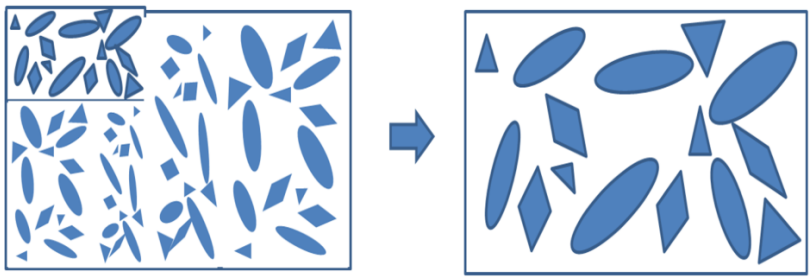

(b) RVE

Figure 2.1: Microstructure: a) RUC and b) RVE

tative of the entire volume of the material and characterizes the heterogeneous materials whose microstructure is statistically homogeneous. Statistically homogeneous means that the statistical averages for RVEs taken over any sub volume of the entire domain will be same as that of the entire volume[37, 38, 39]. The size of RVE was first introduced by Hill in his monograph [37]. The RVE should be large enough to incorporate all the constituents of the composite and should be able to capture the material's behavior as a whole. The effective behavior of the RVE is indistinguishable from the whole material.

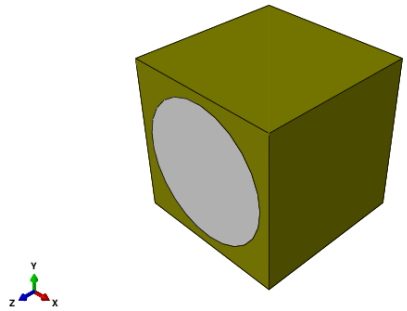

(a) RUC

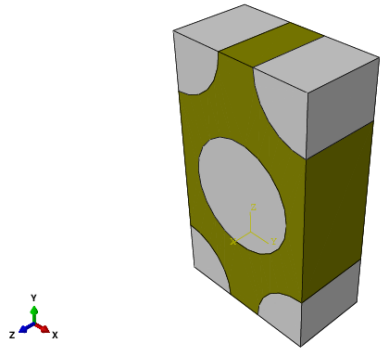

(b) RVE

Figure 2.2: Different Unit Cells : a) Square unit cell b) Hexagonal unit cell

The concept of RUC is such that the entire heterogeneous material is approximated to be periodic, wherein the RUC is repeated to generate the whole material. Drago and Pindera have dealt with the concepts of RUC and RVE in detail[40]. Figure 2.1 depicts the concept of RVE vs RUC. A unit cell is defined as the smallest region that represents the behavior of the larger region with translational or reflectional or rotational transformations. For such regions to exist, there must be a basic pattern (of geometry, strains, stresses etc.) that is repeated periodically throughout the domain. The Figure 2.2 shows different unit cells generally adopted for unidirectional fibers (micro scale).

Li[41] has explained the derivation of some unit cells as per Voronoi packing. In the current study the square packing has been adopted.

2.2.1 PBC and HBC

Numerical Homogenization with RUC requires not only choosing the best RUC out of the heterogeneous periodic material but also implementing appropriate PBCs [42, 41, 43].

The requirements/advantages of using PBCs have been listed as follows:

- **Requirements**
  - No gap or overlap between neighboring RUCs is permitted i.e. at the boundary, displacement continuity is preserved.
  - Traction continuity is preserved between periodic surfaces.
  - In case of axial perturbations, the deformations should be along the perturbation.
- **Advantages**
  - The whole simulation process of the micro structure is managed through 3 control-nodes referred to as 'Dummy nodes'.
  - All types of perturbations are applicable.

On the other hand, HBCs are also used in micromechanics approach to simulate the properties of the entire domain from RVEs. These are applied when the geometry is not periodic in nature and the representative volume of the entire domain could be identified. Sun and Vaidya[44] have predicted the effective elastic moduli of unidirectional composite using FE Analysis of RVE along with HBCs.

- **Requirements**
  - These boundary conditions are similar to that at macro scale. Any boundary condition at the structural level can be transferred directly to the RVE.

- Any Rigid Body Rotation if present should be avoided.

- **Advantages**

  - The whole boundary condition can be applied to the RVE either along the boundary or on the whole body .
  - All types of perturbations are applicable- thermal/ structural so on.
  - The HBCs are less time consuming than PBCs.

In the current analysis, since our focus is on RVE, we have resorted to HBCs on the RVE. The far field strains are applied to the composite so as to produce homogeneous fields in the body. Sun[44] derived the relationship between far field strain and the displacements at the boundary of the unit cell as follows:

$$\begin{aligned} \overline{\boldsymbol{\epsilon}}_{ij} &= \frac{1}{V}\int_V (\boldsymbol{\epsilon}_{ij})dV \\ &= \frac{1}{V}(\int_{v^f} \boldsymbol{\epsilon}_{ij}dV + \int_{v^m} \boldsymbol{\epsilon}_{ij})dV) \\ &= \frac{1}{V}\int_S (u_i n_j + u_j n_i)dS \end{aligned} \tag{2.1}$$

where V is the volume of the unit cell, S boundary surface, u_i is the i^{th} component of displacement and n_j j^{th} component of unit normal to S. Hence, far field strains are applied as displacement boundary conditions on the body as follows:

$$u_i(S) = \boldsymbol{\epsilon}^0_{ij} x_j \tag{2.2}$$

where x_j is the dimension of the unit cell along the normal to surface S and $u_i(S)$ is displacement applied on the surface to produce far field strain $\boldsymbol{\epsilon}^0_{ij}$.

2.3 RVE Construction

When the fiber distribution is uniform, the concept of unit cell can be adopted. But in reality, the microstructure is never uniform. The microstructure will have defects arising from manufacturing processes. The uniform microstructure in UD composites tends to underestimate the damage initiation as they do not take into account the effect of stress concentration arising from non uniformity of the fiber distribution. Trias et al[45] shows that the stresses arising from non uniform fiber distribution has higher stresses than the one with inform distribution.

The fundamental concept in treating microstructure with heterogeneities for evaluating elastic properties and/or failure properties is the RVE. The fundamentals of this concept,under elastic context, were laid down in the pioneering work of Hill [46], who recognized that determining the local stress fields within the microstructure by analytical means was a hopelessly complex task. He also proposed the minimum size of RVE such that the averaged properties are independent of the boundary conditions. However this does not apply if the focus is on the local stress state as in the case of failure initiation[47].

Seguardo et al [48] considered clusters of spherical particles randomly distributed within a homogeneous solid and found that while the overall mechanical properties were weakly affected by the degree of clustering, the local stress fields were significantly enhanced by this non-uniformity. How the fibers are distributed within the microstructure affects the local stress fields. This in turn affects the damage initiation location and mode. Hence, there has been an increased need for incorporating the actual distribution in the failure analysis of composite materials. Approaches based on real images were introduced like [49]. The main disadvantage is the non repeatability and the expensive tools for image analysis.

This opened the doors to the statistical method for generating fiber distribution in the RVEs. Pyrz conducts rigorous study on the construction of microstrucutres based on

Dirichlet function and quantifies them based on second order intensity function $K(r)$[8]. The fiber distribution non-uniformity was studied more generally by Pyrz [50] and Ghosh et al [51]. Pyrz [8], Pyrz and Bochenek [52] and Torquato[53] have carried out studies where the real distribution of fibers were described by random distribution of points. Pyrz [50] in particular proposed methods for microstructure characterization that are suited to relate these to manufacturing induced fiber distribution non-uniformity. We shall resort to these methods for statistical characterization of representative volume elements (RVEs). We shall also consider the presence of voids within the RVEs since these are inevitable in resin infusion processes[54]. While Huang and Talreja [32] analyzed the effect of voids in unidirectional composites on their elastic properties, the effect on damage initiation remains unclear in the context of nonuniform fiber distributions. Our focus here is on clusters of fibers in unidirectional composites resulting from matrix infusion processes.

2.3.1 Algorithm

To begin with, it is assumed that the fibers are arranged in an ordered pattern representing a dry fiber bundle, as shown in Figure 2.3. Upon infusing resin, the fibers get redistributed. The fibers on the outer ring are likely to get displaced more. Taking this physical constraints into consideration, each fiber in the new configuration was given a new position based on the cylindrical coordinates- r, θ with the center of the coordinate system being the center of the center-most fiber (see Figure 2.4).

As shown in Figure 2.4, the coordinate r is the distance of the center fiber from the center of the RVE and θ is the angle measured from x axis to the the vector $\vec{r}$. To begin with, fibers in the outer ring are first given perturbation followed consequently by the fibers in the inner rings. The perturbation is such that each fiber is allowed to pick a new position defined by δr and $\delta\theta$ as shown in Figure 2.4. It can be noted that the δr is a fraction of r , for instance $0.25r$ and so on and $\delta\theta$ is a predefined angular variation. For instance, a realization

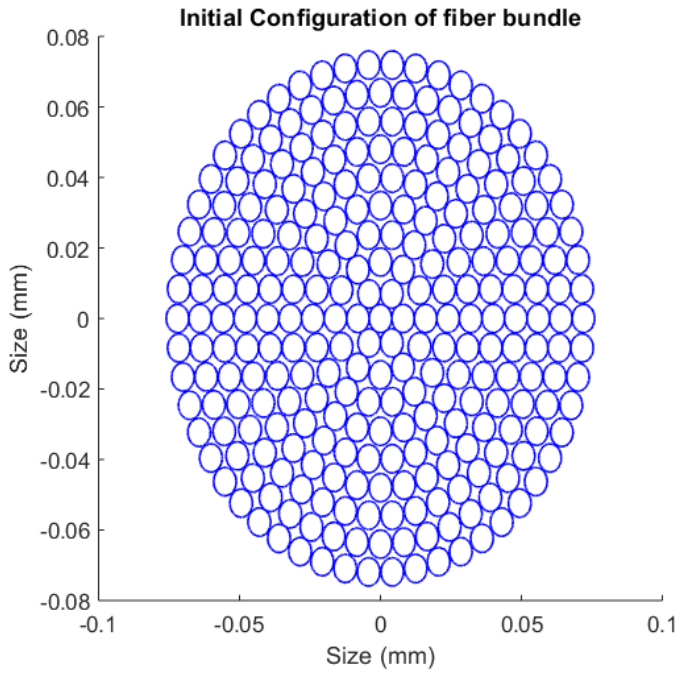

Figure 2.3: Initial Configuration of the Fiber Bundle

with $\delta r = 0.2r$ and $\delta\theta = 15^o$ corresponds to the realization where the new position of each fiber is defined by a random point in an area within a limit of $\pm 0.2r$ and $\pm 7.5^o$. The new position is picked based on uniform random distribution. This also ensures that the fibers on the outer rings get dispersed more than the fibers in the center of the bundle. Starting from the initial configuration in Figure 2.3, the entire process of generating the realization is shown in the Figure 2.5.

The new positions of the fibers are subjected to the following constraints:

- It should be any point within the predefined values of δr and $\delta\theta$.
- It is picked randomly by uniform random distribution.
- It should be such that it is not overlapping with any other fibers.

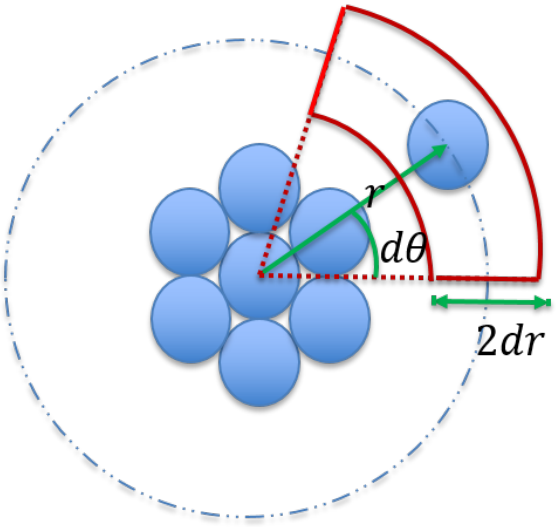

Figure 2.4: Schematic Representation Showing the Plausible New Location of the Fiber

The Figure 2.6 shows the realizations generated for varying radial mobility. The fiber numbers are also marked along with the realizations for comparison purposes. It is quite evident from the figures that the amount of clustering is more when the radial mobility is less.

2.3.2 Need for Statistical Analysis

Another key factor to consider is that for each radial mobility and angular mobility infinite realizations can be generated. Also, each realization will lead to different local stress fields in the matrix. Hence, it is important to consider multiple realizations of the RVE for the stress evaluations and consider the average. In a similar study conducted by Xiaoming et al[55] this minimum number of realizations is adopted as 10. The number of realizations under consideration depends on the standard deviation and variation of the dilatational and distortional strain energy densities and the cost of computation. In the current simulations, the Number of Realizations (NR) is considered 5 based on the standard deviation of the dilatational strain energy density, U_v from the mean U_v.

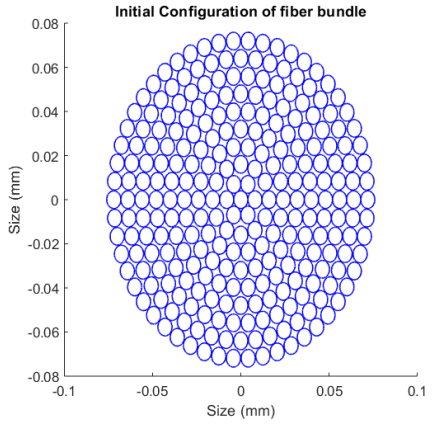

(a) Stage 1 : Initial Configuration

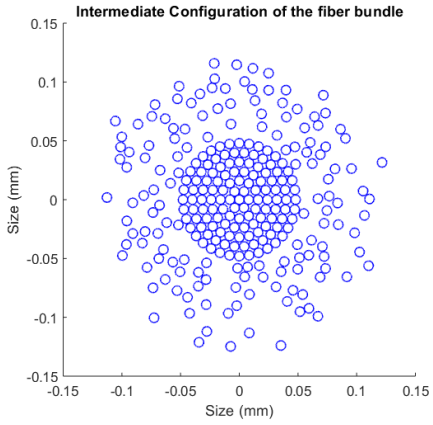

(b) Stage 2 : Next ring of fibers displaced

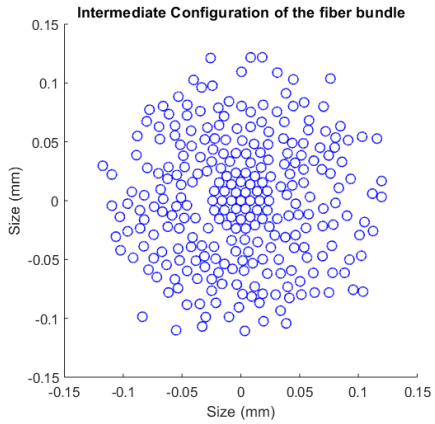

(c) Stage 3 : More rings of fibers displaced

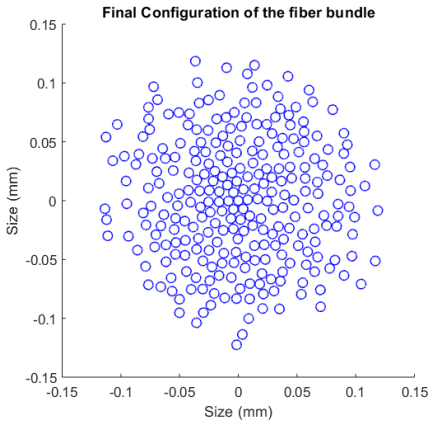

(d) Stage 4 : Final Configuration of the RVE

Figure 2.5: Stages in the Formation of the RVE: Starting from the Initial Configuration shown in Figure 2.3, the Consequent Stages of the Formation of RVE.

2.4 RVE Size

Once the methodology for construction of an RVE has been established, the next step would be to determine the size of the RVE so that it represents the statistical average of the entire composite. Several studies in the past were carried out to determine the size of RVE for average effective material properties. The size of the RVE varies for different cases. As mentioned earlier, the RVE for failure analysis is different from that for average property estimation. In a remarkable work by Pyrz et al[8], several point process is established an

quantified for generation of RVE. In the current analysis, the pair distribution function is utilized to determine the size of the RVE. As shown in Figure 2.8 the pair distribution function $g(r)$ corresponds to the probability $g(r)dr$ of finding an additional point within a circle of radius dr centered at r. It is mathematically represented as (see [8]):

$$g(r) = \frac{1}{2\pi r}\frac{dK(r)}{dr} \tag{2.3}$$

where $K(r)$ is second order intensity function. Figure 2.9shows typical $g(r)$ function for different distributions. Of these Cluster 1 and Cluster 3 are of importance to our analysis. As depicted in case if any cluster is present, then a peak in the $g(r)$ function can be found at that radial distance r. In equation 2.3, $K(r)$ is the additional number of fibers expected to lie within a circle of radius r divided by the density of fibers.

$K(r)$ corrected for edge effects is as follows:

$$K(r) = \frac{A}{N^2}\sum_{k=1}^{N}\frac{I_k(r)}{R_p} \tag{2.4}$$

where N is the number of points, $I_k(r)$ is the number of points in the circle of radius r and and R_p is the ratio of circumference of the circle in W to the entire circumference as shown in Figure 2.10. The quantity $g(r)$ quantifies the likelihood of occurrence of fiber at a particular distance. The peak in $g(r)$ plot indicates that more fibers are found at that nearest neighbor distance and a plateau indicates that the number of fibers remain same for that range of distance as shown in Figure 2.9.

The size of the RVE is measured using the parameter NOR, which is the number of rings around the central fiber in the realization. For instance, in Figure 2.3 NOR is 9. The pair correlation function, $g(r)$ was plotted for different NOR values and it was observed that for N greater than or equal to 9 the $g(r)$ function stabilizes.

Figure 2.11 and Figure 2.12 show the $g(r)$ function plotted for NOR=5 and NOR=9. It can be observed that for NOR=9, the $g(r)$ function reaches nearly stable state. This indicates that beyond N=9 the effect of adding more fibers is statistically insignificant. Thus N=9 is adopted as the size of RVE for further analysis.

2.5 Void Distribution

When resin is infused in the RVE, other than irregular distribution of fiber, voids are also likely to be trapped in between the fibers and also between the fiber bundles. The voids that are trapped inside the fiber bundle are of relatively smaller dimensions and are referred to as micro-voids. The voids that are trapped between fiber bundles or layers of the composite are called as macro-voids[56]. The Figure 2.13 demonstrates the types of voids trapped in a composite. In the current study, micro-voids are relevant to the problem and are taken into consideration. Following are the assumptions made in generating void distribution in the RVE:

- The voids are distributed on the pre-existing RVE for which the stress analysis has been carried out.
- To begin with, the voids are assumed to be circular in cross-section and are distributed randomly in the RVE.
- The voids are distributed in such a way that they occupy space between the fibers in the matrix medium
- The algorithm created takes care that the voids do not overlap with other voids or fibers.

Figure 2.14 shows a typical distribution of the RVE with voids. A statistical analysis on the effect of void volume fraction and void size on damage initiation is also carried out.

2.6 Section Summary

The main intend of this chapter was to introduce the concept of RVE, the need for the same in failure analysis. Since no manufacturing process would yield a perfect distribution of fiber devoid of voids or any inclusion, the RVEs are the smallest unit adopted to capture the local stress fields. We also discussed the corresponding boundary conditions required for an RVE. To compare, we introduce the difference between RVE and RUC, the primary analysis units of micro scale analysis. The required boundary conditions for each have been identified.

The primary focus on generating the RVE is to be able to capture the local stress state accurately. Hence, we identified and proposed a novel methodology for RVE generation which is capable of capturing the local stress field resulting from the manufacturing process. The manufacturing process of concern is resin infusion and the corresponding defects are irregular fiber distribution and presence of voids. The methodology adopted aids in creating multiple realizations of the RVE which can be parametrized by the mobilities of the fibers- radial and angular mobilities. At-least 5 realizations each for the radial and angular mobilities are adopted in the current studies.

The size of the RVE depends on the behavior we are interested in. The size of the RVE is governed by the inter-fiber distance. This is different from the size determined by Hill's criteria for average properties. In case of any average properties, Hill's average criteria for determining the size of the RVE holds true. On the other hand for behavior that involves the understanding of the local fields, especially for failure mechanisms, the RVE size cannot be determined by averaging principles. In the current study since the size depends on the local stress fields, which in-turn depends on the microstruture we resort to the concept of statistical descriptors that utilize the inter fiber distance as the criteria for size determination of the RVE. The current study utilizes the radial distribution function

and second order intensity function for the size determination.We showcase the need for statistical descriptors and utilize them for determining the minimum size of the RVE. The size of the RVE is identified based on NOR as discussed in this chapter. NOR in this study is 9.

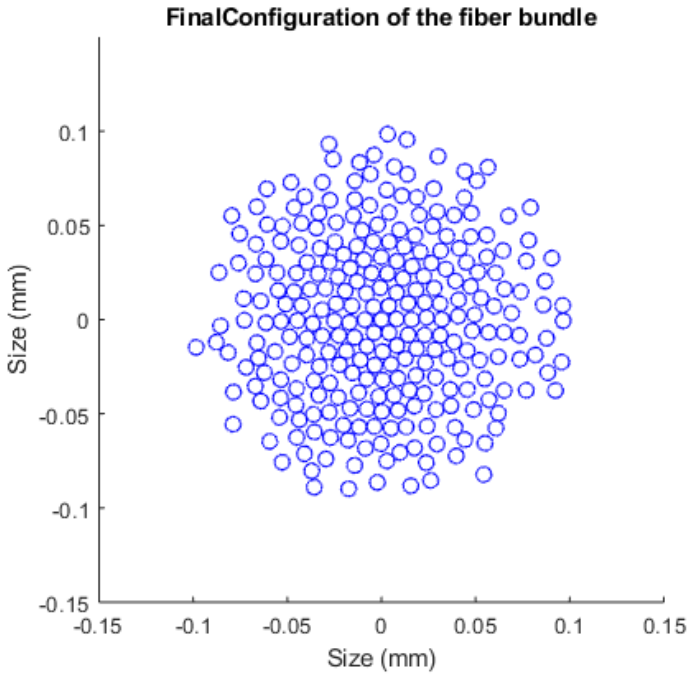

(a) RVE Construction: δ R =0.1

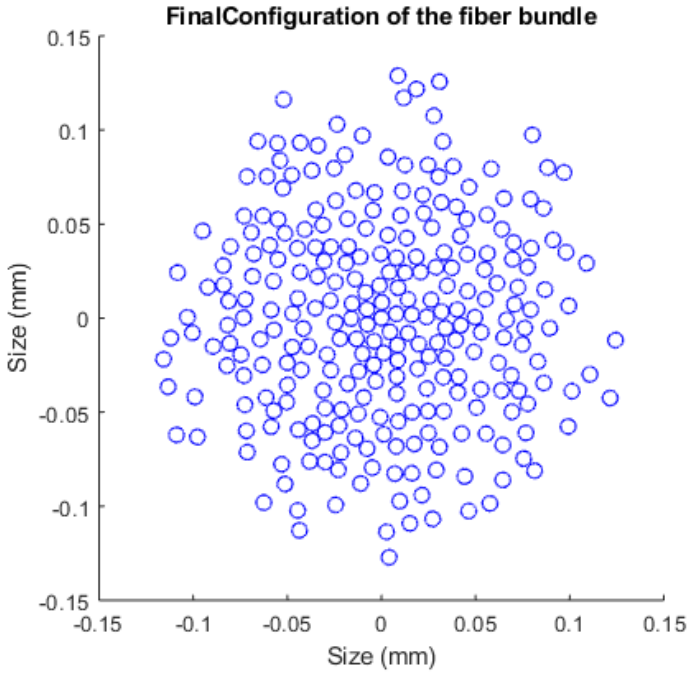

(b) RVE Construction: δ R =0.4

Figure 2.6: RVE Construction: A Comparison with Different Radial Mobility

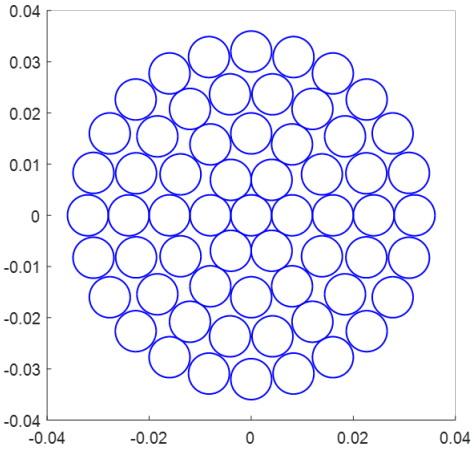

Number of fiber rings around the center fiber → NOR

In figure NOR=4 (for illustration)

Figure 2.7: RVE Size Illustration : NOR

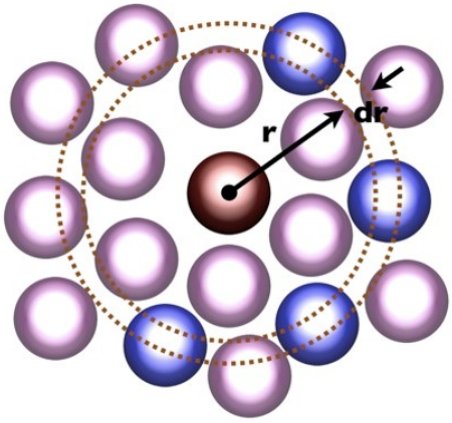

Figure 2.8: Radial Distribution Function Calculation

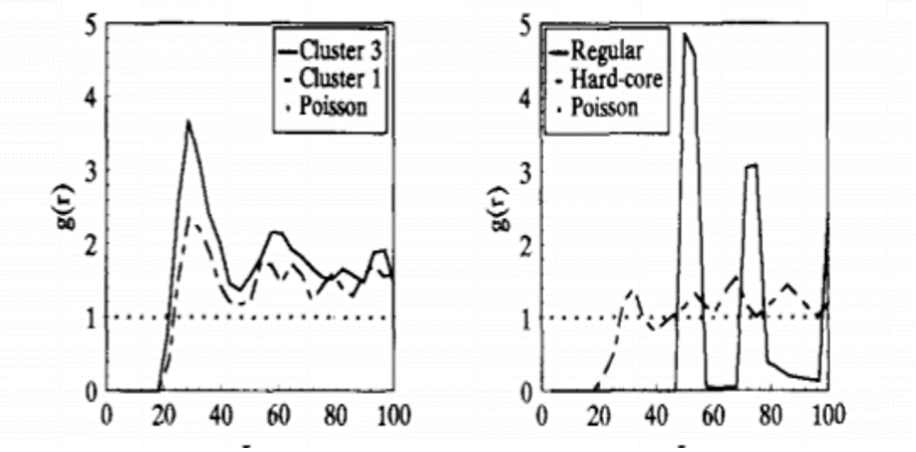

Figure 2.9: Radial Distribution Function Reprinted from [8]

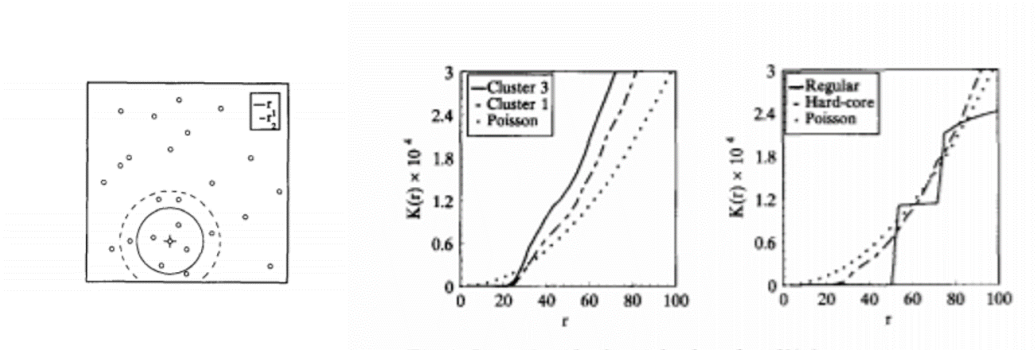

Figure 2.10: Typical K(r) Function Reprinted from [8]

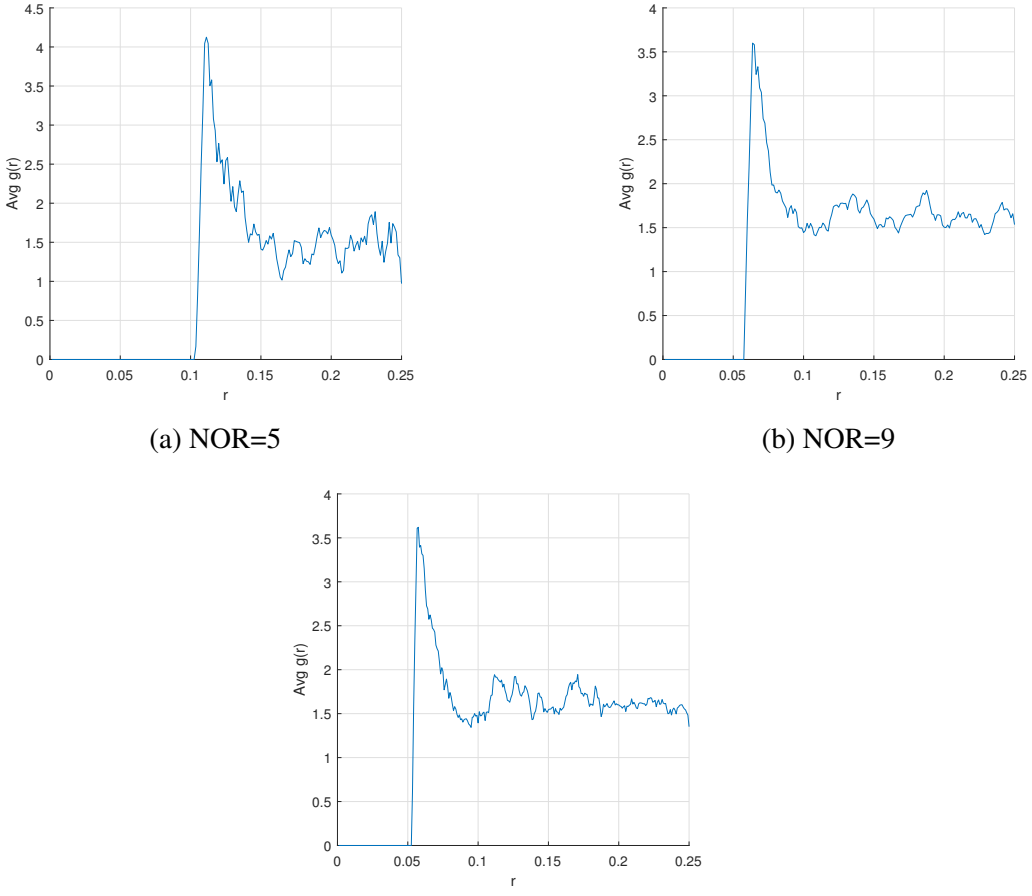

(a) NOR=5

(b) NOR=9

(c) NOR=10

Figure 2.11: Statistical descriptor - Radial Distribution Function $g(r)$ for 3 Values of NOR for Fiber Rings in the Bundle.(a) NOR=5 and (b) NOR=9 (c) NOR=10.

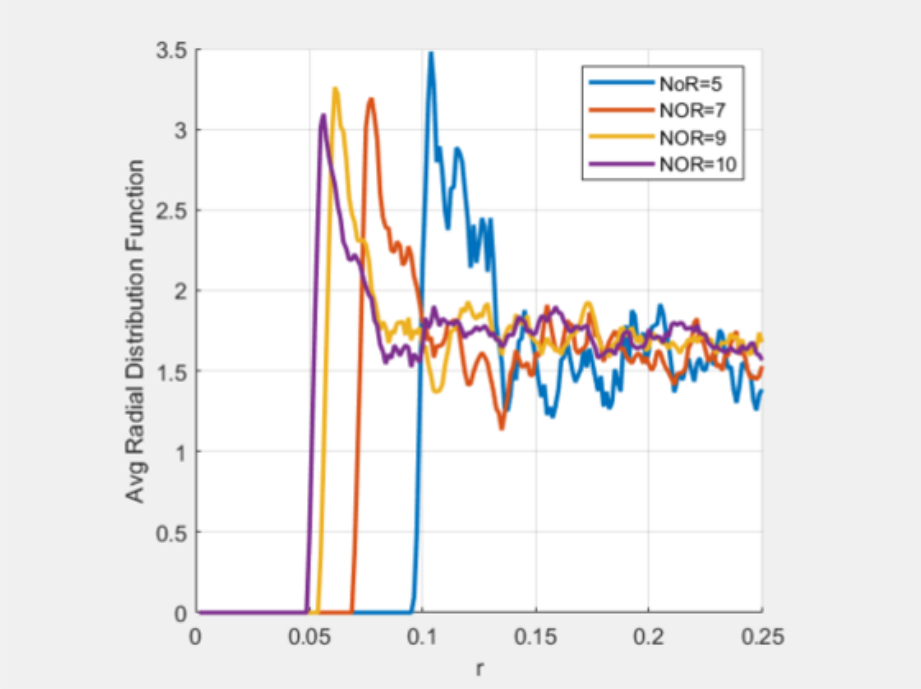

Figure 2.12: Radial Distribution Function

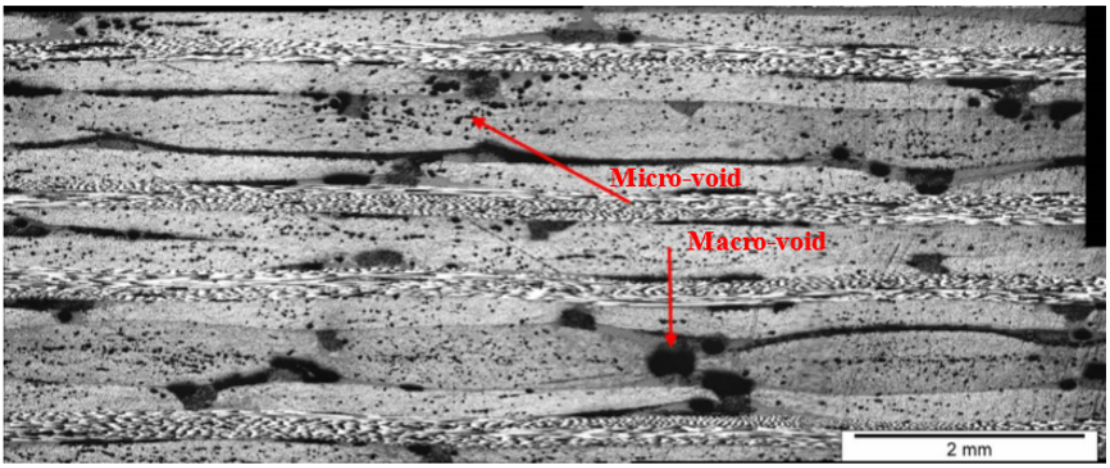

Figure 2.13: Types of Voids : Micro Voids and and Macro Voids Adapted from [9]

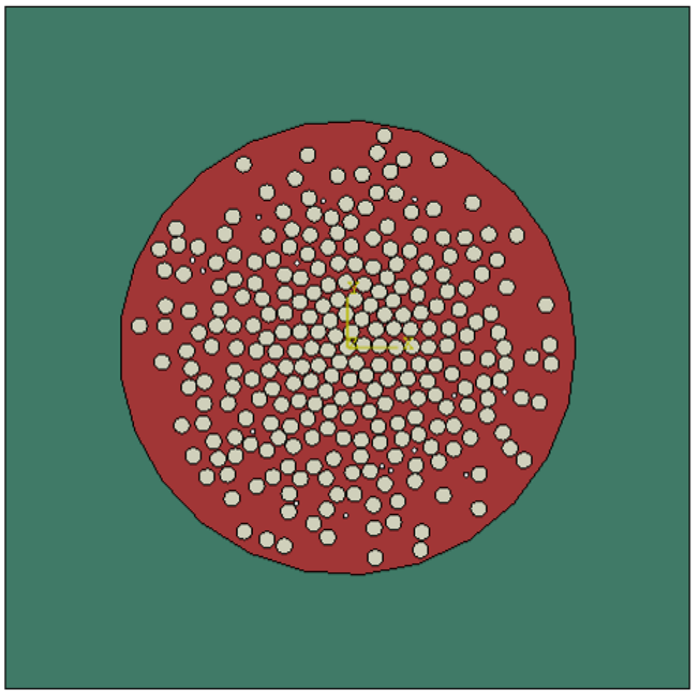

Figure 2.14: RVE with Void Distribution

3. DAMAGE INITIATION CRITERIA

The current composite literature is filled with a number of failure theories for the material. Some of the early theories has been discussed briefly in Chapter 1. Some of the remedies to the current failure theories based on [5] has also been described briefly in the same section. In the current chapter we introduce, the main failure modes in the PMCs under transverse load. As shown in Figure 3.1, when a fiber distribution is subjected

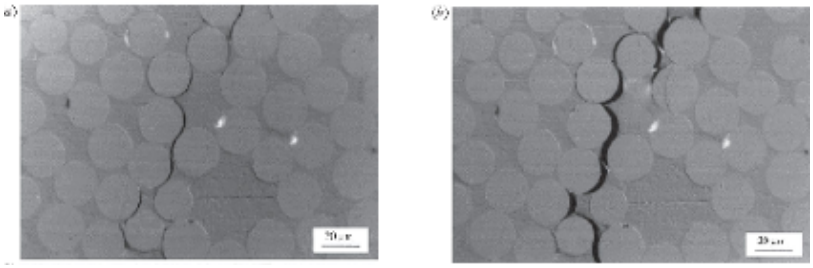

(a) (b)

Figure 3.1: Transverse Crack Formation(a) Fiber matrix debonding (b) Debonds coalesce to crack Reprinted from [4]

to transverse load, failure appears to occur from unstable growth of smaller cracks at the fiber matrix interface. However, there is no single failure initiation mechanism which can be captured at macro length scale based on any of the early failure theories mentioned in Chapter 1. These cracks are shown in Figure 3.1 taken from [4]. If we look closely on the crack as shown in Figure 3.2 it can be observed clearly that the transverse crack is formed from the coalescence of multiple debonds. There are two possible likely precursors to this event.

1. The debonds occur first and then grow into the matrix and the coalescence cause the transverse crack

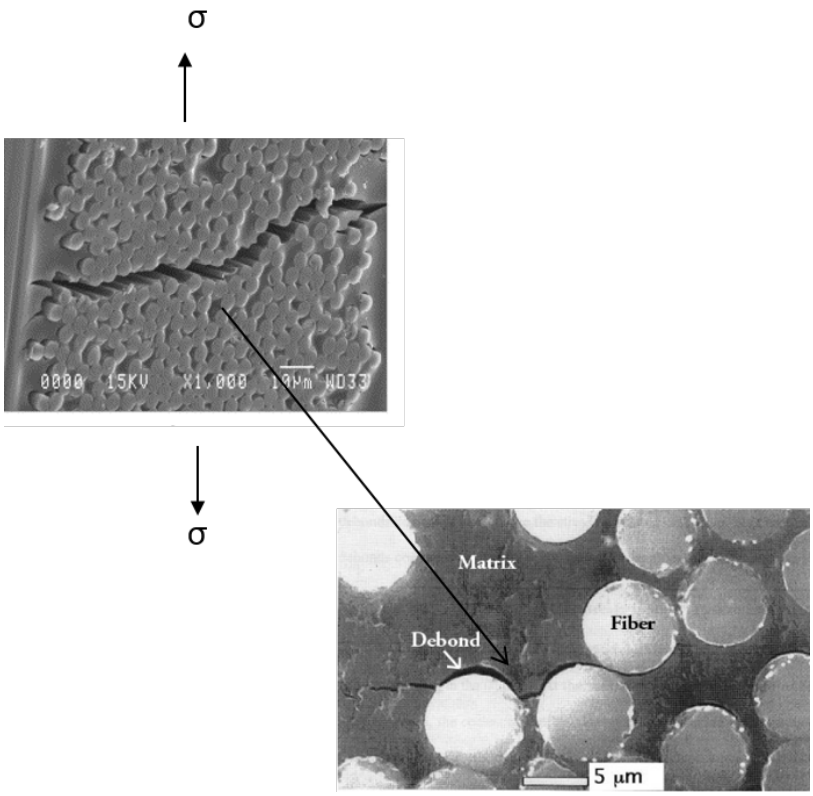

Figure 3.2: Transverse Crack from Coalescence of Debonds Reprinted from [4] Based on [6]

2. The matrix cracks first and then grow into the debonds and coalesce to form transverse crack.

These two likely mechanisms are shown in Figure 3.3.

In a remarkable work by Asp et al [34], two likely mechanisms for failure initiation is pointed out. These mechanisms are fiber/matrix debonding and matrix failure. The mechanism by which the failure initiates depends on the local triaxial stress state. By systematically analyzing the stress state, Asp st al [34] showed that local stress state in a transversely loaded UD composite is as shown in Figure 3.4. The study was conducted for varying the volume fraction and fiber packages. It was observed then that the energy

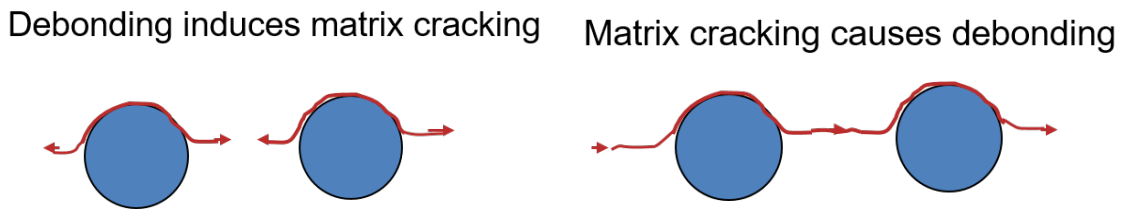

(a) Debonds occurring first and growing into the matrix

(b) Matrix cracking occurs first and grow into the interface

Figure 3.3: Likely Precursors for Coalescence of Debonds Reprinted from [5]

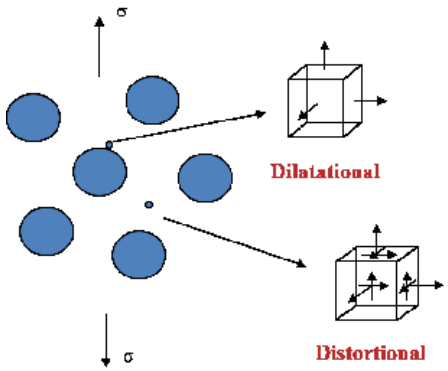

Figure 3.4: Stress State in Different Locations of Composite Reprinted from [5]

density for dilatation was lower than the distortion energy density. Also, the location where these two energy densities reached critical values were based on the stress state as shown in Figure 3.4. The dilational energy density reached critical value close to the fiber matrix interface.

As shown in Figure 3.5, it was observed that there existed points close to the fiber matrix interface, where equi-triaxial stress state existed. When these points experienced stress state such that the dilatational strain energy reached critical value, these points were subjected to point failure by phenomenon called crazing in matrix. This was called cavitation induced brittle failure in glassy polymers and verified for 3 different epoxies[35, 57].The

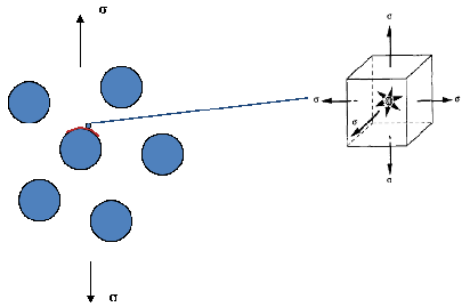

Figure 3.5: Location of Dilatation Driven Damage Initiation Reprinted from [5].

main contributor to the hydrostatic stress state is the microstructure distribution and thermal residual stress. Thermal stresses are created in the matrix during the heating and curing operations. This depends on the rate of heating and cooling as well. This behavior results from differing coefficients of thermal expansion (CTE). Often, the matrix has a greater CTE than do the fiber[58]. This resultant residual stress in the matrix leads to a phenomenon called crazing, which leads to micro-crack and eventually leads to delamination.

In another significant work done at the molecular level by Neagi et al[59], it is been verified that under equi-triaxial stress state, polymers like epoxy tend to formation of the cavities. It was also observed that these cavities tend to grow in size as large as 50% by volume within the epoxy. This finding reinforces the formation of cavity and formation of crack from the cavities when critical strain energy density is reached.

Having explained the possible failure modes in UD composites, lets now look closely at these modes and the likeliness of the mode to reach criticality. As shown in the schematic in Figure 3.6, the two energy densities result in two different mechanisms of failure initiation in the matrix.

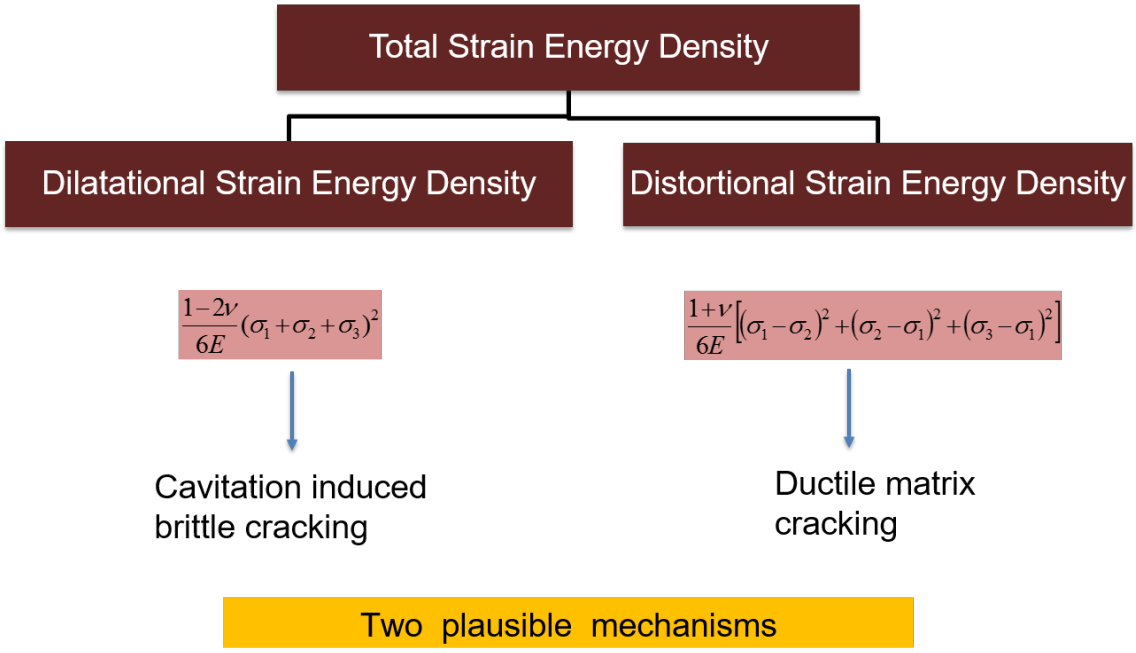

Figure 3.6: Energy Based Damage Initiation Criteria

3.1 Cavitation Induced Brittle Failure:

The criteria for the cavity formation from crazing depends on the local stress state. It is possible only if the local stress state is hydrostatic or nearly hydrostatic (within a tolerance of 20%) and the strain energy density at that point is failure is greater than or equal to the critical strain energy density ((U_v)). In that case, the distortion energy vanishes. This ensures that there is no yielding and the material is under elastic regime. The polymer chains at the point is subjected to equal forces as shown in Figure 3.5. This results in the formation of a cavity which bursts open when the energy is enough to break the polymer chains. This energy is the density is equal to the (U_v). This point failure occurs close to the fiber/matrix in the matrix and results in the fiber/matrix debonding.

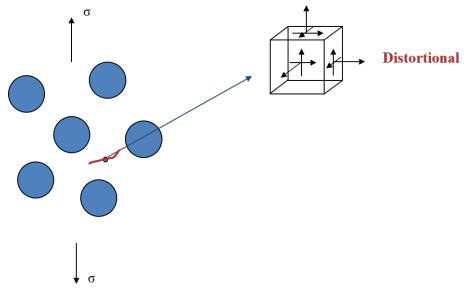

Figure 3.7: Location of Distortion Driven Damage Initiation Reprinted from [5].

3.2 Ductile Matrix Failure:

The criteria for this mechanism is that the material should yield when the criticality for distortional energy is reached. This condition occurs at resin rich areas of a composite. As a result the stress state in the matrix tends to the applied far field stress. This is because the interference from fibers are minimal in those regions. The studies conducted by Asp et al[57, 35, 34] and in the current study, it is observed that the stress state becomes more tri-axial close to the fibers in the matrix rich region under transverse loading. It was confirmed by the studies conducted by Asp. et al [57, 35, 34] that the yielding behavior of epoxies were driven bu the energy of distortion.

Cavitation Induced Brittle Matrix Failure	**Ductile Matrix failure**
Equi-triaxial stress state (tension)	stress state close to applied far field stress
Strain energy density $\geq$ Critical dilatational strain energy density (U_v^{crit})	strain energy density $\geq$ Critical distortional strain energy density (von Mises equivivalent)
location: In matrix close to fiber/matrix interface	location: In matrix rich areas

Table 3.1: Comparison of the Criteria for the Energy Density Driven Failure Initiation

The criteria for the failure initiation from the two mechanism is summarized in Table 3.1.

3.3 Governing Failure Mechanism

Having the knowledge of the two possible failure mechanisms, it is now evident that the driving mechanism is that which reaches the criticality first. There are also a number of theories in literature which states, that the first event of failure is the fiber/matrix debonding. In the case, when the fiber is perfectly bonded to the matrix, fiber/matrix failure initiates when the bond breaks. In that case the bond strength would determine the critical stress. On the other hand all composites inevitably are manufactured with flaws, in which case the failure must be evaluated by energy criterion. The interface properties are hard to determine experimentally and hence faces difficulties due to uncertainties.

We shall follow Asp et al [34] who showed that cavitation-induced brittle failure occurs when the dilatational strain energy density (U_v) at a point reaches a critical value (U_v^{crit}) for the matrix polymer. This component of the strain energy density for linear elastic material is given by,

$$U_v = \frac{1-2\nu}{6E}(\sigma_1+\sigma_2+\sigma_3)^2 \tag{3.1}$$

where σ_1, σ_2 and σ_3 are principal stresses and ν and E are the Poisson's Ratio and Young' Modulus of the material. Based on Asp et al [34], a likely location for the cavitation criterion to be satisfied in a nonuniform configuration of fibers is illustrated in Figure 3.4. Also shown in Figure 3.4 is a likely location of a point in the matrix where the distortional energy density can reach its critical value. This location will then yield if the von Mises criterion holds.

$$U_d = \frac{1+\nu}{6E}[(\sigma_1-\sigma_2)^2+(\sigma_2-\sigma_3)^2+(\sigma_3-\sigma_1)^2)] \tag{3.2}$$

These two energy densities have separate critical values which are obtained experimentally. Once these critical values are exceeded it leads to two different mechanisms of damage initiation based on the energy states. It was shown that when the stress state at a point becomes equi-triaxial and the dilatation energy exceeds the critical value (U_v^{crit}), then cavitation occurs in PMCs. Under this stress state, the distortional strain energy vanishes. Then, an elastic material will not yield but behave in a perfectly brittle manner. As shown in Figure 3.5, this cavitation occurs at a point close to a fiber surface. On the other hand in matrix rich areas, the matrix tends to yield under uniaxial tensile stress. This results in ductile material failure. In a nutshell, when subjected to transverse tension, these two failure initiation modes will compete and failure initiates according to the mode which occurs first[35].

The consequence of cavitation is illustrated in Figure 3.5, which shows a fiber-matrix disbond crack formed when the cavity close to the interface grows unstably. This is likely to occur when the dilatational energy density is produced by hydrostatic tension, in which case, the distortional energy density vanishes, leading to brittle conditions for cavitation. The energy released by unstable cavity growth is then likely to be available for debonding of the interface. As suggested in [35], under transverse tension of a unidirectional composite, two competing mechanisms, viz., fiber-matrix debonding and matrix yielding exist. Crack formation from yielding at a point is, however, a tedious process involving shear banding and ductile cavitation, which requires much higher energy than what goes in the brittle cracking of the fiber-matrix interface.

3.4 Illustration

The systematic study by Asp et al[34], shows the variation of dilatation and distortional energy density for uniform distribution of fibers in matrix. For illustration, we are reproducing the results from Bulsara et al[10]. As shown in Figure 3.8, a RVE with fiber

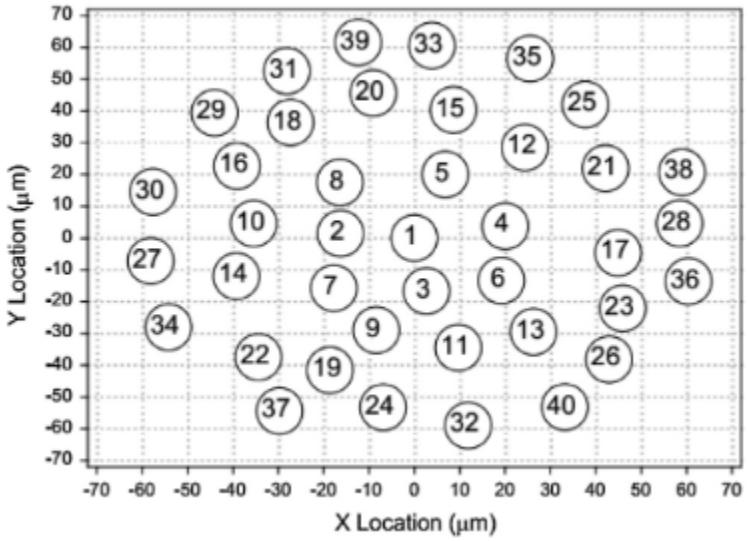

Figure 3.8: Representative Cross Section of UD Composite Reprinted from [10]

distribution reproduced from the image of an actual composite is adopted. This RVE is subjected to the a thermal cool down of 82 ° and a uniaxial transverse displacement. The properties were adopted from that of Asp et al[34].

The Figure 3.9b shows that for the fiber distribution shown in Figure 3.8 the dilatational energy density is always higher than the distortional energy density. Also, Figure 3.9a shows that corresponding to point of max dilatational energy density, there exists points where the ratios of principal stresses are nearly equal. These two are the critical criteria for cavitation induced failure initiation as predicted and proposed by Asp et al[34].

3.5 Section Summary

This chapter deals with a failure analysis mechanism proposed by Asp et al[34]. In PMCs, this mechanism is proven to capture the first event of failure. The theory proposes two mechanisms driven by the local stress state and energy in the matrix. These two mechanisms compete with each other and the one that reaches criticality initially is the driving

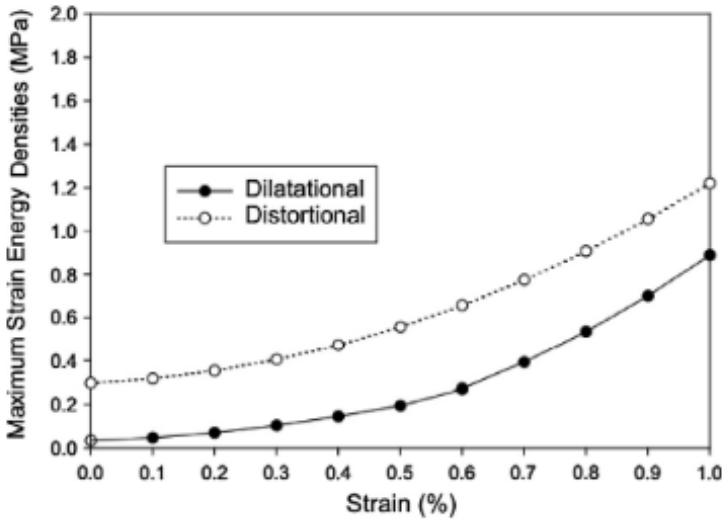

(a) Maximum Value of Energy Density

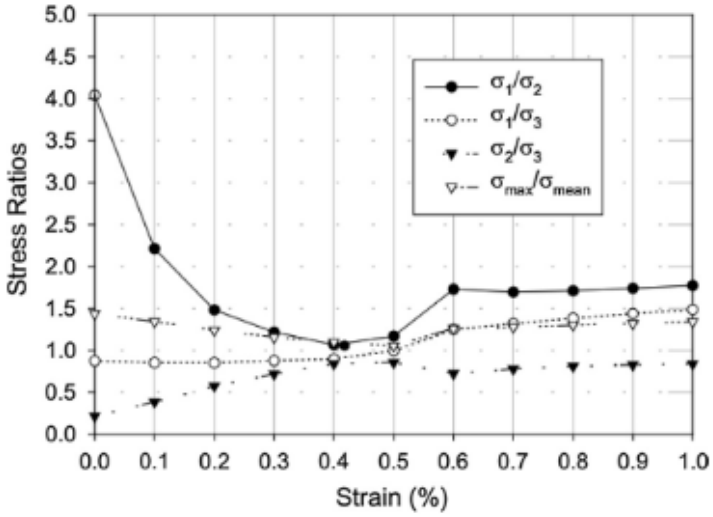

(b) Principal Stress Ratio

Figure 3.9: Principal Stress Ratio and Maximum Energy Density Plotted for the Fiber Distribution shown in Figure 3.8 Reprinted from [10]

mechanism for failure initiation. The critical values for damage initiation based on both energy densities has been determined experimentally.

4. ANALYSIS OF INITIAL FAILURE

4.1 Model Assembly

The local stress fields in the modeling of transverse sections of a unidirectional composite material were determined using the finite element method (FEM). Two dimensional models of the transverse sections were analyzed with the generalized plane strain assumption. The model geometry and finite element mesh were created in Abaqus CAE using python scripting interface and was analyzed with the Abaqus FEA. FORTRAN subroutines were written to extract the relevant stresses and the energy densities from the Abaqus data files.

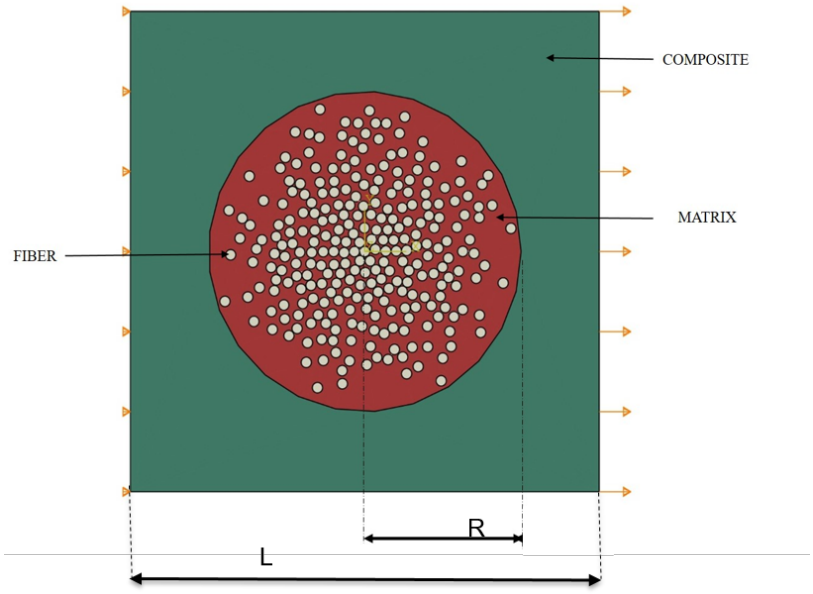

Figure 4.1: Boundary Conditions on the Embedded RVE.

Table 4.1: Properties of the Constituents of the Composite

Material	Young's Modulus (GPa)	Poisson's Ratio	Thermal Expansion Coefficient(10^{-6})
E-Glass	72	0.2	5
DGEBA/DETA	2.07	0.345	66

The RVE generated in a realization is a statistical representation of the fiber distribution in the . Hence, a minimum of 5 realizations were generated and the average of these were taken to determine the damage initiation. The failure initiation sites in a RVE are determined by applying the dilatational energy density criterion for cavitation-induced cracking and the von Mises criterion for yielding. The realizations were generated for each case of varying δr and $\delta\theta$. The properties of the resin and fiber used in the current analysis are tabulated in Table 4.1. The fiber diameter is $8\mu m$. The realizations were analyzed to determine the first failure event.

4.1.1 Mesh Convergence Study

Mesh convergence study was first carried out on the model assembly to ensure the accuracy of the numerical results. The Figure 4.2 shows mesh convergence study for Dilatational Strain Energy Density. The error in U_d is also plotted to ensure the convergence of the criteria. As the mesh density increases, the U_d converges and the mesh density of 150 is adopted in the current study.

4.1.2 Size of Embedding Composite Layer

The size of the embedding composite region was determined by Hill's criterion that uniform displacement at the boundary should yield uniform traction at the same boundary. Based on this, different sizes of the embedding composite layer were chosen and traction

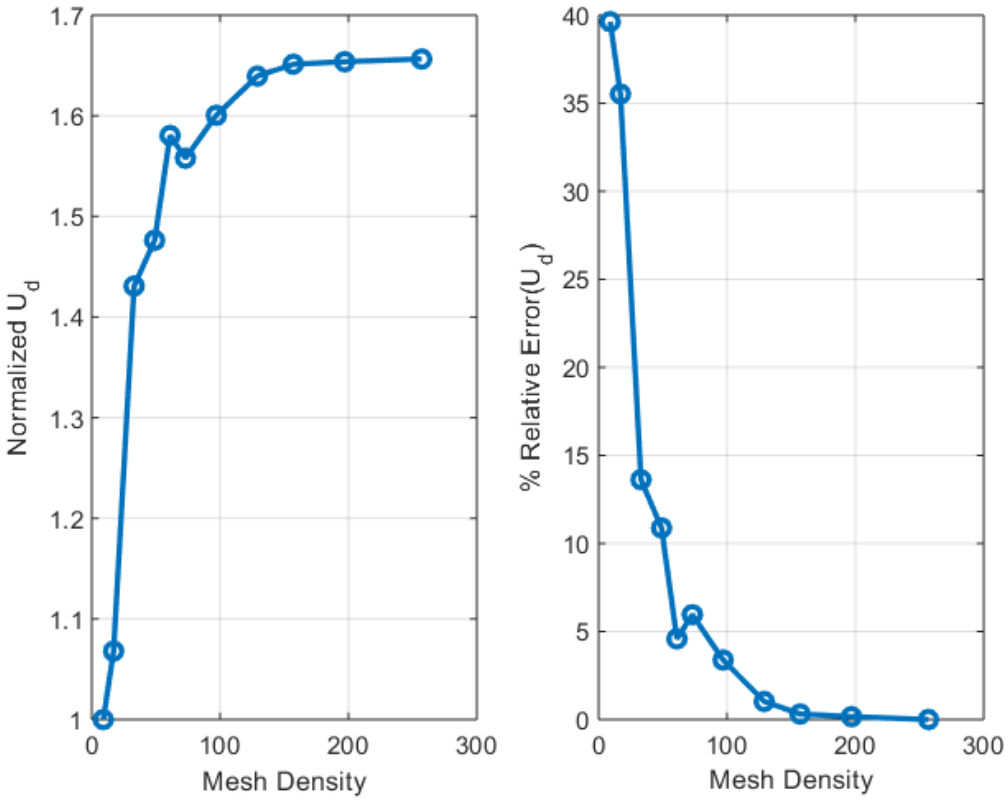

Figure 4.2: Mesh Convergence for U_d.

at the boundary where displacement was applied was monitored. The results are as shown in Figure 4.3. In the further analysis the size of the model assembly, L, was taken to be $5R$.

4.2 Numerical Analysis

4.2.1 FEA: Validation of the Model

Before looking at the damage initiation in RVEs generated, as a preliminary validation, the developed model is validated by replicating the results from a previous study conducted Bulsara et al[10]. The RVE in this study is from the microscopy image. The exact fiber distribution and material properties are adopted from [10]. The realization with the boundary

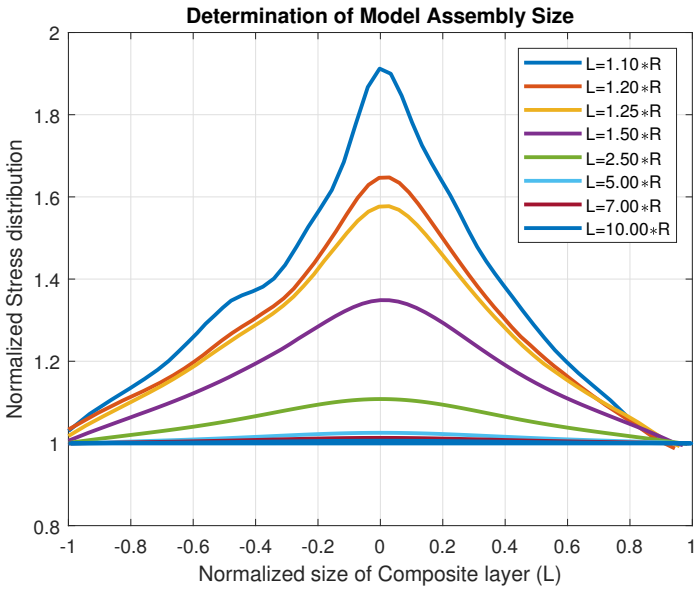

Figure 4.3: Effect of Embedding Composite Layer on the Traction Along the Boundary.

conditions are as shown in Figure 4.4. The model is analyzed in Abaqus with generalized plane strain elements. The max dilatation and distortional strain energy densities are monitored. Along side, the ratios of the max principal stress ratios are also monitored.

The results obtained as shown in Figure 4.5 and Figure 4.6 are identical to the ones predicted by Bulsara. This ensure, the validity of the model and enhances the confidence of the current model to implemented on the new microstructure.

4.2.2 FEA : RVE Analysis

As shown by Asp et Al[34], it is observed that the first event of failure is by cavitation. This failure event reaches criticality much earlier than the distortional driven damage initiation. Hence, the material undergoes brittle failure. For the purpose of explaining a realization with $\delta r = 0.10r$ and $\delta\theta = 15^o$ is taken. This RVE is subjected to thermo-mechanical loading and boundary conditions as discussed earlier. Once the simulations

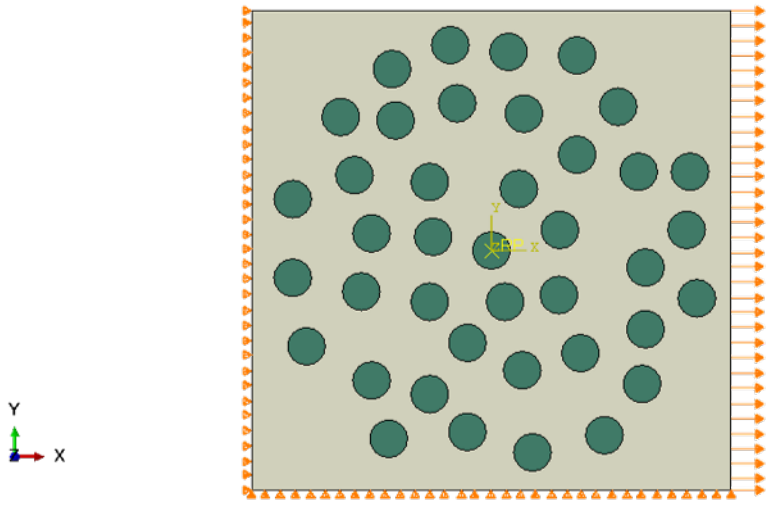

Figure 4.4: RVE with Non Uniform Fiber Distribution and Boundary conditions Adapted from [10]

are carried out in Abaqus FEA software, the stresses at nodes are extracted. The principal stresses, dilatational and distortional strain energy densities are evaluated at the nodes from these stresses. These nodal values are evaluated for increasing applied strain.

As shown in Figure 4.8, there exist points in the RVE which experience nearly equi-triaxial stress state at the applied strain $\geq 0.30\%$. At lower strain values, none of the nodes satisfy condition of nearly hydrostatic stress and hence the plot of principal stress ratios are not valid for lower strains. A 20% tolerance from perfectly hydrostatic stress state is given to the principal stress ratios for a practical implementation of the method. At each strain value the nodes, which satisfy the condition of equi-triaxial principal stress ratio are monitored and from which the node with max dilatational strain energy density is plotted on Figure 4.7a.

A previous work by Asp et al [35] conducted the poker chip test for epoxy polymers and it was observed that the critical dilatational strain energy density for DEBTA resin was 0.17MPa. As shown in Figure 4.8 and Figure 4.7a, at a strain of nearly 0.3% the

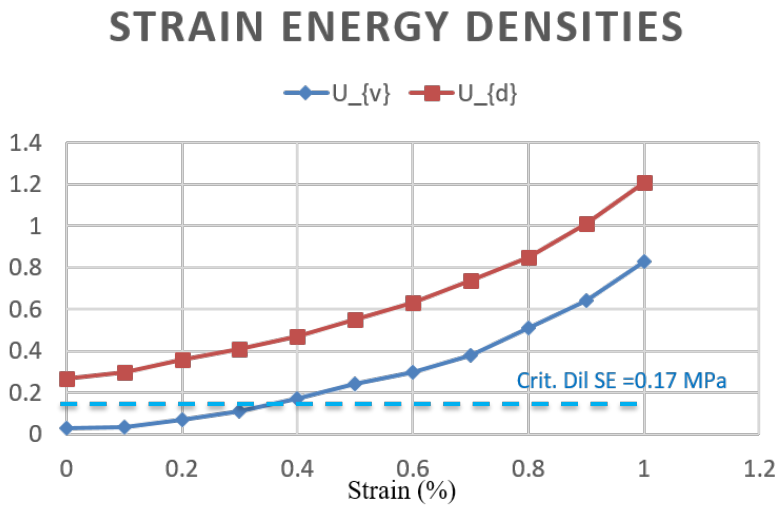

Figure 4.5: Validation: Strain Energy Densities

dilatational strain energy exceeded the critical value of 0.17MPa. Thus the condition for dilatation induced cavitation exists. On the other hand failure by distortional strain energy density initiates at strain of 0.60% applied strain.

Upon investigation of the location for points of cavitation, it is observed that it occurs close to interface between fiber and matrix. It is also observed that there exists multiple 'hot spots'for cavitation and the number of hot spots increases upon increasing the strain. Figure 4.10 shows the locations of cavitations at strain of 0.3%.The same realizations were also analyzed for damage initiation in the presence of micro-voids. The effect of void size on damage initiation was also carried out. The voids distribution was generated using the same algorithm where the voids were added to the existing fiber distribution.

4.2.2.1 Effect of Residual Stress from Thermal Cool-down

PMCs are usually subjected to a thermal cooldown of $\tilde{}$(100-200), which would result in residual stresses in the composite due do difference in thermal expansion coefficients of the constituents. The effect of residual stresses are monitored for both dilatation and

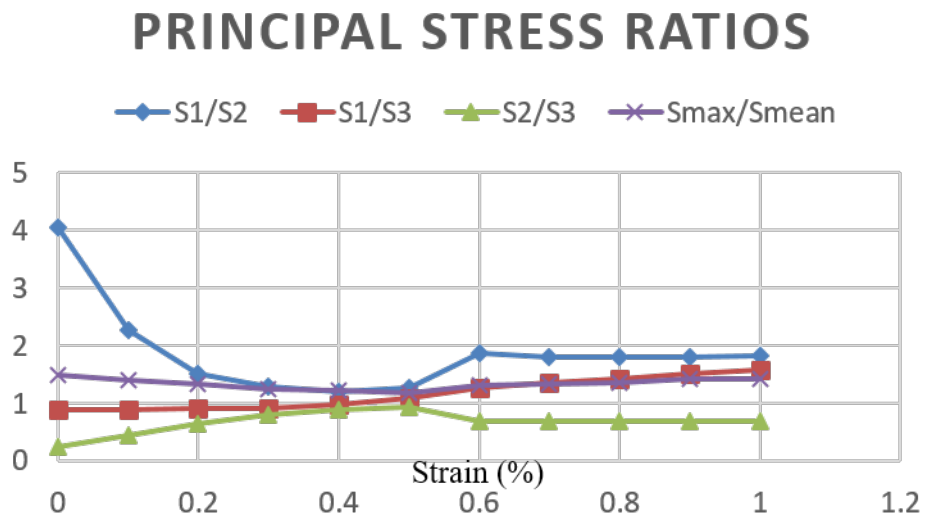

Figure 4.6: Validation: Ratios of Principal Stresses

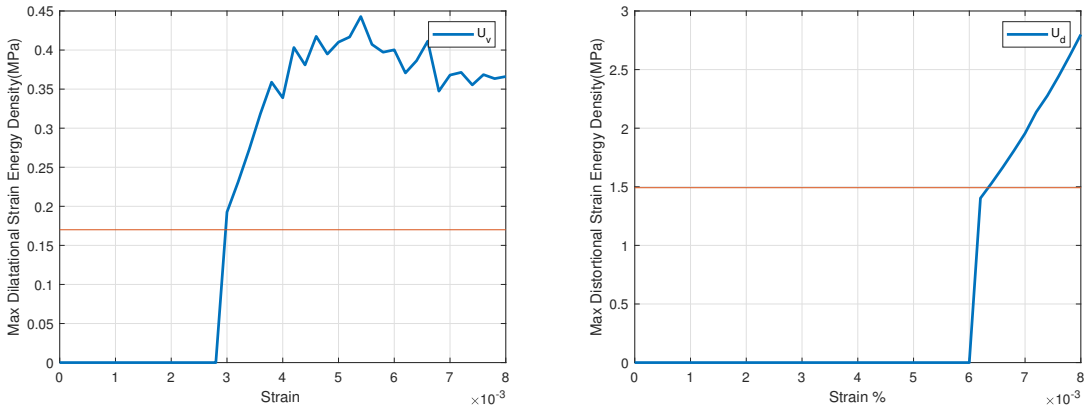

(a) Max Dilatational Strain Energy Density (b) Max Distortional Strain Energy Density.

Figure 4.7: Strain Energy Densities Above the Critical Values

distortion driven damage initiation for varying radial mobility($\delta R = 0.1$ to$\delta R = 0.5$)4.14. It can be observed that for both for both radial mobilities, the dilatation driven damage is more critical than distortional damage criterion for a thermal cooldown of 80-200, with the most critical δT 80. Hence in the current simulations, δT is 82.

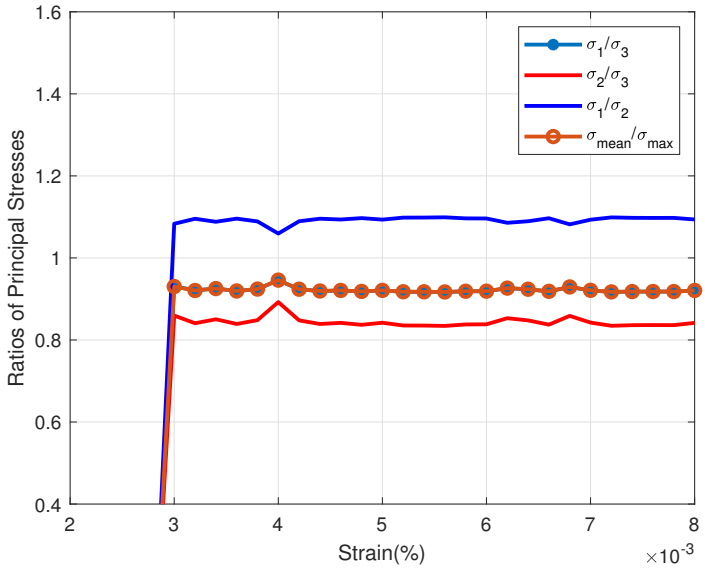

Figure 4.8: Ratio of Principal Stresses in the RVE Corresponding to Point of Maximum Dilatational Strain Energy Density

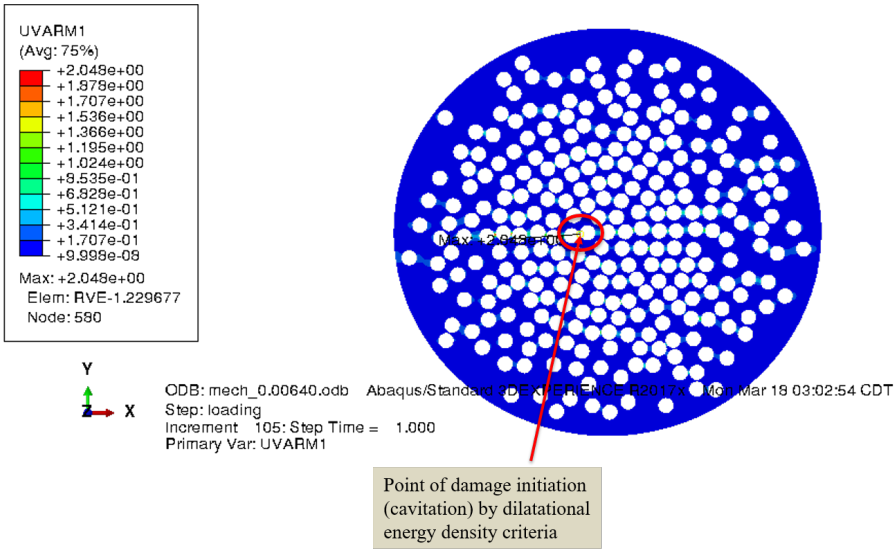

Figure 4.9: Location of Damage Initiation: FEA

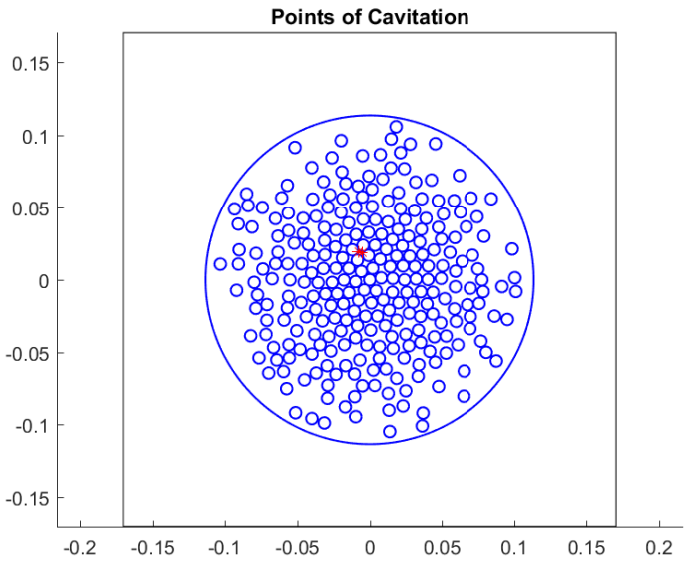

Figure 4.10: Plot Showing Cavitation at Strain=0.4%.

4.2.2.2 Effect of Embedding composite layer

Another key observation is with respect to the stiffness properties of the embedding composite layer. A study is conducted where the homogeneous embedding layer has properties varying from matrix properties to the composite in the initial configuration. The Figure4.13 shows the effect of the embedding composite layer on cavitation in a realization with non uniform distribution of fibers. As the embedding layer has properties close to that of matrix, cavitation due to dilatation becomes less critical. On the other hand, if the RVE is embedded in a composite layer with properties close to that of pristine composite, then the cavitation becomes more critical. Hence, cavitation induced by the presence of localized non uniformity is more critical when the volume fraction of the composite is high. In addition. it is also observed that the number of points of cavitation also increases with the increase in embedding composite stiffness. In further analysis, the embedding

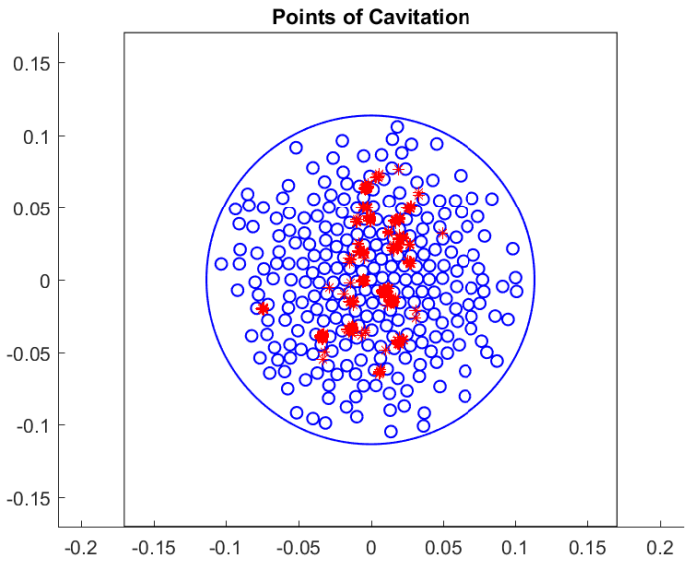

Figure 4.11: Location of Cavitation in RVE at Strain=0.44%.

composite is given the property corresponding to the RVE.

4.2.2.3 Effect of Constituents

The ratio of the stiffness of the fiber to matrix also affects the local stress state in the matrix. For a given epoxy material the damage initiation by dilation driven damage criteria is plotted for varying stiffness of the fiber. It is interesting to note that beyond a particular value the increase in stiffness of the fiber does not affect the failure initiation.

4.2.2.4 Effect of Radial and Angular Mobilities

The FE analysis was carried out for 5 realizations each for varying δr and $\delta\theta$ find the mechanism and location of the damage initiation. The Table4.15 shows the strain to failure initiation by both dilatational and distortional damage initiation criteria. It can be seen that the dilatational failure initiates at lower strain than the distortional failure strain.

Parametric study on damage initiation by cavitation for varying radial mobility are

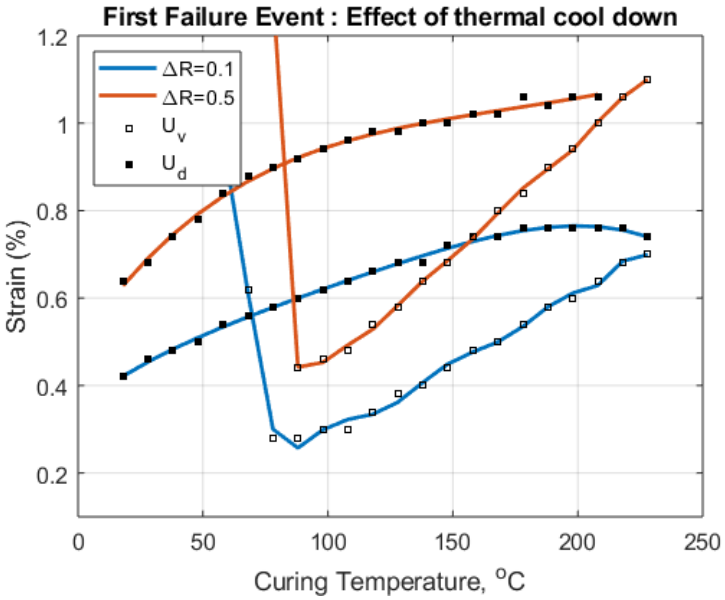

Figure 4.12: Effect of Thermal Cool-down on Residual Stress and it's Effect on Failure Initiation by Dilatational and Distortional Strain Energy Densities

Table 4.2: FE Results for $\delta\theta$ Variation at δR = 0.5R.

$\delta\theta$	Strain Range for Cavitation (%)
5	0.42-0.46
10	0.42-0.48
15	0.44-0.46
20	0.42-0.46

shown in Figure 4.16 and that for varying angular mobilities are tabulated in Table 4.2. It is interesting to note that the criticality of dilatation driven damage initiation increases for lower radial mobilities. As the radial mobility increases the fibers are displaced more and the inter-fiber distance increases The effect of angular mobility on the cavitation and crack formation was also monitored. The results obtained are tabulated in Table 4.2.

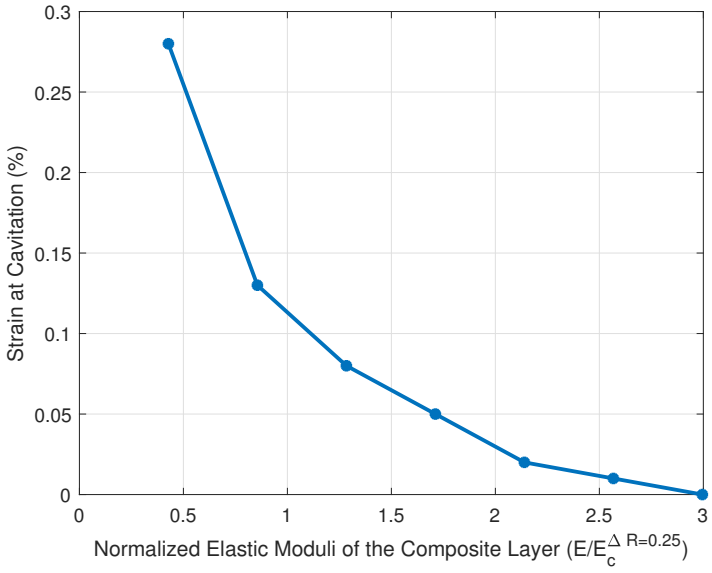

Figure 4.13: Effect of Stiffness of the Embedding Composite Layer to Failure Initiation

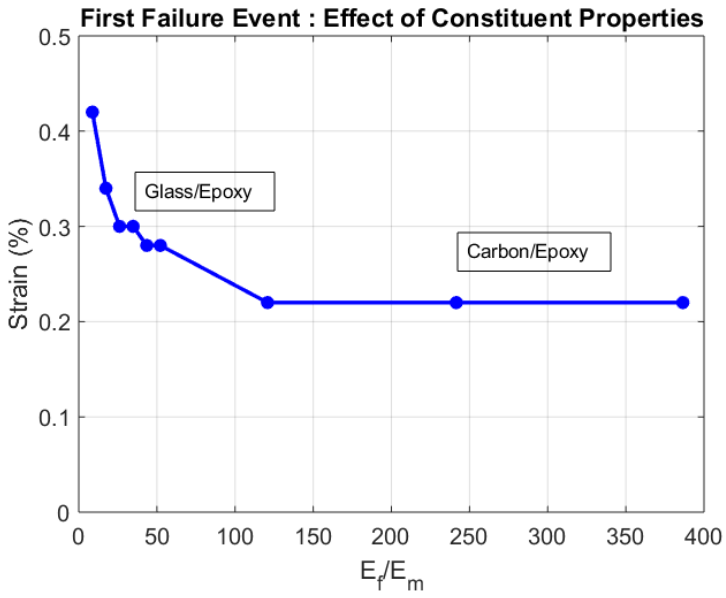

Figure 4.14: Effect of fiber stiffness on Failure Initiation

Sl No	Radial Mobility	Angular Mobility (degrees)	No of Realizations	Dilatational Failure strain (%)	Distortional Failure Strain(%)
1	±0.5r	15^0	5	0.38-0.46	0.88-1.12
2	±0.4r	15	5	0.38-0.40	0.82-0.98
3	±0.3r	15	5	0.34-0.38	0.70-0.78
4	±0.2r	15	5	0.30-0.34	0.66-0.72
5	±0.1r	15	5	0.28-0.32	0.58-0.66

Figure 4.15: Strain to First Failure Event

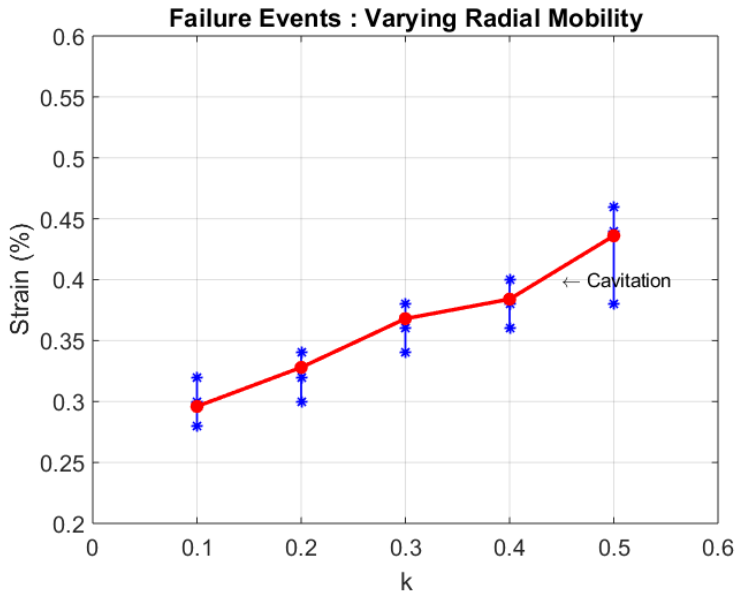

Figure 4.16: Effect of Radial Mobility on Cavitation

The location of the cavitation driven damage initiation is observed to be close to the fiber matrix interface but within the matrix. Hence, it is assumed that this cavitation would lead to fiber matrix interface instantaneously. These debonds later coalesce to form crack. The Figure 4.16 shows the effect of radial mobility on cavitation.

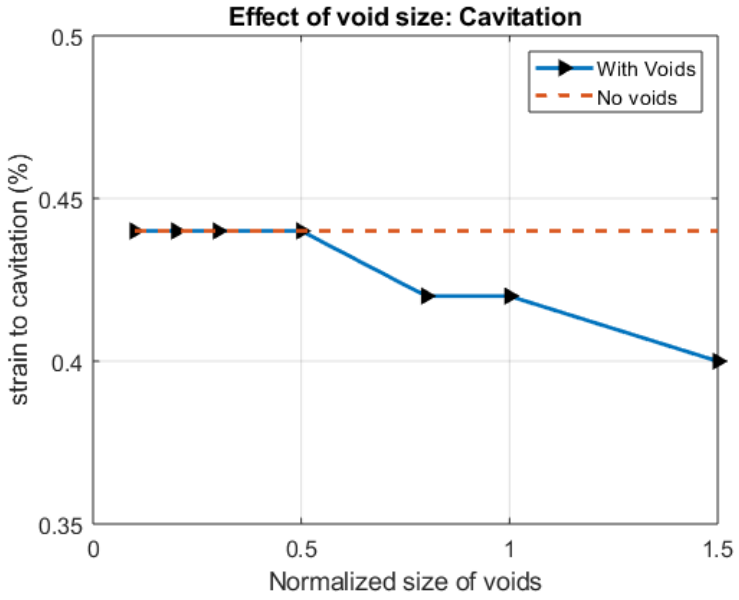

Figure 4.17: Effect of Void Size : Cavitation

4.2.2.5 Effect of Presence of Voids

As mentioned earlier, the voids re distributed in the pre-existing realizations to understand the effect of voids on damage initiation. We look into the effect of void size and void volume fraction on damage initiation.

The Figure 4.17 and Figure 4.18 shows the effect of void size and void volume fraction on dilatation driven damage initiation respectively. The results shown are for realizations with radial mobility of δR 0.5. In Figure 4.17, the volume fraction of the voids are kept constant and the effect shown is for varying the void size. Similarly for the Figure 4.18, the void size is maintained across different volume fractions of void and the damage initiation by cavitation is monitored. It is observed that in both cases, the damage initiates earlier when the voids are present.

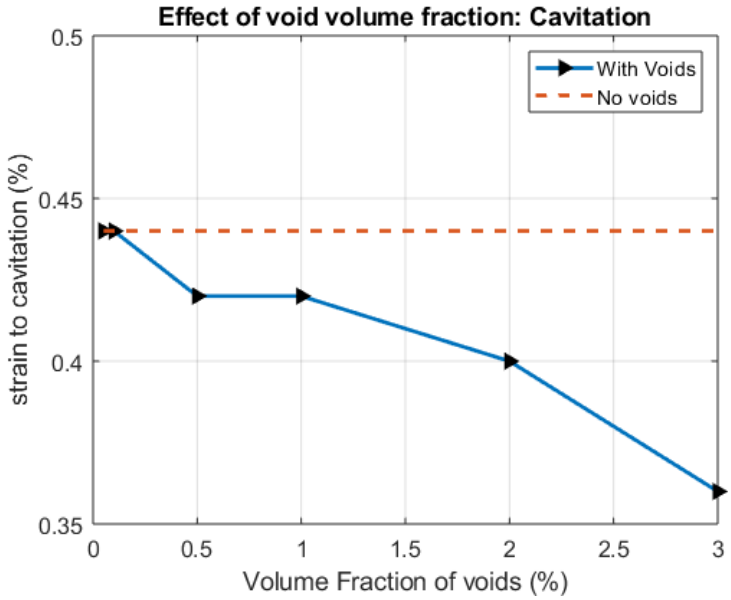

Figure 4.18: Effect of Void Volume Fraction : Cavitation

4.2.3 Second Event of Failure

From the above results, it is evident that the first event of failure is cavitation in PMCs. Since these cavities occur close to the interface, when they burst open by unstable growth, results in debonding, as discussed earlier. Upon further increasing the strain, there exists a stage where multiple locations of debonding occurs from cavitation. These debonds occur in such a way that they can coalesce into a crack. They occur along a line perpendicular to the applied load. At a strain of 0.44%, there exists multiple debonding as shown in Figure 4.10. The debonds occur in such a way that they are aligned approximately normal to the transverse load. Without a detailed analysis, it is assumed here that the individual debonds will coalesce to form a transverse crack instantaneously. The Figure4.19 shows the strain at which the debonds coalesce to form the crack of length 2Φ, where is the fiber diameter. The obtained results are compared to that of the experimental results obtained by de Kok[60]. The results from de Kok are for varying volume fraction of glass epoxy

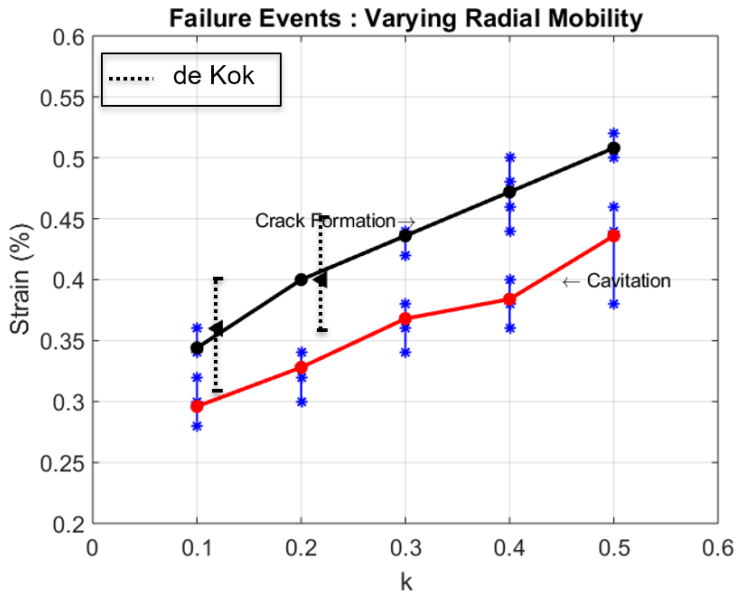

Figure 4.19: Effect of Radial Mobility on Cavitation and Cracking

composites. In the Figure 4.19, increasing volume fraction is in the opposite direction of increasing radial mobility. The experimental results tend to follow similar trend as shown by numerical analysis.

4.3 Section Summary

The current study is a systematic analysis to identify the location and mechanism of damage initiation in PMCs under transverse loading. The damage initiation criteria for realizations with manufacturing defects such as non uniform fiber distribution, presence of voids has been determined based on strain energy density based criteria. Validation of the criteria and model is conducted by replicating the results conducted by Bulsara et al[10].

Statistical analysis of the RVEs were carried out for varying parameters which affect the local stress state in the RVE.The stress and failure analysis for the RVEs generated show that the cavitation dominated brittle failure is the first event of failure in PMCs for varying

angular mobility. The damage initiation by cavitation depends on the local stress fields which in turn depends on the manufacturing process. Parametric study of the significant factors and their effect are as follows:

- **Radial Mobility:**As the inter-fiber distances decreases or when clustering of fibers increase, the damage initiation by cavitation becomes more critical. The manufacturing processes leading to larger radial mobility results in the fibers being dispersed farther away. This condition reduces the favorability for dilatation induced damage initiation.

- **Angular Mobility:** The studies show that the variation in angular mobilities does not hold any significant effect on the damage initiation. This is because the variation in angular mobility does not affect the inter fiber distance, which is critical for damage initiation

- **Constituent Properties:** The stiffer the reinforcement, the more critical the damage initiation by cavitation

- **Thermal Residual Stresses:** The effect of thermal residual stress on the contrary reduces the effect of damage initiation in RVEs. There exists a peak minimum value of thermal cool down for which the effect of residual stress on cavitation is maximum. This is around 80°c.

- **Presence of Voids:** Presence of voids increases the criticality of damage initiation by dilatation. The effect of void size and void volume fraction has been studied.

5. ANALYSIS OF SUBSEQUENT FAILURE EVENTS

In the previous chapter, we carried out a rigorous study to identify the location and mechanism of damage initiation in PMCs under transverse loading. The effect of manufacturing defects and other process related effects were also monitored. In this chapter the focus is on the further events of failure primarily crack formation and the crack advancement. As mentioned earlier, the points of cavitation occurs close to fiber matrix interface. It is assumed that these points of cavitation result in debonds without further investigation of details.

5.1 Crack Formation

As a continuation in study, we monitored further cavitation in the matrix. The number of points of cavitation increases almost instantaneously. Hence, without incorporating for the decrease in the stiffness, we investigate further points of cavitation. The visual inspection of cavitation points in the realizations were observed as shown in Figure 5.1. The strains at which the potential cracks occur are measured. The range of cavitation strain and cracking strain are measured when 2, 4 6 and 8 fibers coalesce to form a crack.

The Figure 5.2 shows the strain at cracking for the varying fiber mobility. Fiber mobility, δR

$$\delta R = kR \tag{5.1}$$

As we can see, the strain at cracking is critical for lower radial mobility. This demonstrates the criticality of brittle cracking in composites with fiber clusters. The increase in strain for the crack to form from 2ϕ to 8 ϕ where ϕ is the fiber diameter is smaller for realizations with lower radial mobility. The crack formation is based on the points of cavitation. In

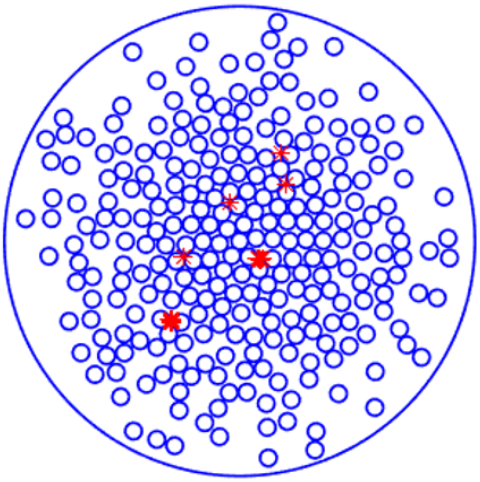

(a) Stage 1: Initial points of cavitation

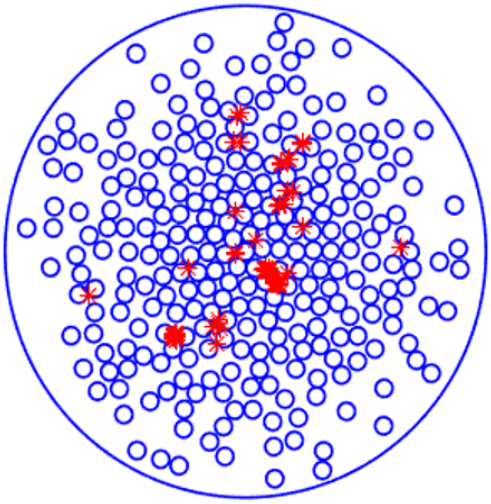

(b) Stage 2: further cavitation formation

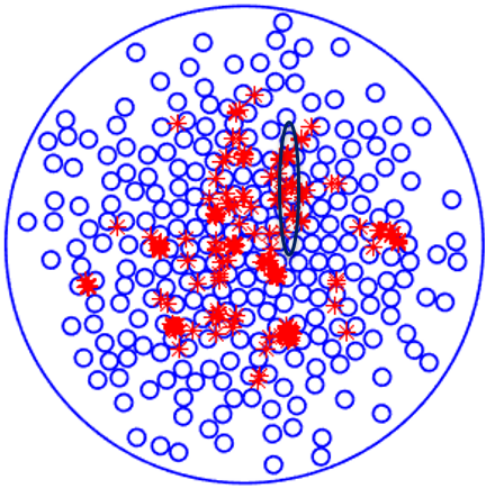

(c) Stage 3: Formation of transverse crack

Figure 5.1: Points of Cavitation upon Loading and Formation of Transverse Crack

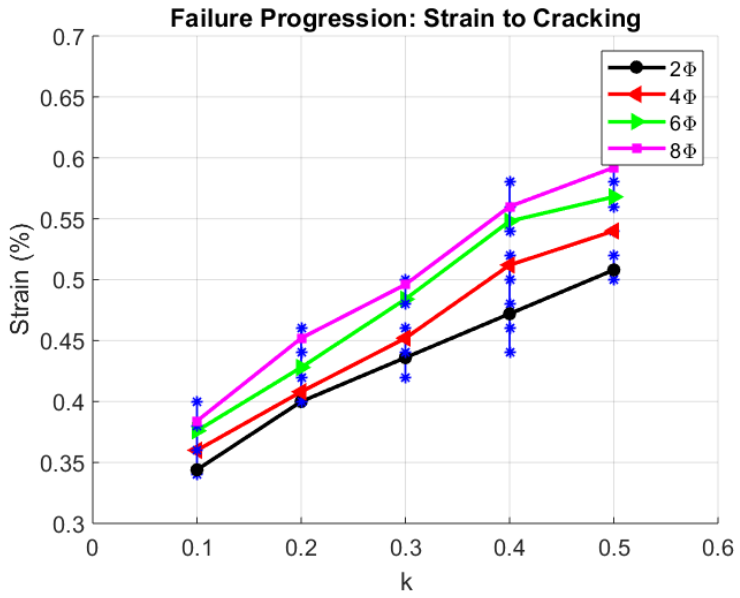

Figure 5.2: Strain at Coalescence of Fibers for Varying Radial Mobility.

the microstructure when the fibers are closely spaced, the condition for dilatation driven damage initiation is enhanced as seen in the previous chapter. These points of cavitation lead to fiber debonding which coalesce to form cracks.

Along with the the strain at cavitation, the number of points undergoing cavitation was also monitored. Thus, we are able to look at the fibers undergoing debonds from these points of cavitation.Some of the terminology we use ahead:

Cavitation Density : It is measure of the number of points within the matrix region in the realization that undergoes cavitation.

$$C_I = \frac{U_{vpts}}{Tot_{pts}} \tag{5.2}$$

(5.3)

where U_{vpts} is the total number of points that have failed by cavitation at a given instant

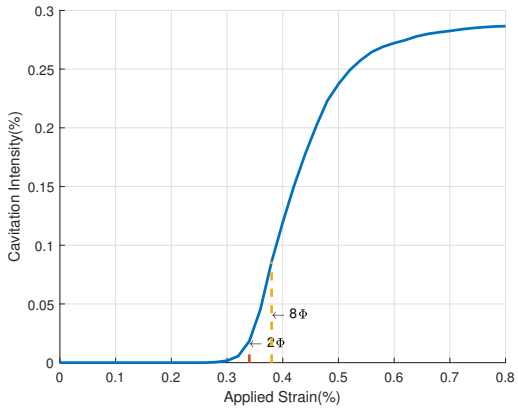

(a) Cumulative Distribution :Points of Cavitation

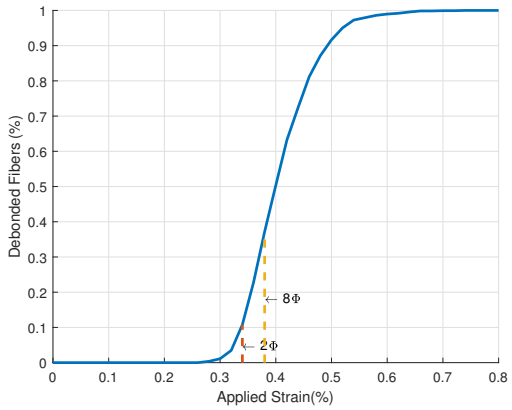

(b) Cumulative Distribution : Fiber Debonds

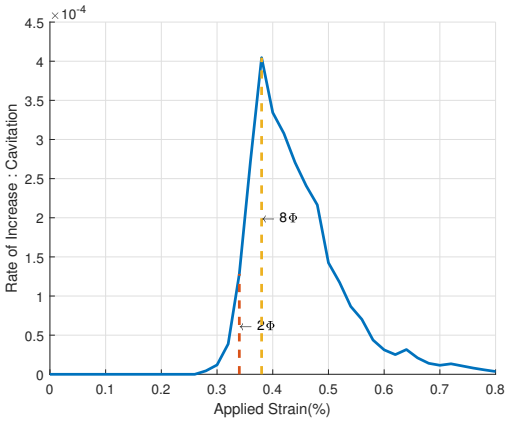

(c) Rate of Increase :Points of Cavitation

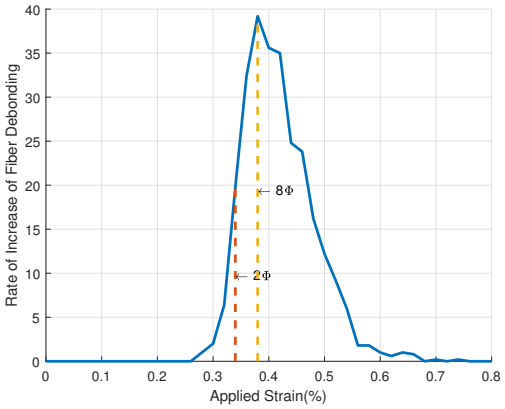

(d) Rate of Increase : Fiber Debonds

Figure 5.3: The Cumulative Increase in Points of Cavitation and Corresponding Fiber Debonds. The Increase in the Points of Cavitation and Debonds for Increasing applied strain for radial mobility of δR=0.1.

and Tot_{pts} is the total number of points in the matrix.

Cavitation growth rate: This is the rate at which the number of points in a realization undergoes under loading. This is related to the cavitation intensity. The cavitation growth rate is the probability distribution function for the cavitation intensity function[61].

Fiber Debond Density: It is the number of fibers debonded at a given instant of load in the realization. The distribution follows a trend similar to the cavitation density. As the load increases, the distribution plateaued to 1 which means all fibers have debonded.

Debond growth rate: It is the probability distribution function for the cumulative distribution of fiber debond intensity.

Now with the understanding of the above parameters we look each of them for all realizations with increasing radial mobility. For the purpose of explaining let us consider the points of cavitation for δR=0.1R as shown in Figure 5.3. The corresponding cumulative distribution of cavitation points are plotted in 5.3a. On the figure is marked the strain corresponding to coalescence of number of fiber debonds leading to crack i.e, 2Φ and 8Φ, where Φ is the fiber diameter. Assuming that each point cavitation leads to the debond of nearest fiber, the cumulative distribution of the fiber debonding is also plotted as shown in Figure 5.3b. From the cumulative distribution, the corresponding probability distribution of the number of cavitation points and debond fibers are generated and are plotted as shown in Figure 5.3c and Figure 5.3d. It is interesting to note that a crack connecting 8 or more fibers are formed corresponding to the strain at which the distribution function for cavitation and debonded fibers reach a peak. When a crack connecting 8 fibers are formed in the core of the RVE with 9 rings of fibers, the crack has covered nearly 50% of the thickness of the RVE. At this stage there are multiple points of cavitation that suggest the probability of formation of multiple cracks.

The same is plotted for other radial mobilities. It is observed that the same phenomenon exists for other cases too but the strain at which these criticalities occur are higher for higher

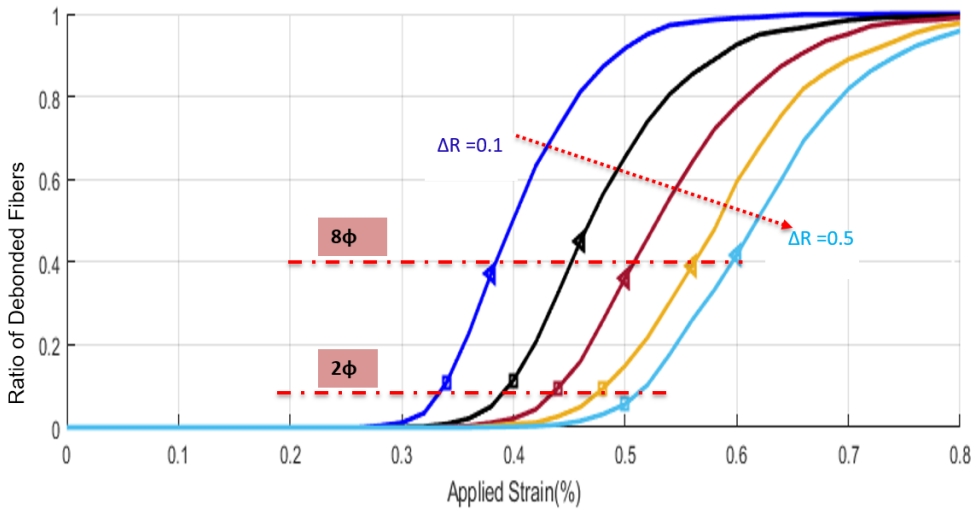

Figure 5.4: Cumulative Debonding of Fibers

radial mobilities.

The Figure 5.4 shows that the cumulative debonding of fibers upon loading for radial mobility. It can be observed from the plot that for increasing radial mobility, the strain at cracking or coalescing of the debonds occur at higher strain. The main observation from this plot:

1. Increasing radial mobility also results in increases in strain at debond coalescing like failure initiation. The strain at which the debond intensity curve starts shows the strain of first cavitation. It can be observed that the strain at cavitation is the strain at which the debond intensity curve becomes non zero.

2. It can be observed that for a particular strain the a distribution with lower radial mobility might have already resulted in a crack on the other hand at higher radial mobility, this strain might not have even triggered the cavitation.

3. The slope of the cumulative debonded fiber distribution curve decreases with increasing radial mobility. This implies the points of cavitation growth decreases with

increasing radial mobility. Hence, the increase in strain required to form a crack of length 2ϕ to a crack of 8ϕ is higher for higher radial mobility.

4. On the Figure 5.4 are marked the strains at which cracks of atleast 2 and 8 fibers coalesce. This is found to occur when atleast 8-12$\%$ and 35-45$\%$ of fibers debond respectively.

5. Extrapolating the above information to another random distribution, with the ability to determine the cumulative debond distribution from the cavitation points in polymer composites, the strain at crack formation corresponding to the coalescence of 2 or more fibers can be determined.

5.2 Crack Driving Force

So far we discussed only the point failure and how it can coalesce to for debonds and eventually a crack. Now, as further step it makes complete sense to replace the coalescing fibers by a crack of equivalent length.For instance, a realization with points of cavitation as shown in Figure5.1c will have transverse crack as shown in Figure5.5. Hence, we replace the fibers and place cracks of length 2ϕ, 4ϕ, 6ϕ and 8ϕ , ϕ-fiber diameter and subject them to the corresponding strains.

The corresponding average strain is applied to the RVE with a crack placed centrally in the RVE. In each realization the location of the crack is ideally different but to generalize , we place the crack on the RVE centrally. Now at-least 4 rings are placed ahead of the crack tip in-order to measure the accurate J Integral.

5.2.1 J Integral

This method is typically used in rate-independent quasi-static fracture. The J Integral provides the energy release associated with the crack growth. It can be related to the stress intensity factor in linear elastic case. In the current analysis, this holds true. The J Integral

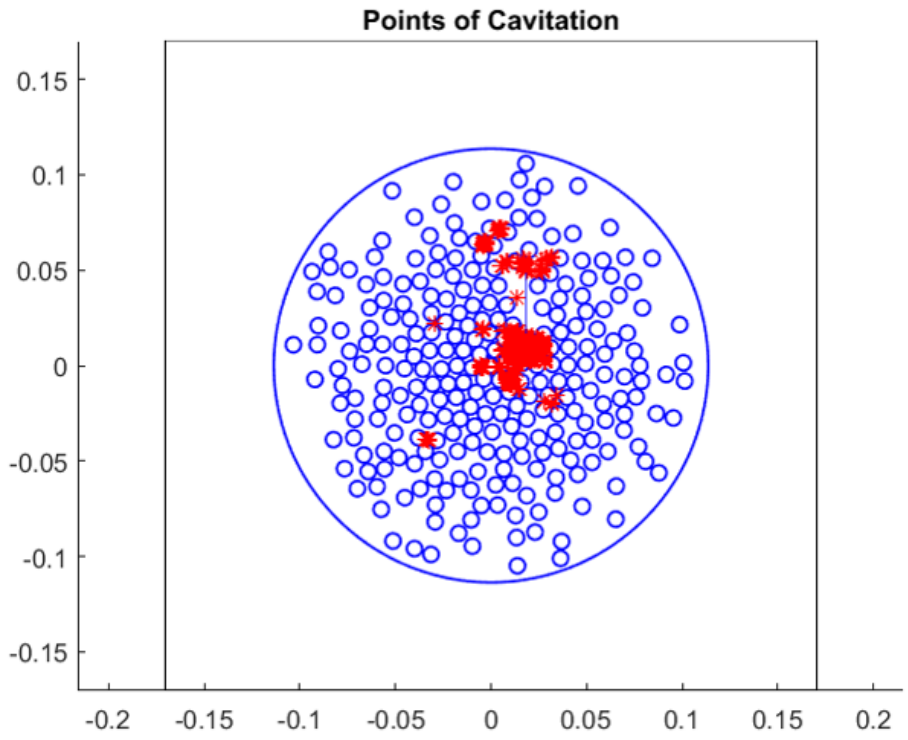

Figure 5.5: Transverse Crack Replacing the Fibers Involved in Coalescing of Fibers

is calculated as follows: For a virtual crack advance $\lambda(s)$ in the plane, the energy release rate is given by

$$J = \int_A \lambda(s)\mathbf{n.H.q}dA \tag{5.4}$$

(5.5)

where dA is a surface element along a vanishing small tubular surface enclosing the crack tip, n is the outward normal to dA, and q is the local direction of virtual crack growth[36,

62]. H is given by

$$H = (WI - \sigma.\frac{u}{x}) \tag{5.6}$$

The J Integral domain independence is a key factor that has to be verified. In the current analysis, special attention is given to ensure the domain/contour independence of the J Integral.

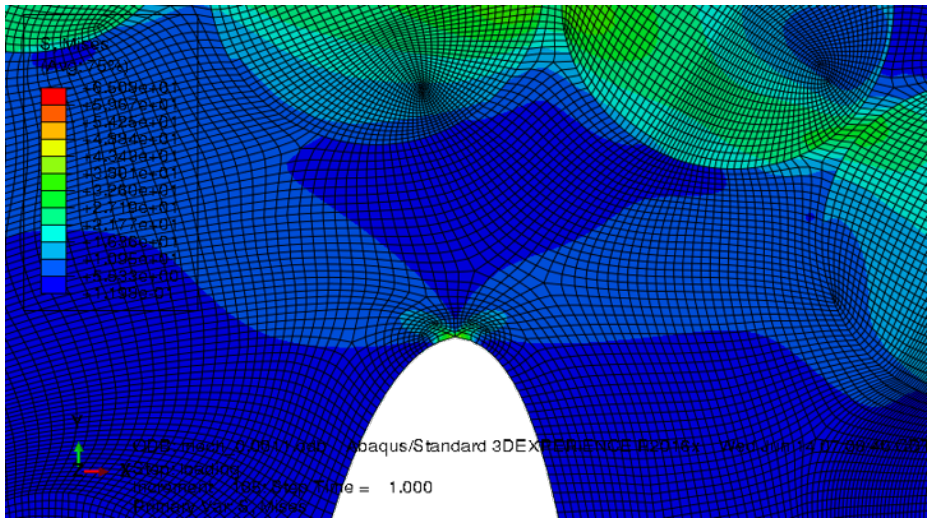

Figure 5.6: Crack Tip

The paths along which J Integral was computed was taken care not to interfere with the fibers in the realization. Also, the paths were placed so as to ensure the J Integral calculation was independent of the path taken. The Figure 5.6 shows that the crack tip and the elements ahead of the The J Integral gives the energy released when a crack advances.

The FE evaluation of the J -Integral for the the crack in elastic regime also allows the computation of stress intensity factor around the crack tip. The crack tip of concern is the one that has maximum J- Integral. Figure 5.8 shows the the stress intensity factor for

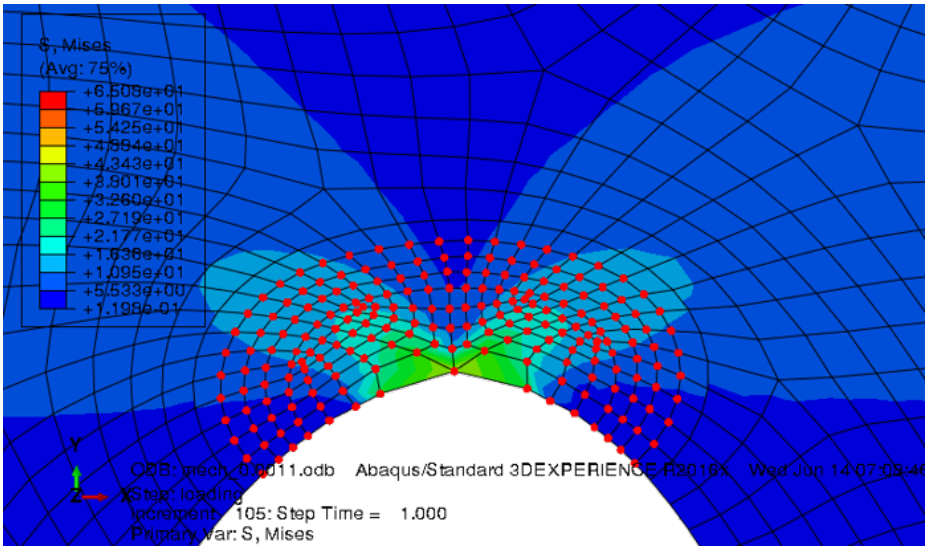

Figure 5.7: Paths for the J Integral Evaluation

the matrix material and the homogenized composite respectively. For the matrix material shown in Figure 5.8a the stress intensity factor is normalized with the K_I for realization with $\delta R = 0.1$ and 2Φ crack length. In the plot shown, the properties of the matrix remain constant. For varying radial mobility the strain applied to the material varies. For higher radial mobility the load applied for the same crack is higher and hence results in the higher K_I.

On the other hand, Figure 5.8b shows the variation of K_I for homogenized composites. As the radial mobility increases, the stiffness of the composite decreases and the K_I for a given crack length is lower than that of the lower radial mobility.

When non homogenized RVEs are considered, the shielding effect of the fibers come into action and alters the J Integral for varying inter-fiber distance. When the radial mobility is low, the clustering of fibers is high, the fibers shield the crack from propagating. On the other hand in the case of higher radial mobility, the fibers are distributed further away. As a result, the shielding from fibers are less and the J Integral decreases from the homogenized

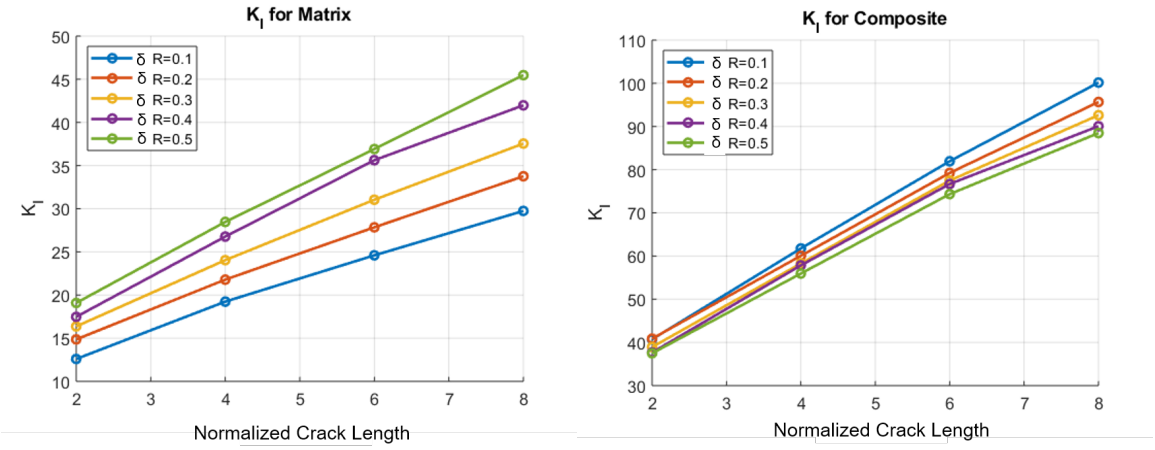

(a) Matrix

(b) Homogenized Composite

Figure 5.8: K_I for Increasing Normalized Crack Length for Homogeneous Media(Normalized w.r.t. fiber diameter)

composite medium.

This would be the expectation. Now in order to compare the energy released from crack propagation, we look at the J Integral released from the identical crack placed an RVE with homogeneous matrix material, composite material and non uniform fiber distribution. This comparison would show the significance of fiber distribution the energy released. We would also look at the effect of fiber mobility on the same.

The J Integral of the RVE for varying radial mobility plotted in the above figures shows that as the radial mobility increases the J Integral for the deviates from the homogenized medium and tends to approach the J Integral of matrix. Also for a given radial mobility with increase in crack length the J Integral shows the same behavior, i.e, it shifts towards the J Integral of matrix material. All the cases show that the J Integral primarily lies between the homogeneous composite and matrix material.

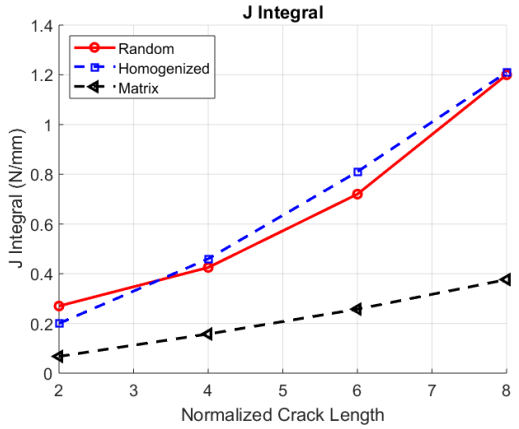

(a) J Integral Variation with Crack Length

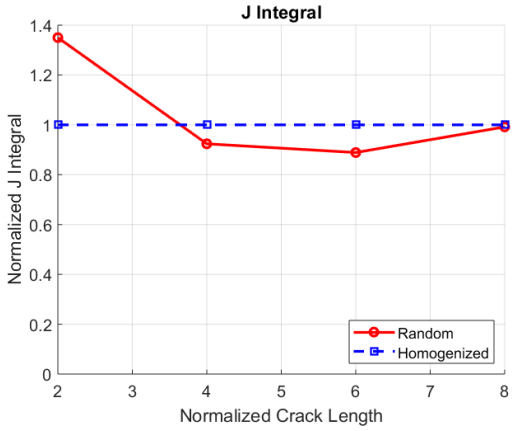

(b) J Integral Deviation from Homogenized Composite

Figure 5.9: J Integral Variation with Crack Length (δ R =0.1), Normalized with that of Homogenized Composite

5.3 Effect of Ply Constraint

So far our studies were limited to the 90° plies alone. It is required to include the effect of 0 ° plies on the failure propagation. Hence, we include the effect of stiffener analogous to the effect of longitudinal plies as shown in Figure 5.14.

There has been few remarkable works carried out by Isida in the 1970s in the field of factors affecting the stress intensity factors of a crack in a plate[63, 11]. Starting with the analysis of Stress Intensity Factors with random array of cracks, he introduced the Laurent series expansion (perturbation technique) for the crack tip stress intensity factor[63]. analyzing the effect of the size , i.e, width and breadth of the plate Isida [64] obtained the correction factor that reflects the specimen geometry and boundary conditions. Well the factor missing is that, all the materials in his consideration were homogeneous and isotropic. Hence in this study, we also aim at comparing the homogeneous results to the remarkable work by Isida and demonstrate the deviation for non uniform stress distribution arising from the non-uniform microstructure. We continue to use the terminology proposed

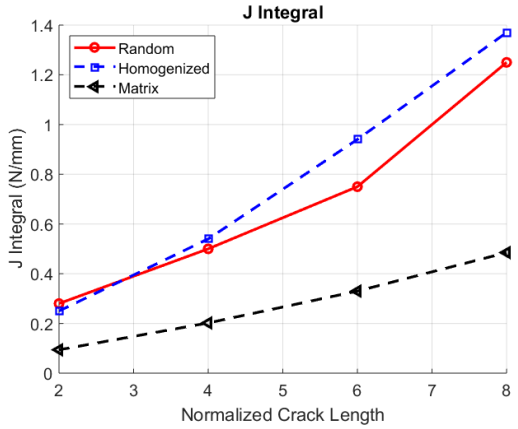

(a) J Integral Variation with Crack Length

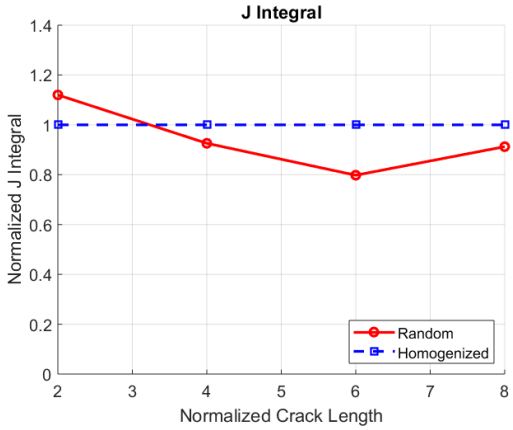

(b) J Integral Deviation from Homogenized Composite

Figure 5.10: J Integral Variation with Crack Length (δ R =0.2), Normalized with that of Homogenized Composite

by Isida.

5.3.1 Analytical Formulation: Comparison of Stiffened and Unstiffened RVE

The stress intensity factor , K_I, for an unstiffened wide plate is given by

$$K_I = \sigma\sqrt{\pi a} \tag{5.7}$$

Isida showed that for the case of stiffened plate, the K_I is obtained as follows[11]

$$K_I = \sigma\sqrt{\pi a}.F(\alpha, \beta, \lambda) \tag{5.8}$$

where α and β are the inertial parameter and extensional rigidity parameter of the stiffener respectively. Both these parameters are dimensionless. λ is the crack ratio,

$$\lambda = \frac{a}{b} \tag{5.9}$$

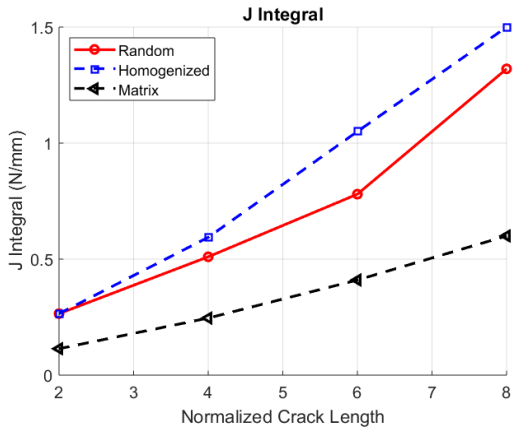

(a) J Integral Variation with Crack Length

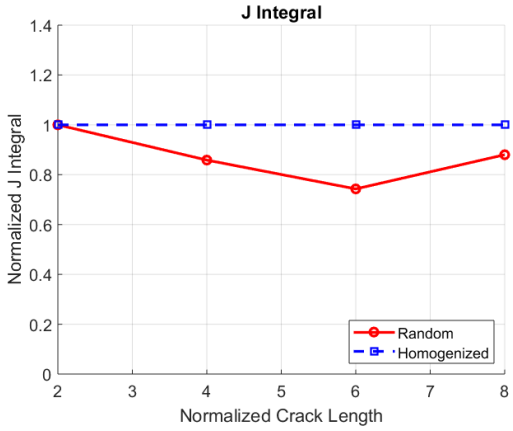

(b) J Integral Deviation from Homogenized Composite

Figure 5.11: J Integral Variation with Crack Length (δ R =0.3), Normalized with that of Homogenized Composite

where b is the plate width and a is half crack length. He has demonstrated the variation of the correction function for various cases. In the current study we utilize the two extremes to compare to the current simulation.

1. Case : Unstiffened strip with central crack:

   α=0 , β = 0 The correction factor for unstiffened strip as shown in Figure 5.15 is

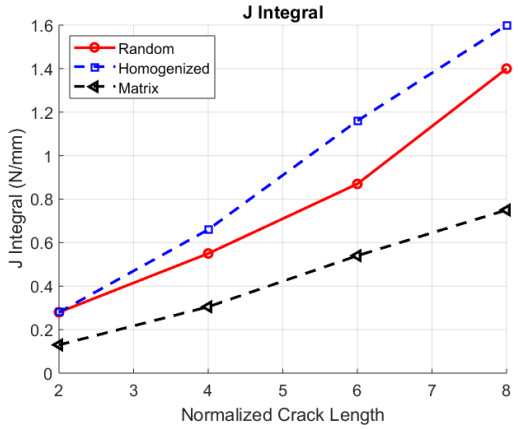

(a) J Integral Variation with Crack Length

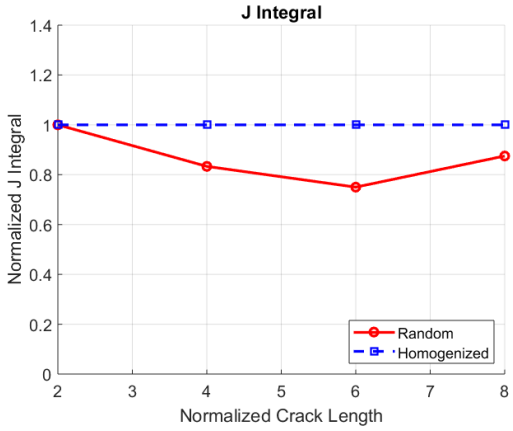

(b) J Integral Deviation from Homogenized Composite

Figure 5.12: J Integral Variation with Crack Length (δ R =0.4), Normalized with that of Homogenized Composite

given by,

$$\begin{aligned} F(0,0,\lambda) =& 1 + 0.5948\lambda^2 + 0.4812\lambda^4 + 0.3963\lambda^6 + 0.3367\lambda^8 + 0.2963\lambda^{10} \\ &+ 0.2684\lambda^{12} + 0.2478\lambda^{14} + 0.2318\lambda^{16} + 0.2186\lambda^{18} + 0.2076\lambda^{20} \\ &+ 0.1980\lambda^{22} + 0.1897\lambda^{24} + 0.1823\lambda^{26} + 0.1757\lambda^{28} + 0.1698\lambda^{30} \\ &+ 0.1644\lambda^{32} + 0.1595\lambda^{34} + 0.1550\lambda^{36} + 0.1509\lambda^{38} + 0.1471\lambda^{40} \\ &+ 0.1436\lambda^{42} + 0.1403\lambda^{44} + 0.1372\lambda^{46} + 0.1341\lambda^{48} + 0.1307\lambda^{50} \\ &+ 0.1255\lambda^{52} + 0.1158\lambda^{54} + 0.0976\lambda^{56} + 0.0660\lambda^{58} + 0.0188\lambda^{60} \\ &- 0.0413\lambda^{62} - 0.1054\lambda^{64} - 0.1593\lambda^{66} - 0.1889\lambda^{68} - 0.1847\lambda^{70} \end{aligned} \tag{5.10}$$

where λ is the crack ratio

2. Case : Wide Panel with clamped edges:

   α=∞ , β = 0 The correction factor for the stiffened strip as shown in Figure 5.16 is

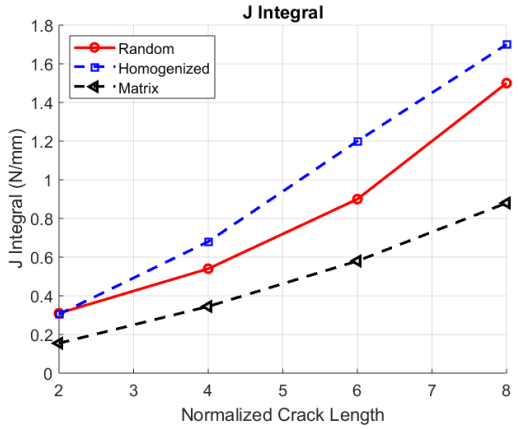

(a) J Integral Variation with Crack Length

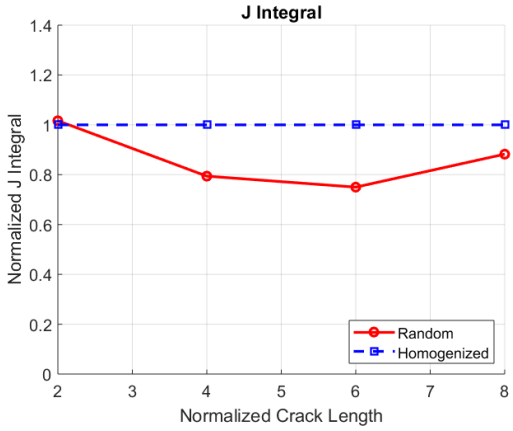

(b) J Integral Deviation from Homogenized Composite

Figure 5.13: J Integral Variation with Crack Length (δ R =0.5), Normalized with that of Homogenized Composite

given by

$$\begin{aligned} F(\infty,\infty,\lambda) =& 1 - 0.4102\lambda^2 - 0.0051\lambda^4 - 0.0701\lambda^6 - 0.0332\lambda^8 - 0.0288\lambda^{10} \\ & - 0.0210\lambda^{12} - 0.0170\lambda^{14} - 0.0140\lambda^{16} - 0.0119\lambda^{18} - 0.0104\lambda^{20} \\ & - 0.0091\lambda^{22} - 0.0082\lambda^{24} - 0.0073\lambda^{26} - 0.0067\lambda^{28} - 0.0061\lambda^{30} \\ & - 0.0056\lambda^{32} - 0.0052\lambda^{34} - 0.0048\lambda^{36} - 0.0045\lambda^{38} - 0.0042\lambda^{40} \\ & - 0.0039\lambda^{42} - 0.0037\lambda^{44} - 0.0035\lambda^{46} - 0.0032\lambda^{48} - 0.0028\lambda^{50} \\ & - 0.0017\lambda^{52} + 0.0006\lambda^{54} + 0.0049\lambda^{56} + 0.0113\lambda^{58} + 0.0191\lambda^{60} \\ & + 0.0257\lambda^{62} + 0.0284\lambda^{64} + 0.0248\lambda^{66} + 0.0145\lambda^{68} - 0.0005\lambda^{70} \end{aligned} \tag{5.11}$$

The correction factor for stress intensity factor is also plotted for varying radial mobility

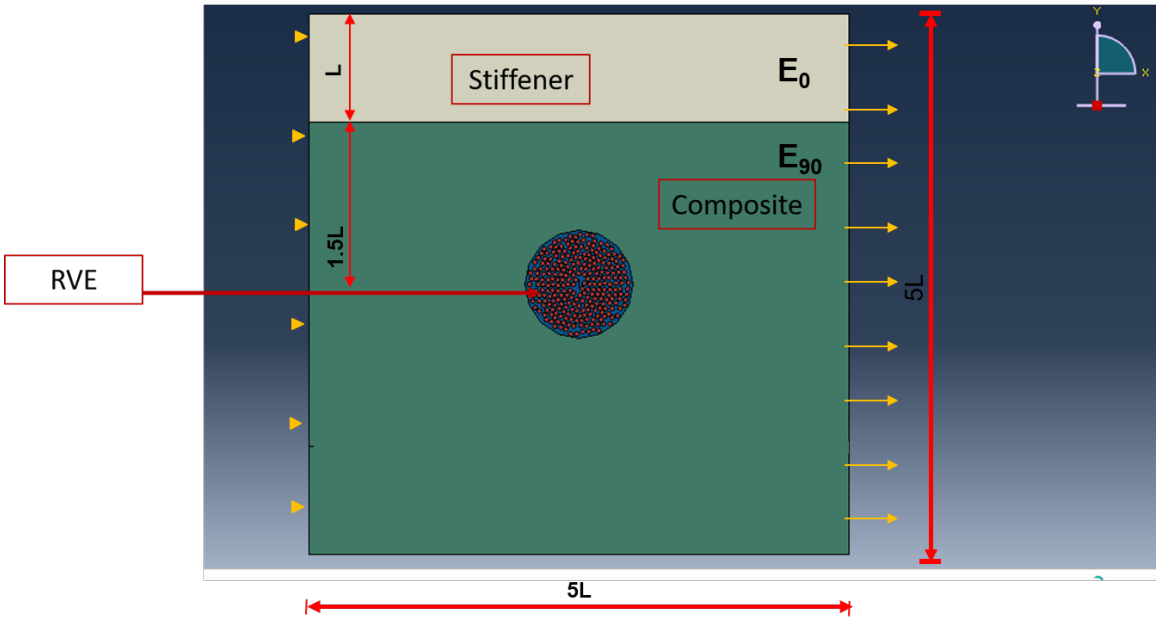

Figure 5.14: Schematic Showing the RVE with Stiffener

for unstiffened RVE. The correction factor is defined as follows

$$K_{IS} = \sigma\sqrt{(\pi a)}F(\delta R) \tag{5.12}$$

$$= K_{IUS}F(\delta R) \tag{5.13}$$

$$\tag{5.14}$$

where K_{IS} is the stress intensity factor for stiffened RVE and K_{IUS} is the stress intensity factor for unstiffened RVE. Hence for homogeneous medium , the correction factor provided by Isida is shown in Figure 5.15. The variation from one with no crack is primarily due to finite size of the RVE

The above analysis conforms to the unconstrained laminate analysis. Also the J Integral shows the driving force for the crack to propagate. These plies act as stiffener. In the further analysis, we look at the effect of the stiffener on the crack propagation.

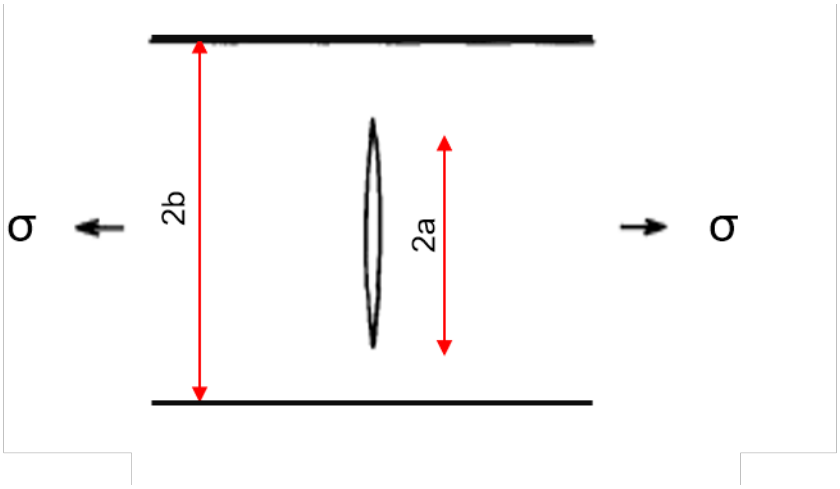

Figure 5.15: Case 1: Unstiffened Strip with Central Crack Adapted from [11]

For this we consider two parameter, the distance of the stiffener from the crack tip and also the stiffness of the crack tip.

5.3.2 Effect of Constraint Location

As a preliminary step, the stiffener is placed at the boundary of the RVE, i.e, at 2.5L from the center of the RVE. Then the size of the RVE is increased and the stiffener being at the edge, thus ensuring the stiffener being further away from the crack tip. Interestingly, as shown in Figure 5.19 the effect of stiffener beyond the size of the RVE determined by Hill's criteria is constant. Once the stiffener comes closer to the crack tip (within the RVE size), the criticality increases. Since RVE is the representative of the entire material. This is applicable at a laminate level too. The effect of the stiffener layer ahead remains constant beyond a particular distance from the crack tip. It is interesting to note that this critical distance is the min size of the RVE determined by Hill's criteria. The J integral plotted in Figure 5.19 is the mean of the J Integral with stiffener for realizations with radial mobility of δR=0.1.

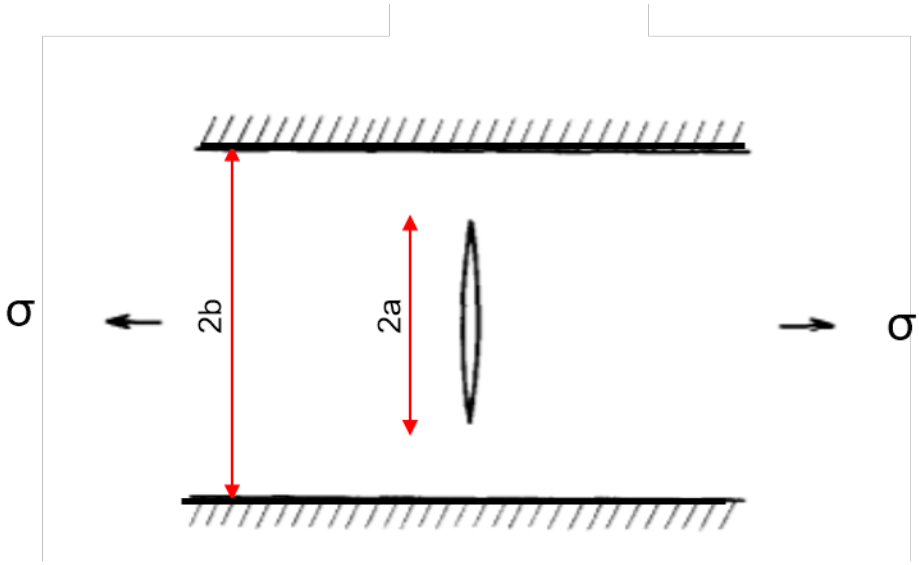

Figure 5.16: Case 2: Stiffened Plate with Clamped Edges Adapted from [11]

5.3.3 Effect of Constraint Stiffness

The effect of stiffness is monitored for the realizations with radial mobility of δR =0.1R, with the stiffness being placed as shown in Figure 5.14. Increasing the stiffness increases the criticality. In the current analysis, the stress intensity factors are monitored for the strain at which crack initiates in an unstiffened RVE. On further analysis, it is observed that the presence of the presence of the stiffener enhances the criticality of cavitation and the strain at which the cavitation occurs and crack initiates are lower than the unstiffened RVE. This makes the Stiffened RVE more critical to transverse cracking due to the presence of constraints from the stiffener.

The effect of stiffness is plotted as shown in Figure 5.20. The presence of the stiffener enhances the criticality for the homogeneous as well as for non uniform distribution of the fibers.

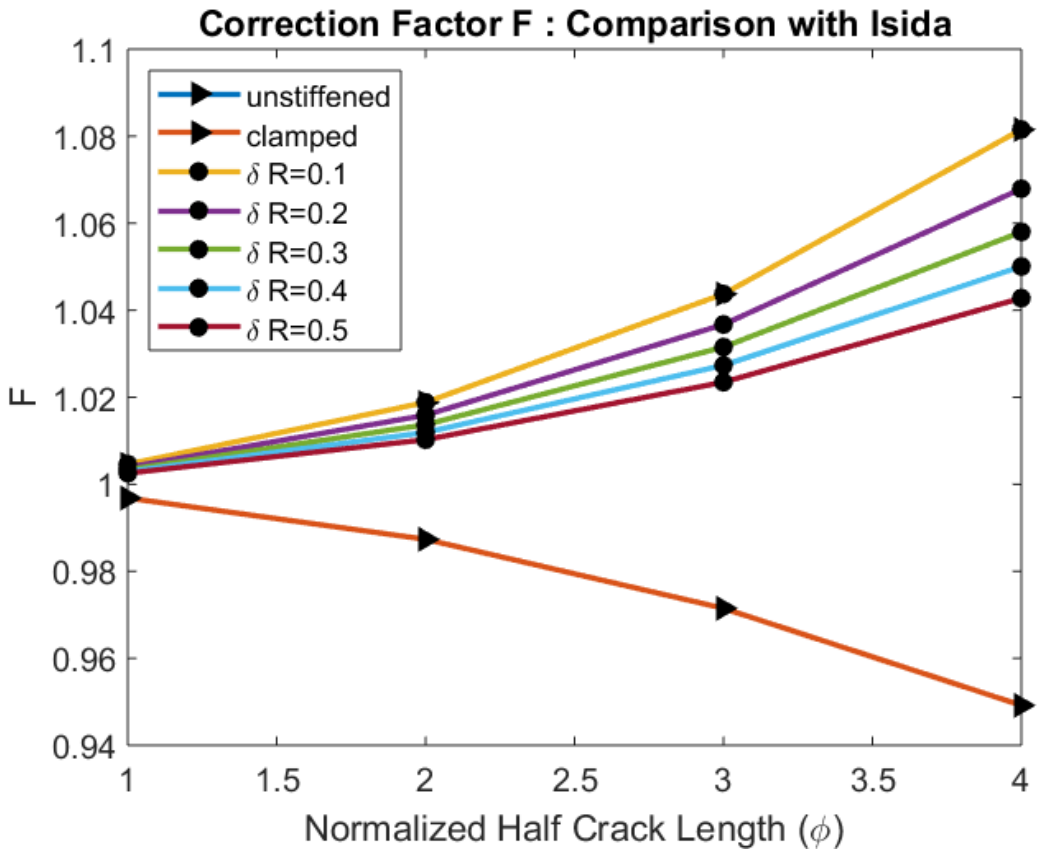

Figure 5.17: Correction factor as Described by Isida[11] for Homogeneous Medium

5.4 Section Summary

In this chapter , we looked at the crack formation and the driving force force for the crack propagation. To summarize,

- **Crack Formation**: Radial mobility has significant effect on the crack formation. The crack formation follows similar trend as the cavitation. The crack formation in the realization with lower radial mobility is more critical than the realizations with larger radial mobility. This is because in realizations with lower radial mobility the inter-fiber distance is lower. This enhances the condition for cavitation. Thus more points of cavitation are formed and the lead to debond formation and trans-

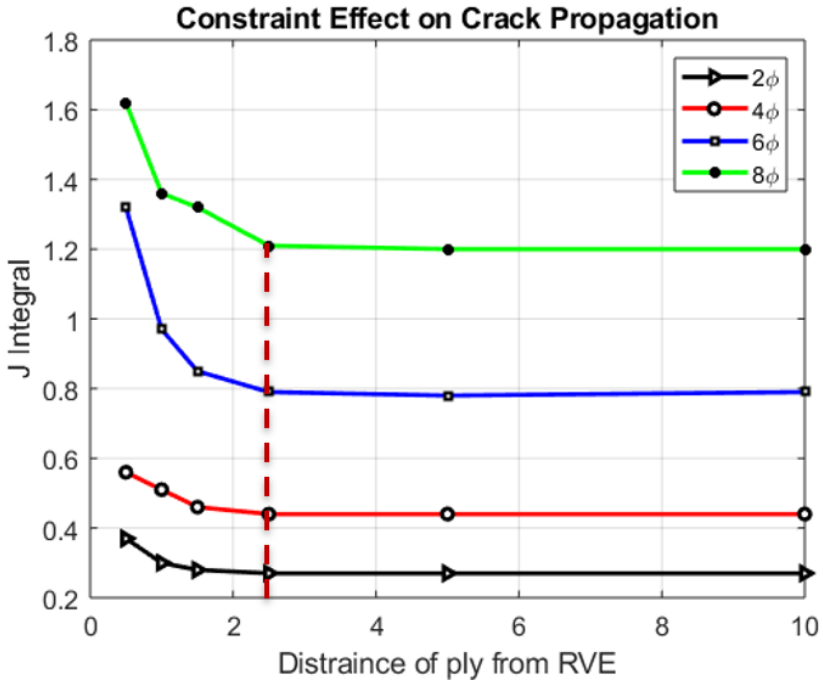

Figure 5.18: Effect of Ply Distance from the RVE for δR=0.5

verse crack. Since these points of cavitation occur instantaneously the material crack formation is brittle in nature.

- **Crack propagation :** A thorough analysis of the J integral, which is also the energy release rate in the current case, shows that as the radial mobility increases, the driving force for crack propagation increases. This is because the effect of shielding from the fibers ahead of the crack tip. In the realization with lower radial mobility this effect is higher.

- **Comparison with homogeneous medium:** The comparison with the homogeneous medium shows that the RVEs with random distribution has lower stress intensity factor than the realizations with homogenized composite medium for smaller crack length. This is also due to the fact that the fibers ahead the crack tip has the shielding

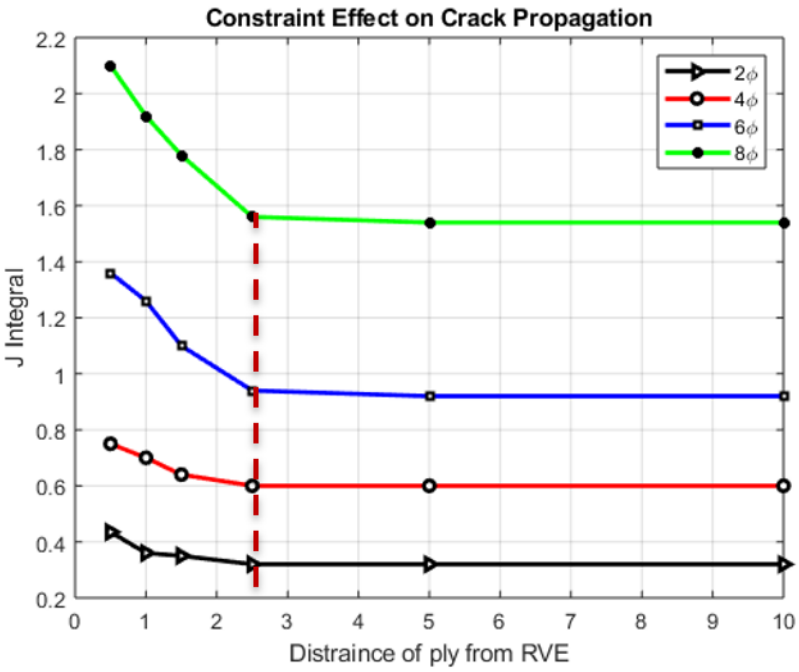

Figure 5.19: Effect of Ply Distance from the RVE for δR=0.1

effect and decreases the crack tip stress intensity.

- **Effect of Ply constraint:**The presence of the 0° plies not only enhances the the cavitation and crack formation but also , decreases the driving force for the crack propagation. The distance of the stiffener from the crack tip has significant impact on the crack propagation. The stiffness of the ply on the other hand has higher impact if closer to the crack. Also, higher the stiffness , higher the J Integral.

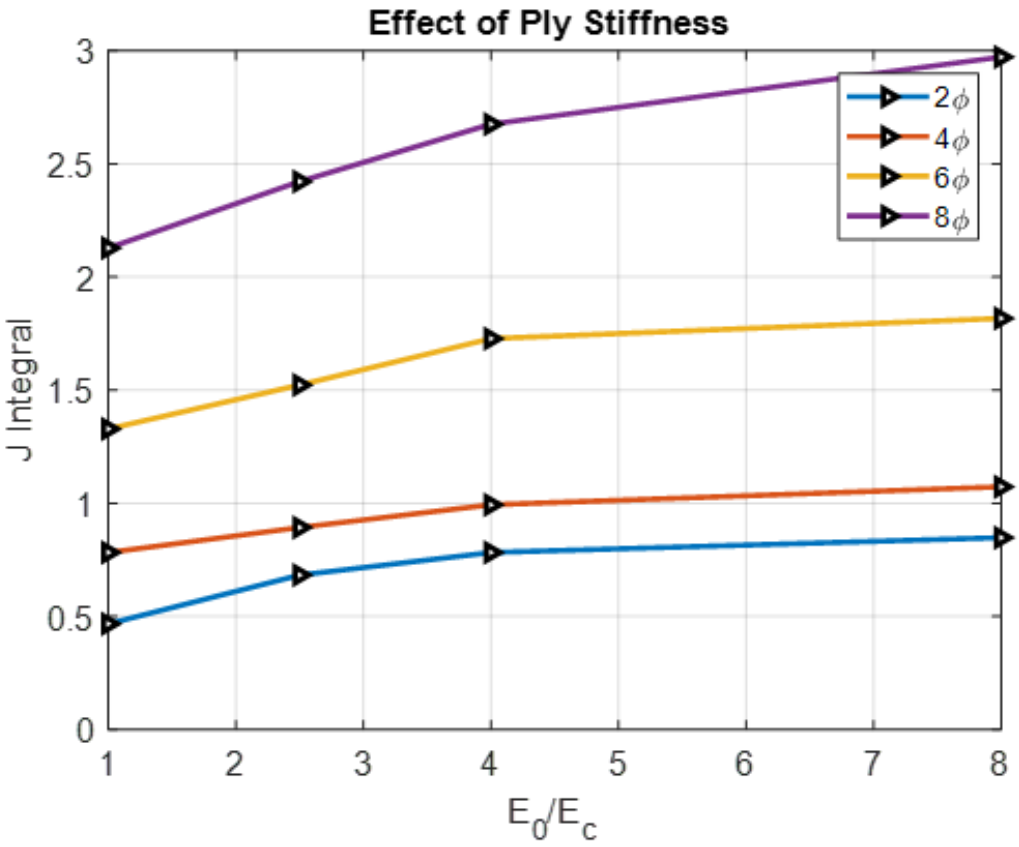

Figure 5.20: Increase in J Integral with Stiffness of the 0° Layer : $\delta R = 0.5$

6. CONCLUSION AND FUTURE WORK RECOMMENDATION

6.1 Summary

In the recent years, polymer matrix composites are being increasingly used in aerospace, automobile and wind turbine industries. They are also finding application in electronic hardware application where reduction of weight without compromising strength is an growing priority. This increase in demand is really promising, yet any composite engineer would be familiar with the fact that full potential of this remarkable material is not yet harnessed completely. This is because of the complex microstructure, anisotropy, and the limited knowledge of the failure mechanisms in composite materials. However, a lot of research is currently being conducted in this field.

In this dissertation, we discuss the current failure mechanisms in composite materials. These failure theories either lack implementation of the physical failure mechanism in composites or consider the composite failure mechanism by homogenization methods. Thus we are unable to capture the failure initiation mechanism accurately. Damage in composite is progressive. It involves multiple length scales and it is extremely important to incorporate multiscale analysis in the failure analysis of composite materials. Also, the boundary conditions and other constraints at each length scale are important for the accurate analysis. Also, equally important is the effect of manufacturing defects. It is impossible for any manufacturing process to render a pristine product without any defects. Each manufacturing process depending upon the quality control would result in certain degree on defects, which affects the failure initiation and propagation as shown in this research. Hence,some of the key aspects that are required for accurately capturing the failure mechanisms in composite materials are multiscale analysis, effect of constraints from the surrounding layer, effect of manufacturing defects etc.

As explained in Chapter 2 the RVE is the smallest unit that can capture the behavior of the entire material. In the current study our focus is on failure initiation and consequent events, which depends on the microstructure. The microstructure on the other hand depends on the manufacturing process. This leads us to the understanding that the manufacturing process has an unavoidable significance on the failure events.For illustration, in the current study we resort to the resin infusion process of manufacturing. Associated with each manufacturing process is the process related defects, which is significant while considering local stress fields. In the current study, we introduced a novel methodology for creating the RVE from resin infusion process. Associated with the resin infusion manufacturing process, we also have defects like irregular fiber distribution and presence of voids. They are taken into consideration in the current study. The analysis shows that these defects have significant effect on both damage initiation and damage propagation. hence, we emphasize the fact that manufacturing defects must be included int failure analysis of composite materials.

The chapter 3, we looks at the damage initiation criteria in polymer composites. Conventionally, the damage initiation criteria in composites are primarily stress based. It was observed that these criteria were not able to capture the damage initiation in polymer matrix composites accurately. The systematic study by Asp et al showed that damage initiation in polymer matrix composites are primarily based on two mechanisms. They are dilatational strain energy based and distortional strain energy based criteria. These mechanisms have completely different failure modes and explained in Chapter 3. The dilatation driven damage is of significant effect in polymer composites and leads to the brittle failure in PMCs. On the other hand, distortion driven which is equivalent to the von Mises criteria results in the ductile failure. Hence, it is important to understand the physics behind the failure initiation and further events and then incorporate them in the failure analysis.

With the implementation of the above mentioned requirements for failure analysis, a

systematic study is conducted to study the effect of these manufacturing defects on failure events. The rigorous analysis shows that the damage initiation is primarily dilatation driven. This occurs by the formation of cavities in as the polymer chains pull apart. This cavity bursts open close to the fiber matrix interface within the matrix. This results in the debond formation in the fiber matrix interface. Previous studies conducted by the group show that these debonds coalesce and form a crack. The current research shows that these points lie on a vertical straight line normal to the applied load. Thus, leading to the formation of a transverse crack.

This is of great significance, since the strain at which damage initiates by dilatation strain energy density is much lower than the ductile failure criteria. This strain at which damage initiates correlates to the experimental results carried out by Asp et al in the past. Thus this failure criteria captures the physics behind the failure initiation accurately in PMCs and also predicts the strain to failure initiation.

As further step we also look at the factors that contribute to the damage initiation by cavitation. They are the microstructure- which consists of the irregular fiber distribution and the voids, constituent properties and thermal residual stresses. Parametric studies of these factors on the damage initiation is carried out and are demonstrated in the Chapter 4. The studies show that as the radial mobility of the fibers have significant effect on the damage initiation. As the fibers are dispersed or distributed further away the damage initiation by cavitation becomes less critical. The more fiber clustering results in the damage initiation by cavitation more critical. Similarly, the parametric study on constituent properties show that as the reinforcement becomes more stiff, the damage initiation by cavitation becomes more critical but reaches a plateau.

As a next step, we look at the formation of crack and the propagation of crack. These consequent events of failure are dealt in Chapter 5. The studies show that the crack formation follows the trend similar to the cavitation. Crack formation is more critical for lower

radial mobility as there are more points of cavitation in realization with lower radial mobility. The strain at which these cracks are formed are monitored . The strains at which 2, 4 6 and 8 fiber debonds coalesce and form a crack is monitored. The strain at which the crack forms are compared with the experimental results from de Kok.

The concept of J Integral is adopted to monitor the crack propagation. The corresponding J Integrals for the crack tip is evaluated and compared with the homogenized composite and matrix material for reference. The comparison shows that the J Integral for non homogenized medium is typically lower than that of the homogenized medium. This shows that the crack growth is more critical in random distribution of fibers over homogenized medium. And this criticality increases with radial mobility (outcome of manufacturing process) and crack length. It is also interesting to note that as the radial mobility and the crack length decreases, i.e., when a small crack is present in the fiber cluster region, the J Integral for the crack is higher. This is primarily because of the shielding effect of the fibers ahead of the crack tip. This effect increases with the increasing fiber cluster formation.

At this point, it is relevant to look into the effect of the longitudinal plies ahead of the crack tip. The location and the stiffness of the 0° layer affects the crack propagation . The stiffer plies prevent the crack from propagating transversely. The studies show that with the increase in distance between the crack tip and the stiffener, the significant effect of the stiffener remains negligible beyond a certain limit. This limit is the minimum size of the RVE as determined by Hill's criteria at which the crack starts to show the effect of stiffener. However, the distance of the crack tip to the stiffener has significant effect once the 0° plies are closer than this limit. Similarly, increase in stiffness enhances the shielding effect.

6.2 Concluding Remarks

The work presented in this dissertation intends to study the failure mechanism in PMCs-UD composites in particular under transverse loading. Based on the studies,

- The failure analysis in composite materials require multiscale analysis.
- It is very evident that the failure initiation and propagation in PMCs are governed by the microstructure of the RVE as well as the constituent properties. Hence, homogenization of composites is not the right method for failure analysis.
- It is very essential to understand the physics behind the failure mechanisms and implement them in the composite material failure analysis.
- Manufacturing defects plays a significant role in the failure analysis. In most cases, these defects enhances the criticality of both failure initiation and subsequent events.

6.3 Future Work Recommendations

The study on failure mechanisms in composite materials is an wide research area and there is more work required to the better understanding of failure mechanism. In the current work, damage initiation mechanism and location has been determined for the PMCs. It was assumed that when cavitation occurs in the matrix close to the fiber matrix interface, it results in the debond formation. This is obvious as the cavity would grow into the weakest plane which is the interfaces. But unless proven, it is a gap in the area. This is a potential area of research on how the cavitation grow into a debond. Another recommendation is studying the crack growth into the interface causing delamination and eventually the fiber breakage. In the current analysis, we focused on 2 D generalized plain strain. This ignores the fiber misalignment in the composite. Hence, a 3 D analysis which includes the fiber misalignment is a potential area of research. Also, in that case modeling voids of spherical or ellipsoidal shape makes more physical significance.

REFERENCES

[1] A. K. Kaw, *Mechanics of composite materials*. CRC press, 2005.

[2] "2014-2023 global composite aerostructures market outlook." Web, 2014.

[3] C. FAULDES, "Experience and lesseons learned of a composite aircraft," in *30th Congress of the International Council of the Aeronautical Sciences*, 2016.

[4] E. Gamstedt and B. Sjögren, "Micromechanisms in tension-compression fatigue of composite laminates containing transverse plies," *Composites Science and Technology*, vol. 59, no. 2, pp. 167–178, 1999.

[5] R. Talreja, "Assessment of the fundamentals of failure theories for composite materials," *Composites Science and Technology*, vol. 105, pp. 190–201, 2014.

[6] R. Talreja, "Studies on the failure analysis of composite materials with manufacturing defects," *Mechanics of composite materials*, vol. 49, no. 1, pp. 35–44, 2013.

[7] R. Talreja and C. V. Singh, *Damage and failure of composite materials*. Cambridge University Press, 2012.

[8] R. Pyrz, "Quantitative description of the microstructure of composites. part i: Morphology of unidirectional composite systems," *Composites Science and Technology*, vol. 50, no. 2, pp. 197–208, 1994.

[9] S. G. Advani and K.-T. Hsiao, *Manufacturing techniques for polymer matrix composites (PMCs)*. Elsevier, 2012.

[10] V. Bulsara, R. Talreja, and J. Qu, "Damage initiation under transverse loading of unidirectional composites with arbitrarily distributed fibers," *Composites science and technology*, vol. 59, no. 5, pp. 673–682, 1999.

[11] M. Isida, "Analysis of stress intensity factors for the tension of a centrally cracked strip with stiffened edges," *Engineering Fracture Mechanics*, vol. 5, no. 3, pp. 647–665, 1973.

[12] R. M. Jones, *Mechanics of composite materials*. CRC Press, 1998.

[13] P. K. Mallick, *Composites engineering handbook*. CRC Press, 1997.

[14] P. Mallick, "1 - overview," in *Materials, Design and Manufacturing for Lightweight Vehicles* (P. Mallick, ed.), Woodhead Publishing Series in Composites Science and Engineering, pp. 1 – 32, Woodhead Publishing, 2010.

[15] S. L. Knoeller and N. Rome, "Polymer matrix composite manufacturing induced defects," *Advanced Materials, Manufacturing and Testing*, vol. 5, pp. 7–10, 2009.

[16] D. Hull and T. W. Clyne, *An introduction to composite materials*. Cambridge university press, 1996.

[17] O. o. T. A. U.S. Congress, *Advanced Materials by Design*. Washington, DC: U.S. Government Printing Office, 1988.

[18] A. B. Strong, *Fundamentals of composites manufacturing: materials, methods and applications*. Society of Manufacturing Engineers, 2008.

[19] M. J. Hinton, A. S. Kaddour, and P. D. Soden, *Failure criteria in fibre reinforced polymer composites: the world-wide failure exercise*. Elsevier, 2004.

[20] V. Azzi and S. Tsai, "Anisotropic strength of composites," *Experimental mechanics*, vol. 5, no. 9, pp. 283–288, 1965.

[21] R. Hill, "A theory of the yielding and plastic flow of anisotropic metals," *Proceedings of the Royal Society of London. Series A. Mathematical and Physical Sciences*, vol. 193, no. 1033, pp. 281–297, 1948.

[22] S. W. Tsai and E. M. Wu, "A general theory of strength for anisotropic materials," *Journal of composite materials*, vol. 5, no. 1, pp. 58–80, 1971.

[23] Z. Hashin, "Failure criteria for unidirectional fiber composites," *Journal of applied mechanics*, vol. 47, no. 2, pp. 329–334, 1980.

[24] A. Puck, J. Kopp, and M. Knops, "Guidelines for the determination of the parameters in puck's action plane strength criterion," *Composites Science and Technology*, vol. 62, no. 3, pp. 371–378, 2002.

[25] C. Sun, "Strength analysis of unidirectional composites and laminates," 2000.

[26] R. B. Pipes and B. Cole, "On the off-axis strength test for anisotropic materials1," *Journal of Composite Materials*, vol. 7, no. 2, pp. 246–256, 1973.

[27] S. Swanson and M. Nelson, "Failure properties of carbon/epoxy laminates under tension-compression biaxial stress," *Composites*, vol. 86, pp. 279–86, 1986.

[28] R. D. Jamison, K. Schulte, K. L. Reifsnider, and W. W. Stinchcomb, "Characterization and analysis of damage mechanisms in tension-tension fatigue of graphite/epoxy laminates," in *Effects of defects in composite materials*, ASTM International, 1984.

[29] J. Lambert, A. Chambers, I. Sinclair, and S. Spearing, "3d damage characterisation and the role of voids in the fatigue of wind turbine blade materials," *Composites Science and Technology*, vol. 72, no. 2, pp. 337–343, 2012.

[30] A. Scott, I. Sinclair, S. M. Spearing, M. N. Mavrogordato, and W. Hepples, "Influence of voids on damage mechanisms in carbon/epoxy composites determined via high resolution computed tomography," *Composites Science and Technology*, vol. 90, pp. 147–153, 2014.

[31] J. Wang, K. Potter, K. Hazra, and M. Wisnom, "Experimental fabrication and characterization of out-of-plane fiber waviness in continuous fiber-reinforced composites," *Journal of Composite Materials*, vol. 46, no. 17, pp. 2041–2053, 2012.

[32] H. Huang and R. Talreja, "Effects of void geometry on elastic properties of unidirectional fiber reinforced composites," *Composites Science and Technology*, vol. 65, no. 13, pp. 1964–1981, 2005.

[33] K. Chowdhury, R. Talreja, and A. A. Benzerga, "Effects of manufacturing-induced voids on local failure in polymer-based composites," *Journal of Engineering Materials and Technology*, vol. 130, no. 2, p. 021010, 2008.

[34] L. Asp, L. A. Berglund, and R. Talreja, "Prediction of matrix-initiated transverse failure in polymer composites," *Composites Science and Technology*, vol. 56, no. 9, pp. 1089–1097, 1996.

[35] L. Asp, L. A. Berglund, and R. Talreja, "A criterion for crack initiation in glassy polymers subjected to a composite-like stress state," *Composites Science and Technology*, vol. 56, no. 11, pp. 1291–1301, 1996.

[36] A. Documentation and U. Manual, "Version 6.10," *Dassault systemes*, 2010.

[37] R. Hill, "Theory of mechanical properties of fibre-strengthened materials: I. elastic behaviour," *Journal of the Mechanics and Physics of Solids*, vol. 12, no. 4, pp. 199 – 212, 1964.

[38] Z. Hashin, "Analysis of composite materials—a survey," *Journal of Applied Mechanics*, vol. 50, no. 3, pp. 481–505, 1983.

[39] J. Aboudi, S. M. Arnold, and B. A. Bednarcyk, *Micromechanics of composite materials: a generalized multiscale analysis approach.* Butterworth-Heinemann, 2012.

[40] A. Drago and M. J. Pindera, "Micro-macromechanical analysis of heterogeneous materials: macroscopically homogeneous vs periodic microstructures," *Composites Science and Technology*, vol. 67, no. 6, pp. 1243–1263, 2007.

[41] S. Li and A. Wongsto, "Unit cells for micromechanical analyses of particle-reinforced composites," *Mechanics of Materials*, vol. 36, no. 7, pp. 543 – 572, 2004.

[42] S. Li, "General unit cells for micromechanical analyses of unidirectional composites," *Composites Part A: Applied Science and Manufacturing*, vol. 32, no. 6, pp. 815 – 826, 2001.

[43] Z. Xia, Y. Zhang, and F. Ellyin, "A unified periodical boundary conditions for representative volume elements of composites and applications," *International Journal of Solids and Structures*, vol. 40, no. 8, pp. 1907–1921, 2003.

[44] C. Sun and R. Vaidya, "Prediction of composite properties from a representative volume element," *Composites Science and Technology*, vol. 56, no. 2, pp. 171 – 179, 1996.

[45] D. Trias, J. Costa, J. Mayugo, and J. Hurtado, "Random models versus periodic models for fibre reinforced composites," *Computational materials science*, vol. 38, no. 2, pp. 316–324, 2006.

[46] R. Hill, "Elastic properties of reinforced solids: some theoretical principles," *Journal of the Mechanics and Physics of Solids*, vol. 11, no. 5, pp. 357–372, 1963.

[47] R. Talreja, "Multi-scale modeling in damage mechanics of composite materials," *Journal of materials science*, vol. 41, no. 20, pp. 6800–6812, 2006.

[48] J. Segurado, C. Gonzalez, and J. Llorca, "A numerical investigation of the effect of particle clustering on the mechanical properties of composites," *Acta Materialia*, vol. 51, no. 8, pp. 2355–2369, 2003.

[49] M. Hojo, M. Mizuno, T. Hobbiebrunken, T. Adachi, M. Tanaka, and S. K. Ha, "Effect of fiber array irregularities on microscopic interfacial normal stress states of transversely loaded ud-cfrp from viewpoint of failure initiation," *Composites Science and Technology*, vol. 69, no. 11-12, pp. 1726–1734, 2009.

[50] R. Pyrz, "Correlation of microstructure variability and local stress field in two-phase materials," *Materials Science and Engineering: A*, vol. 177, no. 1-2, pp. 253–259, 1994.

[51] S. Ghosh, Z. Nowak, and K. Lee, "Quantitative characterization and modeling of composite microstructures by voronoi cells," *Acta Materialia*, vol. 45, no. 6, pp. 2215–2234, 1997.

[52] R. Pyrz and B. Bochenek, "Topological disorder of microstructure and its relation to the stress field," *International journal of solids and structures*, vol. 35, no. 19, pp. 2413–2427, 1998.

[53] S. Torquato, "Random heterogeneous media: microstructure and improved bounds on effective properties," *Appl. Mech. Rev*, vol. 44, no. 2, pp. 37–76, 1991.

[54] N. Kuentzer, P. Simacek, S. G. Advani, and S. Walsh, "Correlation of void distribution to vartm manufacturing techniques," *Composites Part A: applied science and manufacturing*, vol. 38, no. 3, pp. 802–813, 2007.

[55] X. Chen and T. Papathanasiou, "Interface stress distributions in transversely loaded continuous fiber composites: parallel computation in multi-fiber rves using the boundary element method," *Composites science and technology*, vol. 64, no. 9, pp. 1101–1114, 2004.

[56] Y. K. Hamidi, L. Aktas, and M. C. Altan, "Formation of microscopic voids in resin transfer molded composites," in *ASME 2003 International Mechanical Engineering*

Congress and Exposition, pp. 65–76, American Society of Mechanical Engineers, 2003.

[57] L. E. Asp, L. A. Berglund, and P. Gudmundson, "Effects of a composite-like stress state on the fracture of epoxies," *Composites science and technology*, vol. 53, no. 1, pp. 27–37, 1995.

[58] M. Wisnom, M. Gigliotti, N. Ersoy, M. Campbell, and K. Potter, "Mechanisms generating residual stresses and distortion during manufacture of polymer–matrix composite structures," *Composites Part A: Applied Science and Manufacturing*, vol. 37, no. 4, pp. 522–529, 2006.

[59] A. Neogi, N. Mitra, and R. Talreja, "Cavitation in epoxies under composite-like stress states," *Composites Part A: Applied Science and Manufacturing*, vol. 106, pp. 52–58, 2018.

[60] J. De Kok and H. Meijer, "Deformation, yield and fracture of unidirectional composites in transverse loading: 1. influence of fibre volume fraction and test-temperature," *Composites Part A: Applied Science and Manufacturing*, vol. 30, no. 7, pp. 905–916, 1999.

[61] R. E. Walpole, R. H. Myers, S. L. Myers, and K. Ye, *Probability and statistics for engineers and scientists*, vol. 5. Macmillan New York, 1993.

[62] T. L. Anderson, *Fracture mechanics: fundamentals and applications*. CRC press, 2017.

[63] M. ISIDA, "Analysis of stress intensity factors for plates containing random array of cracks," *Bulletin of JSME*, vol. 13, no. 59, pp. 635–642, 1970.

[64] M. Isida, "Effect of width and length on stress intensity factors of internally cracked plates under various boundary conditions," *International Journal of Fracture Me-*

chanics, vol. 7, no. 3, pp. 301–316, 1971.